Swansea University
Prifysgol Abertawe

Advanced Packaging Solutions for Shelf Life Management of Fresh Food

by

Alaa Alaizoki

Submitted to Swansea University in fulfilment of the requirements for the Degree of Doctor of Engineering (EngD)

Swansea University

2022

Abstract

Liquid residues and moisture within the packaging is a big challenge to fresh food packaging, particularly for liquid-exuding food, such as meat, fish and poultry. The free-moving liquid (exudate) in the bottom of plastic food trays adversely affects the safety, quality and presentation of packaged meat products. However, the current food packaging solutions to isolate meat exudate including the addition of absorbent meat pads are not efficient, restricting the recycling process of plastic packaging and increasing plastic waste that ends up in landfill and oceans.

This work reports the development of innovative plastic packaging solutions capable of effectively isolating the meat exudate within the packaging itself, ensuring more sustainable and recyclable plastic food packaging. The developed solutions include three innovative technologies:

Geometry modification of liquid-holding recesses integrated into plastic food tray. The raised rims of the modified recesses act as capillary geometrical valves, enhancing the liquid pinning and pressure barrier. This results in an approximately 2.8 times increase in liquid retention capacity of the recesses, compared with a design without raised rims.

Surface modification of liquid-holding recesses with oxygen plasma treatment. The localised plasma treatment of recess walls implants polar oxygen groups on the wall surfaces. This induces contrast in the surface wettability between plasma treated walls and untreated outer edges of the recesses, increasing their liquid pinning and pressure barrier, thus their liquid retention capacity. The functionality induced by plasma treatment was reserved long enough (> 60 days) for increasing the liquid retention capacity of ~2.2 times in comparison with untreated recesses.

Surface modification of open-cell polymeric foam with oxygen plasma treatment. The plasma treatment results in improving the surface wettability of foam porous structure due to introducing polar oxygen groups on the pore walls. The improved wettability increases the sucking capillary pressure acting on the foam pores, allowing for higher liquid uptake and absorption of open-cell foam. The plasma treatment has sufficiently long effect on wettability improvement (> 60 days) to be used for the treatment of plastic foam packaging with an increase in the liquid absorption capacity of ~8 times.

This work has led to developing innovative and sustainable plastic meat packaging for effective self-isolation of meat exudate. The plastic packaging trays incorporated with recesses are fully recyclable with liquid retention capacities comparable to the conventional absorbent meat pads. Therefore, plastic food packaging with liquid isolation capability can be manufactured with no need for additional absorbent components. The plasma treatment of open-cell polymeric foam can also replace the use of chemical wetting agents for facilitating liquid absorption, protecting human health and environment.

Declarations and Statements

This work has not previously been accepted in substance for any degree and is not being concurrently submitted in candidature for any degree.

Signed.....

Date.....23/02/2023.....

This thesis is the result of my own investigations, except where otherwise stated. Other sources are acknowledged by footnotes giving explicit references. A bibliography is appended.

Signed.....

Date.....23/02/2023.....

I hereby give my consent for my work, if relevant and accepted, to be available for photocopying and for inter-library loans **after expiry of a bar on access approved by the University**.

Signed.....

Date.....23/02/2023.....

The University's ethical procedures have been followed and, where appropriate, that ethical approval has been granted.

Signed.....

Date.....23/02/2023.....

Publications

The following peer-reviewed journal articles have been integrated into the thesis chapters:

Alaizoki A, Phillips C, Hardwick C, Parker D, Deganello D. Enhanced liquid retention capacity within plastic food packaging through modified capillary recesses. J Food Eng. 2022 Jun 1;323:111010.

This article has been published in the *Journal of Food Engineering*.

Alaizoki A, Phillips C, Parker D, Hardwick C, Griffiths C, Deganello D. Effect of plasma treatment on improving liquid retention capacity of capillary recesses for food packaging applications. Food Packag Shelf Life. 2021 Dec 1;30:100759.

This article has been published in the *Journal of Food Packaging and Shelf Life*.

Alaizoki A, Phillips C, Parker D, Hardwick C, McGettrick J, Deganello D. Improvement in liquid absorption of open-cell polymeric foam by plasma treatment for food packaging applications. J Appl Polym Sci [Internet]. 2022 May 139(17):52015.

This article has been published in the *Journal of Applied Polymer Science*.

Authorship Declaration

Candidate	Name and College
Author 1 (Candidate)	Alaa Alaizoki – Faculty of Science and Engineering, Swansea University
Author 2	Christopher Phillips – Faculty of Science and Engineering, Swansea University
Author 3	Craig Hardwick – Klockner Pentaplast
Author 4	David Parker – Klockner Pentaplast
Author 5	Chris Griffiths – SPECIFIC IKC, Swansea University
Author 6	James McGettrick – Faculty of Science and Engineering, Swansea University
Author 7	Davide Deganello – Faculty of Science and Engineering, Swansea University

Author Details and their Roles:

Paper 1 (**Enhanced liquid retention capacity within plastic food packaging through modified capillary recesses**)

Located in Chapter 5

Candidate (Author 1) contributed to Investigation, Conceptualisation, Methodology, Writing – original draft, Visualisation.

Author 2 contributed to Supervision, Writing – review & editing, Validation.

Author 3 contributed to Resources, Supervision, Project administration.

Author 4 contributed to Supervision.

Author 7 contributed to Conceptualisation, Supervision, Methodology, Writing – review & editing, Validation, Project administration.

Paper 2 (**Effect of plasma treatment on improving liquid retention capacity of capillary recesses for food packaging applications**)

Located in Chapter 6

Candidate (Author 1) contributed to Investigation, Conceptualization, Methodology, Writing – original draft, Visualization.

Author 2 contributed to Supervision, Writing – review & editing, Validation.

Author 3 contributed to Supervision.

Author 4 contributed to Resources, Supervision, Project administration.

Author 5 contributed to Resources.

Author 7 contributed to Conceptualisation, Supervision, Methodology, Writing – review & editing, Validation, Project administration.

Paper 3 (**Improvement in liquid absorption of open-cell polymeric foam by plasma treatment for food packaging applications**)

Located in Chapter 7

Candidate (Author 1) contributed to Investigation, Conceptualization, Methodology, Writing – original draft, Visualization.

Author 2 contributed to Supervision, Writing – review & editing, Validation.

Author 3 contributed to Supervision.

Author 4 contributed to Resources, Supervision, Project administration.

Author 6 contributed to Review and Resources.

Author 7 contributed to Conceptualisation, Supervision, Methodology, Writing – review & editing, Validation, Project administration.

We the undersigned agree with the above stated "proportion of work undertaken" for each of the above published peer-reviewed manuscripts contributing to this thesis:

Signed Candidate (Author 1) _____

Author 2_____

Author 3_____

Author 4_____

Author 5_____

Author 6_____

Author 7_____

Contents

Acknowledgements

Having accomplished this chapter of my life, I would like to give a huge thank you to the people supported me during my study journey at Swansea University. I am very thankful to the EngD scheme and M2A team for providing great learning environment and support over these years.

I am thankful to my supervisors Davide Deganello and Chris Phillips for their guidance and support, especially the motivation during difficult times. Under their supervision, I learned to be creative, dedicated and patient. A big thank you to Klockner Pentaplast (kp) and my industrial supervisors Craig Hardwick and David Parker for their support and help, encouraging me to succeed as innovative engineer. I would like to thank Alex Holder, James McGettrick and Chris Griffiths for their support and training on different test facilities.

To my great lady, Zeina, who firmly stood and backed me to succeed and overcome obstacles. Thank you, my love.

To my Dad and Mum, I know you would be pleased and proud of me even though you are not with me in this life.

Finally, a big thank to my family and friends, who have always been supportive and loving.

List of Figures

List of Tables

Abbreviations/Acronyms

PET	Polyethylene terephthalate
PE	Polyethylene
PP	Polypropylene
PS	Polystyrene
PVC	Polyvinyl chloride
LDPE	Low-density polyethylene
PSE	Pale-soft, exudative
WCA	Water contact angle
L-W	Lucas-Washburn
PE	Pork exudate
DC	Direct current
AC	Alternating current
CMC	Carboxymethyl cellulose
BSA	Bovine serum albumin
DI	Deionised
ASTM	American Society for Testing and Materials
SEM	Scanning electron microscope
AFM	Atomic force microscopy
XPS	X-ray photoelectron spectroscopy
LT	Low torque
SF	Secondary flow
IPA	Isopropyl alcohol
CAD	Computer-aided design
RMS	Root mean squared roughness
Ra	Average roughness
O/C	Oxygen/carbon

Selected Symbols

γ	Surface tension	wt%	Weight percentage
θ	Contact angle	G'	Storge modulus
W_a	Work of adhesion	G''	Loss modulus
r_w	Roughness factor	δ	Phase angle
P	Proportion area of a solid surface	d	Diameter
$\Delta\theta$	Contact angle hysteresis	H	Physical quantity related to d_s/d_e
P_o	Atmospheric pressure	ψ	Expansion ratio
R^{-1}	Meniscus curvature	n	Porosity
ρ	Density	L	Long
g	Gravity acceleration	W	Width
z	Capillary liquid height	T	Thickness
ΔP_c	Capillary/Laplace pressure	R	Absorption capacity
r	Radius	α	Draft angle
h_e	Equilibrium liquid height	O%	Oxygen percentage
η	Liquid viscosity	C%	Carbon percentage
t	Time	N%	Nitrogen percentage
β	Inclination angle	Si%	Silicon percentage
ω	Expansion opening angle	RH	Relative Humidity

Chapter 1

Introduction

1.1 Food Packaging: Functionalities and Challenges

Food packaging has a vital role in prolonging food shelf life and ensuring safer and fresher food in the supply chain.[1] The packaging provides a protection to contained food from various physical and chemical contaminants, and it inhibits the growth of spoilage and pathogenic bacteria. It also facilitates promotion and convenience of packaged food within food markets.[2–5] Plastic packaging is the most used packaging for food products in the supply chain, particularly after increased safety concerns and customers' demand for packaged food during the coronavirus pandemic.[6] Food packaging value in the global market is estimated to reach US$ 378.58 billion in 2022.[7] Thermoplastic polymers account for the majority of plastic materials used in food packaging, such as polyethylene terephthalate (PET), polyethylene (PE), polystyrene (PS) and polypropylene (PP).[8] These plastic materials are appealing to the food packaging industry as they are low-cost, transparent, light and offer excellent mechanical and barrier properties.[9] Plastic packaging constituted 40.5% (~19.9 million tonnes) of the annual European demand for plastics in 2020.[10] Food packaging can be made from flexible and rigid plastics, taking several forms (e.g. trays, films and pouches) to address market demands in terms of appearance, convenience, practicality and ease of use.[8,11]

The development of food packaging functionalities is gaining more interest in the light of growing demand for safer, healthier and longer shelf-life food. Further, the global population is estimated to exceed 9 billion in 2050, and the supply chain will be required to secure 70% more food.[12,13] These factors stress the key role of functionalised food packaging in reducing food waste and securing adequate food supply,[3,5,8] particularly since 1/3 of globally produced food is wasted as equivalent to 1.3 billion tonnes/year.[14] The large food waste across the food chain also makes a profound impact on the global economy with lost value of US$ 1 trillion/year.[15] Therefore, the packaging industry has been driven to develop packaging solutions to address current challenges of packaged food products, such as limited shelf life and exuded liquid of food.[1,3,16]

Liquid residues and moisture within the packaging is still a big challenge to fresh food packaging, in particular for liquid-exuding food, such as meat, fish and poultry. These meat products are perishable and tend to excrete liquid (exudate) in the packaging trays during their shelf life,[3,17] as shown in Figure 1.1. High exudate content has a negative impact on the packaged meat as it accelerates quality deterioration and compromises safety of the packaged meat. This is due to the increase in water activity, and thus greater proliferation of microorganisms responsible for spoilage and limited shelf life of the packaged meat products.[3,18] This can undermine the efforts to meet the increased meat consumption with currently more than 20% of meat supply wasted.[19] The free-moving exudate in the meat packaging also provides an unsightly appearance to consumers and it can leak from the packaging trays.[18]

Figure 1.1: A plastic tray with meat exudate collected in the bottom of tray.

Isolation of the meat exudate has traditionally been achieved with polymeric or paper-based soak away pads (Figure 1.2) in contact with the meat. These pads in themselves are not recyclable and have to be removed by the customer, are often glued in place, and act as barriers to the recycling of the plastic trays.[20,21] Therefore, it is crucial to develop packaging solutions to isolate the released exudate from packaged meat products.

Figure 1.2: Plastic meat tray with absorbent pad (tray and pad source: Klockner Pentaplast Group).

While plastic food packaging contributes to the sustainability and waste reduction of food products, the growing use of plastic packaging has itself a concerning environmental impact.[9] More than 30% of the global production of plastic materials (>300 million tonnes/year) is designated for plastic packaging.[7,22] These plastic materials are not generally biodegradable and more than half of the plastic packaging including most plastic food packaging are intended for a single use and then sorted as packaging waste. This exacerbates the environmental burden of plastic packaging with < 10% of plastic waste being recycled. Most plastic packaging is sent to landfill or ends up in the oceans,[7,23–26] as shown in Figure 1.3. Oceans annually receive 5-13 million tonnes of plastic waste with estimation to exceed fish quantities by 2050.[27] Recycling of plastic waste is the most efficient approach to minimise the environmental

footprint and achieve greater sustainability of plastic food packaging.[9] However, plastic packaging manufactured from multilayers or different types of polymers, and difficulty in removing food residues are the major constraints on the recyclability of plastic packaging. This makes the plastic recycling impracticable with high cost and complexity of separating and processing of these plastic materials.[7,16] Therefore, this work will investigate the development of fully recyclable plastic food packaging with embedded functionalities to isolate the liquid residues of packaged food products. This can lead to more sustainable food and packaging over the supply chain.

Figure 1.3: Environmental challenge of plastic packaging waste (photo source: waste360).

1.2 Thesis Objectives and Layout

This thesis aims to explore different innovative packaging solutions for scavenging and isolation of meat exudate within plastic meat packaging itself and without the need for additional components. This is based on the functionalities of capillarity and interfaces with a focus on enhancing capillary pressure and liquid pinning to increase liquid retention. These functionalities are gained through modification of both the geometry and surface chemistry of plastic meat packaging.

The thesis reporting this work has been laid out as follows:

- Chapter 2. Literature review: This chapter reports reviews of current literature on meat exudate, surface wettability and capillary phenomena, capillary valves, porous materials and surface modification of polymers.

- Chapter 3. This chapter reports a description of the materials and methods used for characterising the meat exudate and new packaging solutions. The first stage of this work was to prepare simulant liquids of meat exudate, with appropriate surface tension and rheology, to evaluate the liquid retention capacity of the packaging solutions with various modifications. The second stage was to apply surface and geometrical modifications to the packaging solutions, characterise the properties of packaging samples and test their liquid retention capacity.
- Chapter 4. This chapter reports the rheological and physical characterisation of pork meat exudate in addition to the formulation and characterisation of exudate simulants.
- Chapter 5. This chapter reports the investigation of the ability of specifically designed thermoformed recesses in the plastic film tray to trap liquids.
- Chapter 6. This chapter reports the investigation of the use of targeted oxygen plasma treatment as a means of improving the trapping of liquids through the different wetting abilities of the plastic tray face and recesses.
- Chapter 7. This chapter reports the studies on the application of oxygen plasma treatment as alternative means of chemical wetting agents to enhance the liquid absorption capacity of open-cell polymeric foam.
- Chapter 8. Conclusions and recommendations: This chapter reports the key outcomes of this work with recommendations for future work.

Chapter 2

Literature Review

2.1 Introduction

This chapter first explores the characteristics of meat exudate in terms of how it is formed, physical properties and the challenges it presents in food packaging. This enables the formulation of effective simulant liquids for assessing the liquid retention of new packaging solutions. Current methods for dealing with meat exudate are discussed followed by a review of the underlying phenomena behind flow and wetting characteristics of meat exudate. Surface wettability, capillarity and valving phenomena are researched for proposing new technologies that are effective for trapping meat exudate within wells and open-cell foam. These involve geometrical valves and wetting variation-based valves as well as liquid wicking in the porous materials under capillary action. This is followed by a review on surface modification of polymers with a focus on plasma treatment for improving surface wettability and capillary actions.

2.2 Meat Exudate

2.2.1 Exudate Formation and Structure

Liquid exudation from packaged fresh food is problematic to food packaging. Liquid excreted within food packaging is unsightly, affecting the safety and quality properties of packaged food products.[28,29] Fresh meat, seafoods, fish and poultry are naturally liquid-exuding foods and are typically packaged in plastic trays. In the case of prepared packaged foods, this liquid accumulates in the packaging during storage. While this phenomenon is not exclusive to meat products, in this case particularly, the liquid emitted is an undesirable consequence of preparation and storage. Packaged meat products tend to release an exudate (drip) during their shelf life.[3,18] This exudate flows under gravity from the meat surface as a result of protein denaturation and lateral shrinking of muscle fibres during the post-mortem period.[30,31]

Meat muscle primarily consists of 75% water in addition to 20% proteins, while other components, such as lipids, minerals and vitamins only form smaller portions of the meat. The water content of muscle can be found in three different forms based on the structural bonds with meat proteins (free, immobilised and bound water). Most water is retained under forces of capillarity or charge attraction in compartments and

channels between structural myofibrils, meat cells and filaments.[31] This water can be re-distributed inside the meat structure during post-mortem period with a decrease in pH of the muscle due to glycolysis and formation of lactic acid.[30,32] The increased environmental acidity induces equal positive and negative charges of muscle proteins leading to a reduction of their capacity to hold and bind water. Myofibrils also undergo contraction and shrinkage leading to a reduction in the size of structural muscle cells and cross-section of the fibres with nearly 9%. This results in a decrease of the spaces available to hold entrapped water inside meat muscle.[31,32] Therefore, the muscle water is expelled from the structural gaps and drained as meat exudate under gravity.[33]

The exudate expressed from fresh meat is estimated to be around 1-3 wt% of the red meat cut weight and it can reach 10 wt% for pale-soft, exudative (PSE) pork meat.[31] This liquid loss also increases as a consequence of meat handling or processing, such as cutting and freezing.[34] The meat exudate is an aqueous liquid containing soluble sarcoplasmic proteins with a mixture of amino acids and enzymes.[35] The protein concentrations can reach 112 mg for each millilitre of the meat exudate.[31] Exudate content of proteins can vary according to the amount of exudate expressed from meat. Various works reported that protein concentration is negatively proportionate with the volume of released exudate. This can be explained by the dilution effect as the increase in water released from muscle tissues results in diluting the proteins concentration in the exudate[36-40] The sarcoplasmic proteins in meat exudate are water soluble and have low molecular weights. These proteins are globular with more than 500 proteins primarily in the form of enzymes in addition to myoglobin.[30,41] The molecular weights of sarcoplasmic proteins are less than 100 kDa, and more specifically in the range of 17-92.5 kDa.[30,42] Many researchers have analysed the protein composition of meat exudates. Protein analysis carried out by Ursu et al.[43] for pork exudate showed that it primarily contained protein bands with molecular weight ranging from 20 kDa to 100 kDa. These bands are consistent with protein bands found in pork exudate by Di Luca et al.[44] as the most abundant bands were 83, 68, 63, 42, 31 kDa. Bowker et al.[37] found that the majority of soluble proteins detected in beef exudate had molecular weights of 47, 43, 36 kDa. However, further breakdown of sarcoplasmic proteins occurs during meat ageing and proteins with lower molecular weights can be observed in the meat exudate. Proteins with high

molecular weights > 100 kDa were also detected in meat exudate including proteins with 167 kDa in beef exudate.[37] These protein fractions originate from breakdown of myofibrillar proteins through proteolysis processes during meat ageing.[44] This degradation of myofibrils proteins was also observed during ageing stage of beef by Laville et al.[45]

2.2.2 Rheological and Physical Properties of Meat Exudate

The presence of soluble proteins in meat exudate has a significant impact on its rheological and physical characteristics. These are manifested in higher viscosity and lower surface tension of meat exudate when compared with pure water.[33,43,46] This might affect the ability of packaging systems to retain this liquid. Literature indicates that there is a range of properties for meat exudate depending on the meat type and other considerations, such as ageing. Meat exudates typically have a range of viscosities < 10 mPa.s and reduced surface tensions down to 50 mN/m as reported in several works. Pork exudate characterised by Ursu et al.[43] showed Newtonian flow properties with viscosity values ranging from 3 to 10 mPa.s at a temperature of 20 °C, and the surface tension as low as 50 mN/m. Shibata-Ishiwatari et al.[46] found that beef exudate had a viscosity of 3.12 mPa.s at 20 °C. The viscosity of beef exudate was also between 3 and 4 mPa.s as reported by other work.[47] However, the viscosity was higher for exudate expressed from aged meat due to the increase in protein concentration with more protein fractions being degraded and dissolved in the meat exudate.[47]

2.2.3 Challenges of Exudate in Meat Packaging

Meat exudate presents a major challenge to the meat packaging industry. This exudate is usually expressed from meat surface and accumulated in the meat plastic trays. Consumers perceive the free-moving exudate as unattractive and unhygienic, leading to a rejection of the product at point of sale. The exudate can also leak from the meat packaging during handling and display on the shelf.[18,48] The meat exudate has a high content of soluble nutrients transferred from the meat structure including amino acids, vitamins and soluble sarcoplasmic proteins.[49,50] This offers a rich media of nutrients with high water activity for greater proliferation of existing pathogenic bacteria and spoilage microorganisms. This can limit the meat shelf life and result in compromised meat safety and deterioration of meat quality characteristics.[3,18] Kim et al.[51] studied the effect of pork exudate on the microbial activity inside meat packaging

during chill storage at a temperature of 1 °C. They found that removing the exudate from the packaging bags resulted in a considerably lower load of microorganisms.[51]

2.3 Conventional Plastic Packaging Solutions for Exudate Scavenging

Fresh meat products are normally packaged in polymeric trays and sealed with thin flexible film.[18] Isolation of the meat exudate in these trays has thus far been addressed by different packaging solutions. An absorbent pad is commonly placed between the contained meat and bottom of packaging tray to absorb the meat exudate. It can be in different forms including multi-layered pads, paper sheets, blankets, or non-woven polymeric layers with incorporated superabsorbent material.[52–54] These absorbent pads immobilise the exudate in their absorbing bulk leading to a reduced water activity inside the plastic packaging.[55,56] Incorporation of meat trays with liquid-holding micro-wells is also another approach to trap the released meat exudate in film packaging. This includes arrays of micro-wells with hexagonal shape to act as a liquid retention system.[57] A polymeric foam tray with an open-cell structure is another packaging solution as soak-away for the meat exudate as reported in different patents.[58–60] This absorbent tray has an interconnected porous structure and draws the meat exudate into the foam pores through perforations made in the tray skin.[61] The liquid absorbency of polymeric foams is attributed to their porosity and pore interconnectivity, which ensure a network of interconnected voids accessible to the wicking liquids.[62,63]

The current food packaging solutions for liquid scavenging have various drawbacks. Micro-wells and foam are not sufficient to hold the volume of exudate and only absorbent pads are appropriate at the moment.[55,57,64] Additional components such as absorbent pads and foams present a problem in terms of recycling of the packaging film since soaked pads and foams are non-recyclable, and these are often glued to the packaging and must be manually removed.[9,65,66] This makes the recycling of plastic meat packaging impractical and increases the environmental footprint of plastic packaging waste that ends up in landfill and oceans.[7] Saturated absorbent pads can also be separated, and inadequate apertures on the outer pad film can cause tearing of the pad film and direct contact between the absorbing layer and packaged product.[55] Further, foam trays and pad-embedded trays of meat products are usually tilted at different angles (45°, 70°) during shipping and displaying that may

result in noticeable accumulated exudate at the tray edges.[67] Therefore, it is of a great interest to develop sustainable and innovative packaging solutions to isolate the released exudate away from the packaged meat products that does not rely on additional components.

2.4 Surface Tension and Wettability Phenomena

Surface wettability and surface tension are crucial phenomena in nature and practical sciences, such as physics and engineering. These are attributed to the molecular interactions that occur at material interfaces, giving liquids their characteristic surface forces and defining the liquid spreading on solid surfaces.[68,69] Several solutions and phenomena, including capillarity, are based on liquid surface tension and wettability of solid surfaces that can be observed in nature. For example, moisture collection by patterned surface wettability of Namib desert beetles and non-wetting properties of lotus leaves and butterfly wings for self-cleaning surfaces.[70,71] These and other bioinspired wettability-based solutions can be exploited to explore innovative solutions for liquid isolation within food packaging. Hence, capillarity and capillary valving phenomena will be investigated to develop food packaging capable to isolate and retain the meat exudate. The interaction of the exuded liquid with the packaging material surface/bulk will determine the extent to which the liquid can be trapped or retained within the packaging. While the properties of the liquid are due to the type of meat product and its treatment, the packaging may be manipulated to change the liquid/solid interaction.

2.4.1 Surface Tension

Surface tension and surface energy are important physical characteristics of liquid and solid materials, responsible for interactions taking place on the interface of contacting surfaces. These include liquid wicking and adsorption onto solid surfaces, surface wettability and adhesion that are utilised in various technological applications, such as packaging, textiles, pharmaceutical products, coating and printing.[68] The surface tension is particularly crucial to meat exudate as it will determine the potential mechanisms to trap meat exudate in food packaging. The surface tension is attributed to attractive intermolecular forces expressed on the top boundary layer of a material, and originates from the cohesive intermolecular forces between the material molecules as no outer neighbouring molecules are present to interact or balance this layer. These

surface forces are directed towards the material bulk to minimise the surface area, thus, generating a meniscus for liquid materials. Any increase in the material surface increases the imbalance of molecules existing on the top surface layer and induces more forces towards the bulk. This is not the thermodynamically favourable state of materials. Therefore, surface tension tends to reduce the liquid surface area. The increase in the material surface requires additional force to overcome the dominant force of surface tension. This is observed in floating insects like gerridae on water where the surface tension forces are larger than the gravitational forces exerted by the insect on the water surface. The surface tension is commonly determined as the force required to increase a length unit presented in terms of N/m for liquids. For solid surfaces, the equivalent surface tension is referred to as surface free energy, defined as the work needed to increase a unit of surface area and estimated in J/m^2.[72–74]

The surface tension of liquids can be determined by direct methods, such as pendant drop and capillary rise techniques, while the measurement of surface free energy of solid surfaces is carried out by indirect approaches that rely on contact angle measurements of known liquids and semiempirical models.[75] The surface free energy depends on the chemical surface structure of solid materials, and it is divided into polar and dispersive components. The polar component is attributed to hydrogen and inductive bonds, while the dispersive component accounts for various dispersive forces, such as van der Waals and other London forces.[76] The surface free energy and its components are commonly determined by measuring the contact angle of test liquids with known surface tensions and using one of the semiempirical models referred in different indirect methods, such as Fowkes, Geometric mean and Zisman.[75,77] Therefore, solid material surfaces with molecules interacted in their bulks by primary bonds have high surface free energy, such as metals and inorganic materials. On the other hand, organic materials generally express lower levels of surface free energy, particularly the polymers as their surfaces lack polarity and the polymer chains are bonded with weak forces, such as van der Waals and London forces.[72,73]

2.4.2 Surface Wettability

Wettability is a surface characteristic of materials that reflects the affinity of a liquid to spread and adhere to another surface. It can be observed as wetting or non-wetting behaviours in nature and various technological applications, such as water droplets on

plant leaves, oil-water separation technology and printing.[71,72,78] Wetting phenomena occur when surfaces of liquid and solid material are in direct contact as the outer molecular layers on the interface interact to balance their surface forces. This causes formation of a liquid/solid interface. The resulting adhesive forces on interface are based on molecular interaction of the dispersive and polar elements of both liquid and solid material on the interfacial area.[79]

The wetting and spreading depend on the surface chemical structure and acting forces that include electrostatic, van der Waals and other long-range forces. The wetting properties of solid material surfaces can be characterised by the contact angle (θ) formed at the three-line interface between solid, liquid and air in equilibrium. The measured contact angle of a liquid drop on a flat surface or liquid meniscus on a 3D geometrical structure surface allows to determine the surface wettability.[69,80] This contact angle reflects the competition between the molecular cohesive forces exerted by the liquid to reduce its surface and the adhesive forces on the liquid/solid interface to extend the liquid spreading in the thermodynamic equilibrium.[68] These molecular interactions are extremely weak between low density fluids, such as air with the solid or liquid surface.[81] Based on the measured contact angle, the wettability of a solid surface can show different thermodynamic states that can be explained by full and partial wetting regimes under equilibrium conditions. As a liquid tends to completely wet the solid surface forming a thin liquid layer, a contact angle of 0° is achieved. For a liquid partially wetting the solid surface, a characteristic drop with contact angles > 0° can be obtained in equilibrium as illustrated in Figure 2.1. There are two distinguished cases for the partial wetting states, which include wettability with contact angles < 90° known as wettable surface and corresponding to hydrophilic surface regarding water as a wetting liquid. This partial wettability occurs as the solid surface has surface energy enough to compensate the surface tension of the wetting liquid. On the other hand, a partial wetting state with contact angles > 90° accounts for a non-wettable surface with a finite shaped drop. This corresponds to hydrophobic surface regarding water as a wetting liquid.[69,72,82]

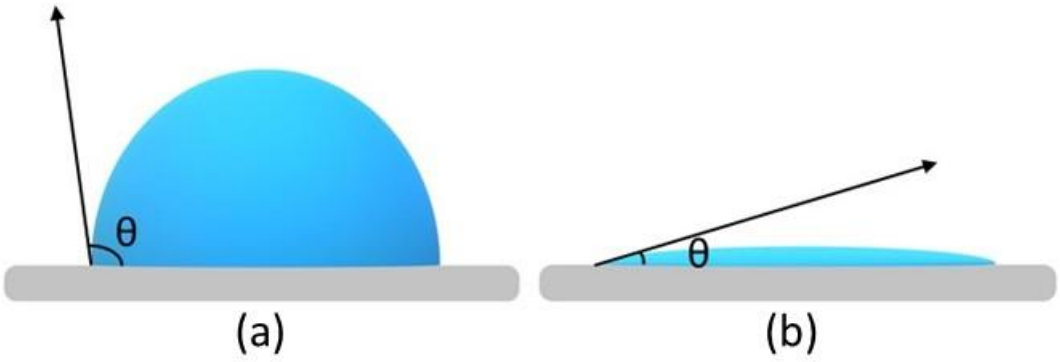

Figure 2.1: (a) non-wettable solid surface (contact angle $\theta > 90°$), (b) wettable solid surface (contact angle $\theta < 90°$). Figure was redrawn from Grundke et al.[69]

Surface wettability of solid materials is governed by their surface chemical composition, surface free energy and topography. It is also dependent on liquid surface tension.[83,84] The mechanism of wetting behaviour is defined by Young's model according to the thermodynamic theory of adsorption. This model considers a liquid drop is settled on a smooth, uniform and solid surface in thermodynamic equilibrium (Figure 2.2) with no impact of any external forces on the deposited drop, such as gravity.[68,85] Young's model relates the resulting static contact angle (θ_e) at the three-phase interface with three characteristic interfacial tensions as shown in equation (2.1)[69]:

$$\cos \theta_e = \frac{\gamma_{sv} - \gamma_{sl}}{\gamma_{lv}} \qquad (2.1)$$

The contact angle can be measured by the sessile drop technique that is based on analysing the drop shape profile. Therefore, the surface wettability increases for higher surface free energy of solid surface represented by solid/vapour interfacial tension (γ_{sv}), and for lower solid/liquid interfacial tension (γ_{sl}) and liquid/vapour interfacial tension (γ_{lv})[68]. On the other hand, the wetting behaviour involves formation of adhesive forces on the liquid/solid interface as the contacting surfaces tend to minimise the energy on their interface in equilibrium condition.[68,71] This is represented by the work of adhesion (W_a) needed to separate the contacting surfaces of liquid and solid phases as given by Dupré equation (2.2)[68]:

$$W_a = \gamma_{sv} + \gamma_{lv} - \gamma_{sl} \qquad (2.2)$$

This equation can be modified to relate the work of adhesion with the contact angle and liquid surface tension by introducing Young's model, which leads to Young-Dupré equation (2.3) for work of adhesion[68]:

$$W_a = \gamma_{lv}(1 + \cos \theta_e) \qquad (2.3)$$

Figure 2.2: Equilibrium contact angle (θ_e) and three-phase interfacial tensions (γ_{sv}, γ_{sl}, γ_{lv}) according to Young's model. Figure was redrawn from Grundke et al.[69]

2.4.2.1 Effect of Surface Topography and Chemical Composition on Surface Wettability

Although the wetting behaviour of a liquid on solid surface is commonly characterised through Young's model by measuring the static contact angle, this approach is only valid when the solid surface is consistent regarding chemical uniformity and surface smoothness. However, solid surface characteristics are highly dependent on the surface topography and chemical heterogeneity of a solid surface. Most surfaces of real-world solid materials are non-ideal exhibiting a degree of roughness or chemical non-uniformity, which affect the contact angle in the thermodynamic equilibrium. Therefore, the surface chemical composition and roughness are considered when studying the wettability and surface energy of non-ideal solid surfaces.[68,69,76] The surface free energy of non-ideal solid surfaces is determined by measuring the apparent contact angle in thermodynamic equilibrium. This angle may deviate from the Young's contact angle (θ) on an ideal surface due to the effect of surface roughness or chemical heterogeneity. Wenzel determined the correlation between the apparent/Wenzel contact angle (θ_w) on a rough surface and Young's contact angle on corresponding ideal surface.[86,87] This was based on using roughness factor (r_w) to include the effect of surface roughness in Young's model. The surface roughness was found to influence the surface energy of solid surface and interfacial tension between solid and liquid materials. The roughness factor represents the ratio of rough surface area to the

equivalent smooth surface area, and it can be embedded in Young's model as shown in equation (2.4)[69]:

$$r_w(\gamma_{sv} - \gamma_{sl}) = \gamma_{lv}\cos\theta_w \qquad (2.4)$$

The apparent/Wenzel contact angle on the non-ideal rough surface can also be estimated from the Young's contact angle and roughness factor as shown in Wenzel equation (2.5)[69]:

$$\cos\theta_w = r_w\cos\theta \qquad r_w > 1 \qquad (2.5)$$

The roughness parameter r_w in Wenzel equation >1 reflecting that rough surface has a larger contacting surface than the corresponding smooth geometric surface. Consequently, the surface roughness has a considerable impact on the apparent surface wettability leading to an increase in the magnitude of the wetting or non-wetting (repellency) of solid surfaces. This is observed in the decrease in measured contact angle on rougher surfaces with intrinsic contact angles < 90° that exhibit improvements in the wetting and spreading behaviours. On the contrary, any increase in roughness of hydrophobic surfaces with intrinsic contact angles > 90° results in higher contact angles and improved surface repellency.[69].

Surface wettability is also influenced by the chemical heterogeneity of solid surfaces. The effect of heterogeneous surface was described by Cassie, who defined the contact angle on a solid surface with two different chemical components. The overall apparent contact angle (θ_c) according to Cassie was found to be dependent on the proportion of each surface component and corresponding to local contact angle on each surface component as shown in the Cassie equation (2.6)[68]:

$$\cos\theta_c = P_1\cos\theta_1 + P_2\cos\theta_2 \qquad (2.6)$$

where P_1 is the fractional area of the component 1 of surface with its local contact angle θ_1, P_2 is the fractional area of the component 2 of surface with its local contact angle θ_2.[68]

The heterogeneous solid surfaces (chemically or topographically) can show various apparent contact angles with mechanical stabilities of a deposited liquid drop. The apparent contact angle can take a range of contact angle values as the liquid drop tends to advance or retract from its position in equilibrium. Therefore, a contact angle hysteresis phenomenon can be used to reflect the effect of surface heterogeneity on

these dynamic contact angles and wettability of solid surfaces. The hysteresis induces pinning to a liquid drop as it advances on non-ideal solid surface towards new non-wetted surface. This causes increases in the contact angles of advancing drop sides until reaching a maximum value. On the other hand, the liquid drop boundary can be pinned when the drop side is retracting leading to decreases in the contact angle until reaching a minimum value. These maximum and minimum values of apparent contact angles are the characteristic advancing (θ_a) and receding (θ_r) angles respectively. The difference between these extreme angles determines contact angle hysteresis ($\Delta\theta$), which arises from the deviation from the ideal smooth and uniform solid surface as given by the equation (2.7)[68,69]:

$$\Delta\theta = \theta_a - \theta_r \qquad (2.7)$$

Contact angle hysteresis is determined by measuring the advancing and receding angles of a liquid drop using dynamic measuring methods. These include contact angle measurements when increasing and decreasing the volume of the sessile drop or using a tilting plate.[88]

The effect of surface roughness on contact angle hysteresis is crucial in characterising the solid surface wettability and it was first studied by Johnson et al.[89] It has been demonstrated that contact angle hysteresis for rough surfaces increases with the degree of roughness as the advancing contact angle becomes larger and receding contact angle becomes smaller. The increase in surface roughness can induce a capillary effect when it reaches a specific degree depending on the geometrical topography. The resulting capillary forces facilitate liquid wicking into the confined surface grooves and features when the Young's contact angle < 90°. This leads to a reduction in advancing contact angles, thus improving the surface wettability. However, the hydrophobic rough surface with Young's contact angle > 90° will resist the liquid wicking into the structural surface grooves converting the homogeneous rough surface into heterogeneous composite of solid surface and air fractions. This surface configuration occurs due to the air trapped in the surface pores and features that results in a dramatic reduction in surface energy and contact angle hysteresis of the surface as reported by Grundke et al.[69] Therefore, the rough surface can be tuned from homogeneous state described by Wenzel model to heterogeneous state described by air-rough surface composite that is called Cassie-Baxter model as shown in equation (2.8)[90]:

$$\cos \theta_{cb} = P_{sl} (\cos \theta_{sl} + 1) - 1 \qquad (2.8)$$

where θ_{cb} is the total contact angle according to Cassie-Baxter model, P_{sl} is proportion area of contacting liquid drop with solid surface, θ_{sl} is local contact angle of liquid drop on solid surface proportion. This is a special case of Cassie model where the solid surface and air phase represent the two heterogeneous material fractions with different wetting characteristics (complete non-wetting of liquid drop with air proportion, θ = 180°).[90]

2.4.2.2 Exploitation of Surface Wetting Phenomena

Inspired by the natural biological systems, engineered surfaces with special wettability, such as super-repellent surfaces and superhydrophilic surfaces, various functional surfaces have been developed for different technological applications. Synthesis of surfaces with desired wetting properties depends on both surface chemistry and topography.[70] Self-cleaning and water repellency are among the common applications of surface wettability, particularly for fabrics and textiles industry. Surface modification of the fibrous structure of textiles is used to impart superhydrophobic properties, hence self-cleaning functionality. This includes applying a hydrophobic coating onto the textiles, such as silicone coating.[91] Separation of oily components from water is another wettability-based approach for water recovery in industries, such as food and pharmaceuticals, or oil spills remedy in oceans. This involves different techniques including the use of porous polymeric materials (sponges) and filters. These are based on manufacturing materials with affinity for oils (oleophilic) and water repellency (superhydrophobic) that provide micropores permeable to oils and impermeable to water.[70,92] Wettability manipulation was also used to reduce friction resistance in microchannels and develop smart microfluidic devices to perform sample dosing, separation and analysis.[93,94] The advances in surface engineering and functionalisation of solid materials led to many other applications of wettability, such as Biofouling control, fog collection system, antifogging surfaces and water desalination.[70,95]

The wettability also has its applications in food packaging. Surface wettability modification of plastic packaging waste is an important approach in separating different polymer materials prior to recycling process. The separation process is based on adjusting the wettability of mixed polymers. Thus, polymers with varied surface

wettability exhibit different floating behaviours. This technique was applied to mixed PET and polyvinyl chloride (PVC) parts as the main components of plastic bottles used in soft drink industry. The PET could be isolated from PVC by inducing the hydrophilicity on one polymer while the hydrophobicity of the other polymer was maintained. Another application of wettability on food packaging showed that the improved wettability of plastic packaging surfaces increased the rate of biological degradation by microbial colonisation. This was proved for low-density polyethylene (LDPE) treated with corona technology.[68] Antifogging functionality of plastic food packaging is fundamentally dependent on the surface wettability of packaging films. One of the common approaches to impart antifogging properties is the increase in wettability of film packaging surface. Previous antifog LDPE surface was manufactured by the application of hydrophilic pullulan coating, leading to a decrease in WCA from 89.2° to ~24°. The improved wettability of LDPE film allowed for antifog plastic film suitable for food packaging applications.[96] Therefore, the design of plastic packaging with varied wetting properties can provide different surface functionalities desired for food packaging applications.

2.5 Capillarity and Capillary Valving Phenomena

Capillarity and capillary valving are among the most common phenomena based on wettability and surface tension. Liquid flow and retention can be effectively controlled by capillary features and valves. Therefore, capillary-based techniques can be developed and incorporated into the plastic food packaging to allow mechanisms of liquid retention within the bulk or surface of packaging itself.

2.5.1 Capillarity Phenomenon

Capillary-induced wetting (capillarity phenomenon) is a ubiquitous process in nature for transport of water in soil and plants.[80] Capillarity is based on the wettability phenomena and fundamentally depends on liquid surface tension and wetting properties of a solid surface, which can be used to develop new technologies for liquid isolation and liquid flow management within the food packaging. The capillarity accounts for the unique spreading of a liquid on a tilted surface against the pulling effect of gravity, and liquid rising or retracting in a thin tube connected with a liquid reservoir. As liquid wets a vertical or tilted solid surface, it can rise over the wetted surface forming a meniscus due to the acting negative Laplace pressure. This capillary pressure is induced

by interplayed cohesive forces of the wetting liquid with adhesive forces on liquid/solid interface.[71,80] Therefore, capillary forces are generated to drive the liquid meniscus for a certain height (z) until the hydrostatic pressure balances Laplace pressure in equilibrium as shown in equation (2.9):

$$P_o + \frac{\gamma}{R} = P_o - \rho g z \qquad (2.9)$$

where P_o is atmospheric pressure, γ is liquid surface tension, R^{-1} is meniscus curvature of liquid, ρ is liquid density, g is gravity acceleration.[71,80]

The liquid spreading and rising tend to minimise the free energy on the contact line of solid, liquid and air interfaces.[97] Liquid rise and flow in a confined thin tube is one of the most common applications of capillarity where a liquid can spontaneously transit into the tube space. This phenomenon is observed when the capillary tube with small radius is connected to a wetting liquid reservoir, and a differential pressure called Laplace pressure (capillary pressure) is induced by the gradient energy between the interfaces of liquid/solid (wetted region) and air/solid (dry region). This pressure allows pulling capillary forces within the confined tube to drive the liquid to spread on the capillary walls while the cohesion forces of the liquid raise the rest of the liquid mass leading to a liquid column with a curved meniscus. The rise of liquid meniscus in a confined tube differs from the case observed on a tilted flat surface as the meniscus is boosted by the tube curvature.[71,80,98] The Laplace pressure/capillary pressure (ΔP_c) is described by Young-Laplace equation (2.10) for a capillary tube:

$$\Delta P_c = \gamma\left(\frac{1}{R_1} + \frac{1}{R_2}\right) \qquad (2.10)$$

where R_1 and R_2 are principal curvature radii of rising meniscus. For circular capillary tube with radius (r), $R_1 = R_2 = r/\cos\theta$ where θ is meniscus contact angle with tube wall. Therefore, Laplace pressure depends on the contact angle as described in equation (2.11)[99,100]:

$$\Delta P_c = \frac{2\gamma\cos\theta}{r} \qquad (2.11)$$

This pressure gives the liquid meniscus a curved shape and drives the liquid within the capillary tube. The rising liquid experiences an increase in the hydrostatic pressure during liquid transit (imbibition) process due to the increase in liquid column weight as

illustrated in Figure 2.3. The liquid reaches a certain height when the driving Laplace pressure is balanced with the hydrostatic pressure (ΔP_h) in equilibrium, which is given by equation (2.12)[71,101]:

$$\Delta P_h = \rho g h_e \qquad (2.12)$$

where ρ is liquid density, g is gravity acceleration, h_e is height of liquid column in equilibrium.

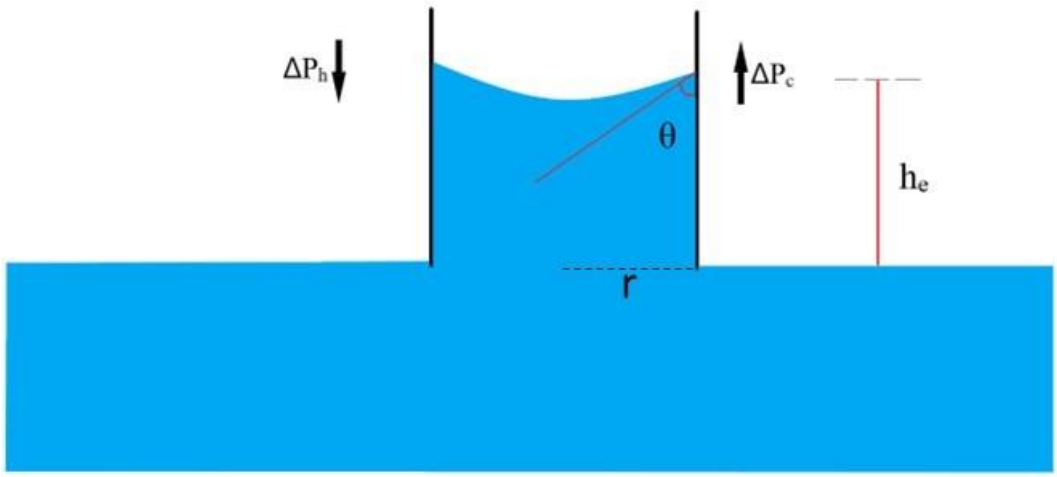

Figure 2.3: Sketch of capillary liquid rise within capillary circular tube with radius (r); equilibrium liquid height (h_e), hydrostatic pressure (ΔP_h), capillary pressure (ΔP_c). Figure was redrawn from Yifan et al.[71]

The dynamic flow of the rising liquid in capillarity is influenced by different forces acting on the meniscus during transit process. These forces include driving capillary force with viscous, gravitational and inertial forces. Lucas-Washburn (L-W) model was an early analysis of liquid flow in a capillarity.[102] It considers a horizontal flow in tube with radius (r) and dominant Poiseuille law for velocity gradient in adjacent liquid layers. The model explained the liquid transit based on a constant contact angle (θ) and under the influence of only driving capillary force against frictional and gravitational forces. This model shows that the liquid meniscus flows to lengths along the capillarity in proportion to the square root of time (t) as described in equation (2.13)[103,104]:

$$h^2 = \frac{\gamma r \cos\theta}{2\eta} t \qquad (2.13)$$

where h is liquid height at time (t) in capillary tube, η is liquid viscosity.

(L-W) model also explained the major mechanism of rising liquid in vertical capillaries under normal gravity, while the effect of gravity and inertial forces on liquid flow kinetics was not considered. These forces have a significant effect on flow dynamics, particularly over a short time scale. Further, the liquid dynamic flow involves generating a dynamic contact angle that is higher than the static angle and proportionate with liquid flow speed. This was manifested in the deviation of the initial stage of liquid flow process from the model of (L-W) law.[102,105] A number of researchers have studied the capillary liquid flow in tubes under different conditions to include more parameters governing the kinetics of rising liquid in capillarity, such as inertial forces and dynamic contact angle.[102,104,106] In equilibrium conditions, capillary force and gravitational force are the only balanced forces as the other forces diminish. This corresponds to the balanced Laplace and hydrostatic pressure. This enables to extrapolate equilibrium liquid height (h_e) inside circular tube that is vertically oriented as shown in equation (2.14)[99]:

$$h_e = \frac{2\gamma\cos\theta}{\rho g r} \qquad (2.14)$$

Therefore, liquid surface tension, surface wettability and size of the capillarity are the key parameters governing the driving capillary force and equilibrium liquid height under normal gravity.[98,99,107] Various studies investigated the influence of these parameters on liquid rise in capillarity. Capillary force is positively proportionate to the liquid surface tension as reported by a previous study,[108] showing an increase in water height (γ: 72 mN/m) of three times that of surfactant solutions (γ: 23 mN/m) within a capillarity of the same size. The study findings also showed a decrease in the height of surfactant solutions with an increase in diameter of the capillary tube.[108] This was in line with another study on the increase in height of imbibed liquids in capillary tubes for smaller radii.[102] The contact angle of a liquid with capillarity walls has a considerable effect on liquid rise height in equilibrium. The contact angle reflects the interaction between capillarity surface and rising liquid. It was found that a lower liquid contact angle on capillarity surface improved the capillary force and increased the liquid height.[102,109] A further factor affecting liquid rise height is the inclination of the capillarity. Barozzi et al.[107] investigated the effect of inclination angle of a capillary tube on the liquid rise heigh. It was reported that tube inclination reduced the impact of gravitational forces acting on rising meniscus. The study involved inclination

angle (β) in the range of 0-88° from the vertical, showing longer liquid extension (L_β) along the capillary tube with the increase in inclination angles as predicted from the theoretical model in equation (2.15)[107]:

$$L_\beta = \frac{H_\beta}{\cos \beta} \qquad (2.15)$$

where H_β is liquid height in capillary tube inclined at angle of β.

2.5.2 Capillary Valving Phenomenon

Capillary valves are an abrupt change in the dimensions or surface wettability of a capillarity which exploit the capillary forces to restrict liquid motion. These valves can be introduced to the food packaging by a special design or surface treatment to enable liquid retention within the packaging itself. The liquid retention and flow can be controlled in capillary channels and features under the effect of capillary forces.[110] The capillary forces govern liquid flow and behaviour in the capillary systems where these forces are magnified in comparison with existing body forces.[80,82] Valving functionality is usually introduced to use the capillary forces in liquid retention and flow control by using passive stop valves in capillary systems and channels.[110,111] These capillary valves are mostly used in micro-sizes and divided into geometrical valves and wetting-based variation valves, which generate a pressure barrier to retain liquids.[112–114] The working principles of valving functionality are based on inducing liquid pinning at the sudden change in geometrical dimensions or surface wettability of a capillary channel. This allows liquid to form a specific pressure barrier preventing liquid flow. Therefore, any increases in the air/liquid interfacial area result in rises in the pressure barrier until reaching a maximum value that is called burst pressure.[113] The use of capillary valves is very common in liquid flow control due to their low cost, simple design, easy fabrication and good anti-clogging properties.[112,115] Capillary passive valves are widely used for liquid manipulation and flow control in various technological applications in biology and chemistry, such as sample handling and analysis in microfluidic devices, liquid micropump and drug delivery.[112,116] Therefore, the functionality of capillary valves can be exploited to improve the liquid retention of recesses of extended sizes that can be integrated into plastic meat trays as a solution for self-isolation of meat exudates.

2.5.2.1 Capillary Geometrical Valves

The geometrical passive valves are a sudden expansion/enlargement in the capillary geometry, where the liquid can be pinned on the diverging capillary walls.[113] The liquid on the passive valve expands and adapts to the geometrical expansion. This induces a liquid pinning effect on the valve walls and generates a capillary pressure barrier to prevent the liquid flow.[113,115,117] For a micro-sized capillary channel with circular cross-section that ends up with a sudden expansion with an opening angle (ω), a liquid forms a contact angle (θ_e) with internal channel wall surface in equilibrium, exhibiting capillary pressure (Laplace pressure) given in equation (2.11). As an external pressure acting on the liquid, the liquid meniscus will be pinned on the valve walls restricting the liquid advancement. Further increases in the external pressure will make the liquid meniscus bulge outwardly forming a convex shape and reducing its radius of curvature. The liquid meniscus will be maintained pinned until the contact angle reaches the maximum advanced angle (θ_a) on the valve walls (Figure 2.4). This corresponds to a maximum pressure barrier on the capillary valve before the liquid can advance and flow. This pressure is called valve burst pressure (ΔP_{gv}) as given by equation (2.16)[113,118]:

$$\Delta P_{gv} = \frac{2\gamma \cos(\theta_a + \omega)}{r} \qquad (2.16)$$

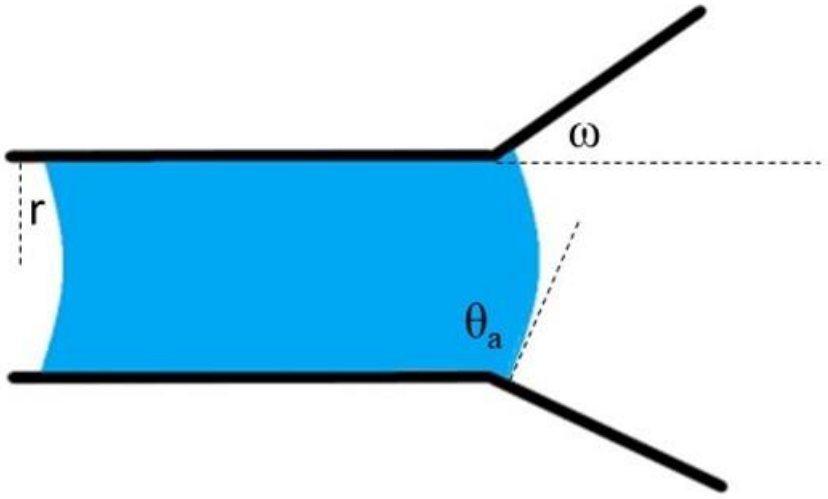

Figure 2.4: Sketch of capillary geometrical valve with opening angle (ω) on a capillary channel with radius (r); θ_a is advanced liquid angle on valve wall. Figure was redrawn from Cho et al.[113]

Various studies investigated the mechanism and functionality of capillary valves to control liquid flow in microfluidic systems.[110,113,118] The burst pressure barrier is the defining feature of geometrical passive valves, and it allows to determine the force needed to overcome the pressure barrier of a certain valve. This pressure is fundamentally governed by different parameters including liquid surface tension, valve opening angle, capillarity size and surface wettability. The magnitude of the pressure barrier increases for liquids with higher surface tensions as reported in previous works.[110,113,118] Other studies found that increases in the size or diameter of the capillary channel led to reductions in the resulting pressure barrier of geometrical passive valves.[111,115] The surface wettability of the walls of a geometrical valve has an impact on the valve pressure barrier. For high surface wettability of valve walls, the valve exhibits a low pressure barrier. This was demonstrated in the research work of Kazemzadeh et al.[119] who studied the effects of capillary surface wettability on liquid burst from a capillary channel at different water contact angles. The capillary channel and valve walls with contact angle of 60° had a convex liquid meniscus on the valve walls with high burst pressure barrier, while the meniscus had concave shape with lower burst pressure barrier for lower contact angle of 20°. This is due to the substantial increase in adhesive forces on the wall surface of capillary valves. These adhesive forces are large on highly hydrophilic surfaces and compete with the cohesive forces on advanced liquid curvature leading to reduced pressure barrier.[119]

The pressure barrier of a geometrical passive valve depends on the expansion valve angle. Valves with larger opening angles result in higher burst pressures. The highest burst pressure of a valve with a specific diameter is attained when the sum of its opening angle and advanced contact angle ($\omega + \theta_a$) $\geqslant$180°.[110,120] Therefore, flow control of highly wetting liquids entails designing capillary valves with very large opening angles to ensure a sufficient pressure barrier.[121] The impact of valve opening angle on the burst pressure barrier was investigated and demonstrated in other studies on capillary passive valves.[111,117] The sharpness of valve opening angle has also a significant effect on the pressure barrier as round opening angles cause gradual increases in the capillary size. This reduces the burst pressure experienced by a liquid on the valve expansion in comparison with a corresponding valve with a sharp opening angle.[113] Capillary valves with round or flat expansion edges (e.g. open end of a capillary tube)

exhibit lower pressure barrier with the increase in their edge width as reported by a previous work.[121]

2.5.2.2 Capillary Wetting-Based Variation Valves

Capillary valves based on surface wetting variation are designed with a sudden change in the wetting properties of a capillary channel.[113] These valves are also called hydrophobic passive valves and can be fabricated by applying a hydrophobic material layer to make patterns on hydrophilic capillary walls.[114,118] The valving functionality is attributed to the pinning of liquid meniscus on the hydrophobic surface introduced to a capillary channel providing the contact angle > 90°. The increase in hydrophobicity of capillary channel walls to fabricate a burst valve can vary from hydrophobic to superhydrophobic surfaces. The sudden change in the surface wetting properties of a capillary channel requires the liquid meniscus to adapt new hydrophobic surface, creating larger contact angle (Figure 2.5). Therefore, the liquid meniscus can generate a pressure barrier restricting the liquid flow or drainage. The valve burst pressure (ΔP_{hv}) that can be achieved for a hydrophobic micro-sized channel with circular cross-section is given in equation (2.17):

$$\Delta P_{hv} = \frac{2\gamma \cos(\theta_a)}{r} \qquad (2.17)$$

where θ_a is the advanced contact angle of liquid on the hydrophobic wall surface.[112–114,122]

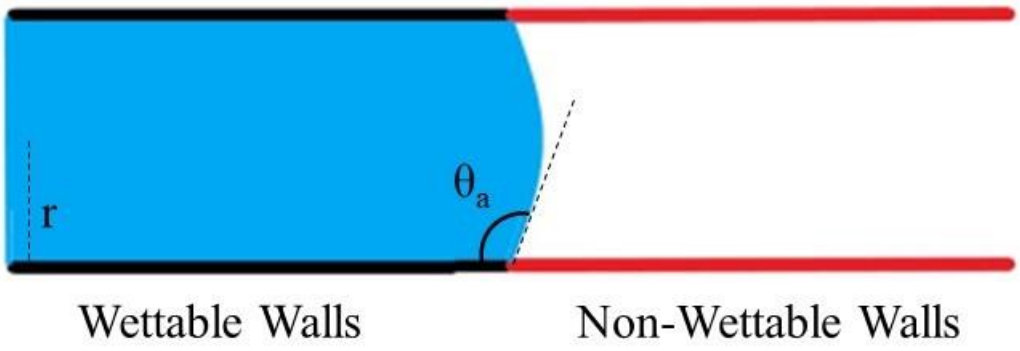

Figure 2.5: Sketch of capillary valve based on wetting variation on a capillary circular channel with radius (r); wettable (hydrophilic) capillary walls vs non-wettable (hydrophobic) capillary walls, θ_a is advanced contact angle on non-wettable wall surface. Figure was redrawn from Feng et al.[114]

The maximum pressure barrier of wetting-based variation (hydrophobic) valves is governed by key parameters comparable to the geometrical valves. These include liquid surface tension, valve dimensions and liquid contact angle on valve wall surface. Smaller sizes of hydrophobic valves lead to increases in the resulting pressure barrier as reported in previous work.[123] However, there is another type of hydrophobic valve used in microfluidic systems that is based on narrowing the hydrophobic capillary channel to allow higher pressure barrier.[114] A sudden enlargement can also be introduced to hydrophobic capillary channels to improve the valving functionality and pressure barrier.[123]

2.6 Liquid Retention and Drainage in Capillarity

The use of capillarity to contain exuded liquids in confined spaces within the food packaging is an effective approach to isolate the liquid/exudate from packaged product. Various means were explored for getting liquid into capillarity, such as recesses and pores. However, liquid must be retained in place and prevented from drainage during handling the food packaging. This requires introducing technologies to trap the liquid inside the capillarity, such as capillary valves. The liquid retention and drainage are common phenomena occurring in nature and have a particular importance in capillary systems for their various technological and industrial applications, such as transfer processes of chemicals. Drainage of a liquid in a closed capillarity with open end (capillary tube, container with capillary orifice) can be initiated as the capillarity is inclined. The mechanism of liquid drainage from the open end of a vertically oriented tube is based on the Taylor finger phenomenon. This involves the formation of an air finger that propagates into the unstable liquid-air interface at the open side of the tube, replacing the liquid with air.[124] Hence, the liquid flows forming a film over the tube walls and drains out of the tube under the influence of gravitational and capillary forces.[124–126]

Liquid drainage and retention in closed capillary systems with open bottom ends were studied during vertical orientation and inclination by different researchers.[125–127] The stability of the liquid meniscus is crucial for liquid retention inside a capillarity. The liquid meniscus within an inclined capillary tube undergoes atmospheric pressure acting upwardly against a hydrostatic pressure in addition to the capillary pressure. Therefore, stable liquid menisci in inclined tubes allow the dominant

atmospheric pressure to maintain the liquid trapped inside the tube cavity while unstable menisci are prone to air finger propagation.[125,126] The capillary pressure largely influences the stability of liquid meniscus within an inclined capillary tube or channel. As tube openings are assumed to have capillary valving functionality, the capillary pressure can also generate a pressure barrier strengthening the meniscus stability and liquid pinning effect.[120] This pressure was sufficiently strong for capillary tubes of small sizes (diameter $\leq$ 9.7 mm) to produce stable meniscus and prevent water drainage as described by Extrand.[125] However, liquid menisci were less stable for larger sizes of the capillary tubes and lower surface tension liquids resulting in water drainage.[125] A comparable study on liquid retention and drainage reported that very low surface tension liquids and large-sized capillary tubes led to easily initiated liquid drainage as the energy required to generate air finger was minimised.[126] Liquid menisci with reduced stability can exhibit sinusoidal shapes as an outward bulge is expressed on one side with increased local hydrostatic pressure. The other side shows inward curvature with reduced local hydrostatic pressure. The bulge side of the liquid menisci tends to pin on the opening edge of tube or orifice generating a pressure barrier against the local hydrostatic pressure.[125,127] It was found by Extrand[125] that liquid maintains trapped in a vertical capillary tube providing the pressure barrier is higher than the local hydrostatic pressure acting on the meniscus. The pressure barrier prevents the liquid meniscus from advancing on the opening edge to impede the liquid drainage. This improves the pinning of the liquid meniscus on the tube opening giving the meniscus more stability and preventing propagation of the air finger.[125] Liquid drainage and retention phenomena also occur for liquid in relatively large capillary tubes and orifices during the inclination process where the meniscus presents advancing bulge and receding curvature. Liquid drainage is initiated when the growing hydrostatic pressure on bulge side of meniscus becomes higher than the pressure barrier as reported in another study.[127] Therefore, capillary valving functionality is essential for enhancing liquid retention and restricting the mechanism of liquid drainage.[120]

2.7 Liquid Uptake into Porous Materials

Porous materials are microstructural composites, contributing to various natural and industrial applications due to their structural characteristics of adequate rigidity and low density. These materials contain micropores, which can act as capillary features with

capability to suck and retain wetting liquids. Therefore, porous materials can be explored to absorb and trap liquid/exudate inside the food packaging. These materials are commonly observed in nature or synthesised from different materials, such as ceramic, metals and polymers that can be used for applications of heat and sound insulation, porous electrodes, bioengineering, liquid filtration and packaging. The porous materials are formed of continuous solid phase with pores occupied with gas or liquid.[128–131] Surface chemistry and structural characteristics of porous materials, such as pore size, porosity and interconnectivity of pores are the most crucial properties responsible for their capacities to absorb liquids.[132,133] Porous material structures with small-sized pores behaving as capillaries, exhibit liquid penetration and wicking when they are in contact with wetting liquids.[134] The characterisation of liquid penetration into a porous structure is important for porous materials, such as foam and fibrous sheets for applications of liquid absorption.[135] The liquid penetration is a capillary suction process of a liquid into porous materials under the effect of capillary pressure acting at the pores.[136,137] This capillary pressure is called displacement or entry pressure as previously described in the Young-Laplace equation (2.11) for a circular capillary tube, considering the radius of pore is (r).

The liquid can wick into the pore space when it wets the pore surface and forms a contact angle smaller than 90°. The capillary pressure and liquid penetration are governed by liquid surface tension, size and wettability of the pores.[133,134] The liquid is driven by capillary forces generated by the difference in surface energy between the wet and dry interfaces of porous material as the wicking liquid wets the pore surfaces.[136,137] Liquid penetration and wicking through porous media are complex phenomena due to irregular morphology and varying sizes of the pores.[138] Equivalent/effective pore radius (r_e) is usually estimated to determine the capillary pressure and model liquid flow across porous structures. Therefore, the corresponding capillary pressure (ΔP_c) can be described in equation (2.18)[137]:

$$\Delta P_c = \frac{2\gamma \cos\theta}{r_e} \qquad (2.18)$$

The liquid penetration involves displacement of the penetrating liquid to the fluid inside the pore space and flow of the liquid behind its front advancing meniscus.[134] The complex geometry of porous media has a significant blocking effect on the liquid wicking due to the induced geometrical hysteresis. As the penetration distance by a

wetting liquid is limited by the widest pore, the penetration distance decreases with an increase in the pore radius.[105] On the other hand, the kinetics of liquid wicking inside porous materials are governed by different forces of capillary, gravity, viscosity and inertia.[139,140] The liquid flow during wicking in the porous materials is commonly considered laminar, where the inertial forces are minimal in comparison with the influence of capillary forces and viscosity,[141] thus the effect of inertial forces on liquid flow can be neglected due to the small size of pores and prevalence of viscous forces.[142] Although porous materials are attributed to their complex porous structure and irregular shapes and sizes of pores, various models have been developed to characterising the liquid flow and wicking inside porous media.[141] These models considered liquid flow in a porous structure to be similar to uniform and parallel capillary tubes as in the Lucas-Washburn model, or capillary tube with alternating cells and throats as in the sinusoidal model. Another model based on Darcy Law considered the relationship between the liquid wicking speed and corresponding pressure gradient exhibited across the porous material.[135,137]

2.7.1 Open-Cell Polymeric Foam

Liquid uptake into the open-cell polymeric foam will be studied as a type of porous materials. Polymeric foams are porous or expanded polymers with a structure of cellular composite that contains gas phase distributed in solid polymer matrix.[63] These foams have complex and irregular microstructure, which are classified into two types including open-cell foam and closed-cell foam.[143] The polymeric foam with open cells is attributed to high permeability to fluids with a network of highly interconnected gas cells and compartments with pores on the cellular walls, while closed-cell foam contains isolated gas cells as their pores covered with polymeric membranes.[130,144,145]

Polymeric foams can be produced through different foaming processes, such as extrusion and injection moulding. The foaming process involves introduction of a blowing agent into the polymeric melt under pre-determined foaming conditions of temperature and pressure.[146] The blowing agent can be a chemical organic compound that decomposes at high temperature generating a gas, such as Azodicarbonamide, or physical agent, such as CO_2.[147,148] Various polymers can be foamed, such as PS, PET and PP, and the open-cell structure of polymeric foams are

often achieved at high foaming temperatures.[146,148,149] Open-cell polymeric foams are desired for their high porosity, fluid permeability and light weight required for applications, such as liquid filtration and absorption, drug delivery systems, energy and sound absorption.[92,145,150]

2.7.1.1 Liquid Uptake of Open-Cell Polymeric Foam

Open-cell foams are widely used as a liquid absorber of sucking and retention of oil, food residues and liquid wastes for applications of water purification, remediation of oil spills and liquid isolation within food packaging.[133,143,151,152] Liquids are penetrated and wicked into the cellular foam structure, similarly to other porous materials, under the influence of the driving Laplace pressure as given by Young-Laplace equation (2.11). Therefore, a reduction in pore size and increase in wettability of the pore surface increases the capillary pressure across the foam pore. Liquids with higher surface tensions also exhibit larger capillary pressures and improved liquid penetration when the liquids wet the pore walls. The liquid absorption performance of polymeric foams can be enhanced by modifying their pore surfaces to be more hydrophilic or hydrophobic depending on the liquid characteristics and application.[133,151] Liquid uptake capacity of open-cell foams depends on different foam structural properties. This includes foam density, open-cell content, porosity and pore size.[151] Lower foam densities lead to formation of larger foam cells with thinner walls that increases their liquid absorption capacity.[153,154] Open-cell content is an important characteristic parameter for liquid uptake as it represents the foam interconnectivity and structure accessible to the liquid.[63] This was manifested in the increased oil uptake of polyurethane foam with higher open-cell content.[154] Pore size also governs the liquid uptake capacity with a direct impact on the driving capillary pressure. The reduced pore size of polyurethane foam led to higher oil uptake capacities as reported by a study.[133] The surface wettability of foam pores is crucial in liquid penetration and absorption. Lower surface wettability of the pores results in a decrease in the liquid uptake capacity and magnifies the impact of geometrical hysteresis.[105]

The wettability of foam pores can be increased by the application of a surface modification treatment, such as plasma treatment and polymer grafting.[155,156] Open-cell polyurethane foams showed high oil uptake capacity and oil/water separation attributed to their superhydrophobicity and superoleophilicity.[155] Wetting agents can

be added to enhance the pore wettability of polymeric foams, facilitating liquid absorption as used in absorbent polymeric trays for food packaging.[152] However, these chemical wetting agents (surfactants) might accumulate in the environment and food chain at high concentrations, introducing potentially toxic effects.[157,158]

2.8 Surface Modification of Polymers

The surface properties of polymers are not always well suited for their end application. Polymeric surfaces exhibit low polarity and surface energy due to the lack of polar groups. This results in poor wettability of polymers, particularly towards water-based liquids, hence polymers may not be suitable for applications based on wettability and capillarity. Polymer surfaces undergo various surface treatments to modify their characteristics for different industrial applications. These treatments target the surface of polymer bulk by introducing functional chemical groups to impart new surface characteristics desired for the polymer product applications.[4,76,159,160] Surface modification treatments of the polymers are advantageous over the bulk treatments for targeting only the outer layer of the polymer structure, maintaining the bulk properties of polymeric materials. These surface treatments are economical, functionalising the surface of polymers to be compatible with different applications without the need to re-shape or manufacture the polymers again.[161]

Polymeric materials can be surface treated for improving their surface properties to suit different applications, such as wettability, adhesive and sealing properties, dyeing, and barrier characteristics.[160,162] One of the common methods of surface modification treatments is to increase surface free energy and wettability of polymeric surfaces by introducing polar functionality, such as oxygen-containing groups to the treated surfaces. This can be achieved by oxygen plasma surface treatment as wettability improvement is particularly crucial for polymers due to their poor polarity and surfaces energy, which restrict the use of polymers for adhesion-based applications.[4,76] On the other hand, polymeric surfaces can be functionalised with more hydrophobic materials, such as silicones and hydrocarbons to further reduce their surface free energy and increase their hydrophobicity. This reduction in wettability is widely used to induce liquid-repellent properties that are used in self-cleaning and anti-fogging applications.[163–165] There are various surface treatment techniques and methods to functionalise and modify polymer surfaces. This includes physical,

chemical and biological treatment approaches.[160,162] Physical methods of surface modification are well suited for functionalisation of polymeric surfaces as these treatments are inexpensive, consistent, scalable with low environmental impact and produce no hazardous chemical waste.[162,166] Physical surface modification methods include various techniques, such as plasma, corona, UV and flame surface treatments that can be used to modify and functionalise the polymer surfaces for different applications.[160,162]

2.8.1 Plasma Surface Treatment of Polymers

Plasma treatment is widely adopted for modification techniques of the polymer surfaces as it can alter the surface hardness, wettability, roughness and improve the adhesion of the treated polymers.[167,168] It is advantageous surface treatment for its desired properties when compared with other physical and chemical treatments.[160] Plasma treatment is environmentally safe, inexpensive and suitable for surface modification of three-dimensional products and polymers with heat sensitivity. It is also a uniform treatment maintaining the bulk characteristics and modifying only the outer surface to a depth range of 0.05-0.005 μm.[159,169,170]

Plasma treatments are classified into thermal and non-thermal types. While the thermal plasma is attributed to very high temperatures, the non-thermal plasma provides excited gases with low temperature and usually called cold plasma. Non-thermal plasma is the more common treatment for surface modification of polymers,[162] and can be categorised into different types based on the working gas, pressure and discharge power. Different gases can be used with the plasma treatment, such as oxygen, nitrogen, hydrogen and air and the plasma glow can be generated under low or atmospheric pressures. Although the low-pressure plasma operates at vacuum with high uniformity and stability, it suffers from the high cost of vacuum equipment and process complexity. This has led to a preference for atmospheric-pressure plasma, which avoids the need for vacuum equipment thus ensuring lower operational costs and facilitating more readily the incorporation of plasma units into production lines. For the discharge power, plasma can be based on direct current (DC) or alternating current (AC). Polymer surfaces are commonly treated by plasma with (AC) discharge due to high efficiency and uniformity. The AC discharge plasma can operate on a wide range of frequencies, which involve radio frequency (kHz) to microwave frequency (GHz).[168,169,171]

2.8.1.1 Plasma Generation and Working Principles

Plasma glow is generated by ionising the molecules of a supplied working gas under the influence of an electric field. The plasma consists of a very reactive gaseous mixture of positively and negatively charged ions, electrons and excited gas molecules with UV irradiation. Neutral and charged oxygen molecules can be found in the oxygen plasma, such as O, O_2^+, O^- and O_2^-.[169,172] The overall plasma is neutral as the quantity of positively and negatively charged species are equal. These charged gas molecules undergo collision with other gas particles within the plasma glow. The charged and non-charged gas particles of the plasma are very reactive and consequently interact with the exposed polymer surface leading to the modification of the polymer surface chemistry and morphology.[169,173] For low-pressure plasma, the electrons in gaseous plasma move faster than other ions and excited species and tend to collide and interact with the polymer surface. This results in generation of an electric potential between the plasma and exposed surface, which works as a driving force to attract the positively charged molecules to the polymer surface so that their interaction rate can reach 100%. Neutral plasma species are also able to interact with the solid surface due to their predominantly random movements.[169] These reactive species with enough potential energy are able to activate the surface and break down the chemical bonds.[174]

Plasma treatment can induce changes in the surface properties of polymers by different mechanisms including etching, crosslinking and polymerisation with chemical modification. Polymer characteristics, working gas composition and process parameters, such as working pressure, discharge power and treatment time determine the prevalent mechanism during the plasma treatment.[167,168,175] Oxygen plasma has widely been used for surface functionalisation of polymers and such treatment usually results in an increase in the oxygen content and surface hydrophilicity of the treated polymer surface. The functionalisation process involves different interactions between the excited plasma species and polymer surface. These interactions are initiated with scission of polymer chains and hydrogen abstraction by the highly reactive oxygen plasma species, such as radical oxygen and hydroxyl groups. This has etching effects that leads to removing parts of the sub-surface of the polymer and forming volatile compounds.[169,176] As well as the plasma process, the etching mechanism is influenced by the characteristics of the polymer being treated, such as degree of crystallinity, which is one of the key properties of a polymer with respect to

the plasma etching rate. The crystalline regions on the polymer surface exhibit higher resistance to the etching process than amorphous regions. This results in increasing the crystallinity content of the plasma-treated polymer as the amorphous parts are etched in preference. This induces modification of the surface morphology forming topographical features at the scale of nanometres that may increase the roughness of the treated polymer surface.[173,174] On the other hand, the scission and hydrogen abstraction processes generate radical sites on the polymer surface. These very active sites react with the excited oxygen species of plasma resulting in implanting new functional oxygen groups on the treated polymer surface, such as C-OH and -O-C=O and C=O as illustrated in Figure 2.6. Peroxy and alkoxy groups can also be among the oxygen groups on the treated polymer surface. These unstable groups can be broken down into different oxygen groups. The polymer surface can be saturated with oxygen groups for extended times of plasma treatments. However, the chemical functionalisation process terminates by the chemical interaction of all free radical sites on the polymer surface.[169] The radical sites can react together forming cross-linked networks of polymeric chains with a significant impact on the properties of the polymer surface, such as wear, shear resistance and adhesion. Plasmas with inert working gases are commonly used to induce cross-linking on the polymer surface.[168,177] The cross-linking process was investigated by a study[177] on Low-density polyethylene (LDPE) surface treated with Argon plasma. Furthermore, the radical sites left on the polymer chain after a plasma treatment remain active and can react with the gaseous molecules in air causing further oxidation of the treated polymer surface.[178] The high capability of plasma treatment to modify the polymer surface properties makes it an effective means for the surface functionalisation with oxygen and other functional groups. The plasma treatment is also clean and eco-friendly with no need to introduce additional materials or change the polymer bulk properties. Therefore, oxygen plasma will be used to implant functional oxygen groups on the polymer surfaces to increase their wettability.

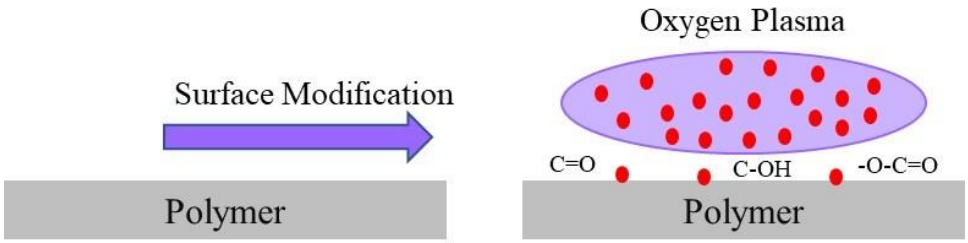

Figure 2.6: Sketch on oxygen plasma treatment of polymer surface; polar oxygen groups (C=O, C-OH, -O-C=O) are implanted on the plasma-treated surface. Figure was redrawn from Puliyalil et al.[174]

2.8.1.2 Ageing Phenomenon (Hydrophobic Recovery)

Surface treatments have transient effects which decay over time. In the context of food packaging, this treatment must give the required functionality from the time the packaging is produced until the product inside is used. Plasma-treated polymer surfaces experience gradual degradation and loss of the gained polarity and surface energy over time. The polymer surfaces revert to a more hydrophobic nature showing a tendency to recover their original surface properties before the plasma treatment. This phenomenon is called hydrophobic recovery (ageing) and reflects post-treatment changes in the surface chemistry of the treated polymers.[172,179,180]

Ageing process of the polymer surfaces is proposed to occur via different mechanisms, such as reorientation or diffusion of the functional polar groups into the bulk of polymers.[79,168] Another mechanism is the conversion of polar groups (C-O) to more stable groups (C=O) that ultimately decrease the concentration of polar groups on treated surfaces as explained in a previous study.[181] The changes in surface properties of aged polymer surfaces after a plasma treatment are usually progressively, but not linearly, observed over time. This can be evaluated by determination of water contact angle (WCA) and chemical composition to reflect the degradation of surface wettability and depletion of polar groups.[179] The hydrophobic recovery of plasma-treated polymer surfaces is often partial, exhibiting some long-lasting surface modification as reported by various studies,[179,182,183] albeit not to the original extent. The surface properties of polymer surfaces experience fast recovery immediately after the plasma treatment while recovery rate slows down over time. Homola et al[182] found that WCA of PET film increased from 36.2° to 51.2° after 6 hours post plasma treatment. The WCA for this film then increased to 55.6° after 90 days of storage time. The ageing process and rate of plasma-treated polymers are

influenced by the storage temperature and environment,[168] plasma working gas, plasma treatment time and polymer type.[169] For feasible application of the plasma to food packaging, plasma treatments would have to factor in the likely shelf life of the packaging. In other words, these treatments would last long enough to cover packing, transport, storage and end use.

2.9 Summary of Review

This chapter has reviewed the relevant literature on meat exudate, wettability and surface tension phenomena, capillarity and capillary valving phenomena, porous materials and open-cell foam, surface modification and plasma surface treatment of polymers. Packaging materials can potentially be modified in terms of their geometry and surface wetting characteristics in a way that offers the ability to trap exuded liquid within the packaging itself. Current packaging solutions are not in themselves capable of trapping meat exudate and require separate soak pads, which have to be removed and act as a barrier to recycling. As a result, a series of experimental trials are required to develop new packaging technologies capable of trapping exudate within the packaging itself, without the need for extra components. The first part of this work will be the development of simulated meat exudate for consistent evaluation of the effects of packaging modification. Following on from this, the geometry of plastic film packaging and surface wetting characteristics of both plastic film and foam packaging will be investigated as means of containing exudate within the packaging. These include the following experiment chapters:

Chapter 4 investigates the rheological and physical properties of pork exudates to formulate simulated meat exudate for testing the liquid retention capacity of the following packaging solutions.

Chapter 5 investigates the modification of recess geometry to incorporate raised rim on the liquid-holding recesses to enhance their geometrical valving functionality, hence the liquid retention capacity.

Chapter 6 investigates the localised plasma surface treatment of liquid-holding recesses to improve their wetting-based valving functionality and liquid retention capacity.

Chapter 7 investigates the plasma surface treatment of open-cell polymeric foam to increase the liquid uptake of foam packaging.

Chapter 3

Materials and Methodology

3.1 Introduction

As stated in the literature review (Chapter 2), there is potential for the development of innovative packaging solutions for isolation and retention of food exudates. These are based on introducing capillary valving functionalities for liquid-holding PET recesses in addition to improving wettability and capillary sucking pressure for open-cell polymeric PS foam. Therefore, a series of experiments were carried out to assess the capacity of these solutions to scavenging and retaining liquids. This chapter describes the materials and methods used in this work, starting with the preparation and characterisation of pork exudate and exudate simulants in Section 3.2. The materials, design and preparation methods of packaging samples are reported in Section 3.3. The geometrical and structural characterisation of samples are described in Section 3.4. Plasma surface treatment and characterisation of sample surface properties are explained in Section 3.5 and 3.6 respectively. Finally, Section 3.7 includes liquid retention and absorption tests of samples.

3.2 Preparation and Formulation of Meat Exudate Simulants

From a research perspective, the direct use of exudate is problematic. Firstly, the exudate will vary depending on the type of meat, storage and preparation method and duration of storage (Section 2.2.1). Secondly, the exudate is an unhygienic material to work with. It changes and degrades over time and can only be obtained in small amounts (millilitres) from fresh meat products. Simulated exudates were, therefore, produced using rheology and surface tension modifiers to mimic the physical and rheological properties of real meat exudates. The exudate simulants are safe, stable and easy to clean liquids, which give physical and rheological behaviours comparable to real meat exudates in a controllable fashion. To benchmark the exudate simulants, fresh pork exudates were characterised in terms of surface tension, shear viscosity and viscoelastic properties. This allows to define the range of surface tensions and flow behaviours that can be exhibited by meat exudates.

3.2.1 Pork Exudate

Pork exudate (PE) was selected as a model of meat exudates to characterise its physical and rheological properties. This is due to the large production volume of pork meat in the world and well documented studies on pork exudate.[184,185] Pork exudate is a pink and aqueous liquid primarily contains sarcoplasmic proteins, enzymes, amino acids and vitamins that are soluble in water.[35,186] Pork meat is mostly packaged in plastic meat trays, where the pork exudate is excreted from the meat surface and accumulated in the bottom of these plastic trays.[17,18] Therefore, pork exudate was taken from fresh packaged pork purchased directly from major retailers (Sainsburys, TESCO, Aldi, Lidl) in Swansea, Wales, United Kingdom. Pork exudates accumulated in the plastic meat trays from each retailer was decanted into separate plastic bottles. Although the exudate content in each tray was varied, the estimated average amount of exudate taken from each tray was ~20 g. The plastic bottles with pork exudates were labelled and stored in refrigerator at temperature of 4 ± 1 °C. Rheological and surface tension characterisation of pork exudate was carried out to produce polymer-based solutions as simulants of the meat exudate. These solutions were formulated with rheology modifiers (Carboxymethyl cellulose and bovine serum albumin, Sigma Aldrich, UK) and surfactant (Triton X-100, Sigma Aldrich, UK) to mimic the rheological and surface tension properties of the characterised pork exudates. The pork exudate itself (Sainsburys superstore, Swansea, Wales, UK) was also used in certain retention tests as a test liquid.

3.2.2 Exudate Simulants

3.2.2.1 Materials

3.2.2.1.1 Carboxymethyl Cellulose

Carboxymethyl cellulose (CMC) with molecular weight of 90,000 g/mol (Sigma Aldrich, UK) was used as a rheology modifier. CMC is a water soluble and cellulose based polysaccharide commonly used in the form of sodium cellulose derivative salt. CMC plays important functional roles as thickener, binder, stabiliser and even as film forming material. It is widely utilised to control the rheological properties of fluids for different applications in food, cosmetic and pharmaceutical industries.[187,188] CMC can be obtained in a range of molecular weights, such as 90,000 g/mol, 250,000 g/mol and 700,000 g/mol to impart different viscosities.[189] Apart from its desired

functional properties, CMC exhibits non-toxicity and good biodegradability.[190] CMC can be dissolved in water to make aqueous solutions with different concentrations. Studies on the rheological characterisation of CMC solutions with low concentrations show dominant viscous properties. In contrast, shear-thinning flow behaviour and viscoelastic properties are attributed to higher concentrations of CMC solutions.[187]

3.2.2.1.2 Bovine Serum Albumin

Bovine serum albumin (BSA) (Sigma Aldrich, UK) was used to mimic the presence of proteins in meat exudate. BSA is a globular protein containing 583 amino acids with a molecular weight of 66400 Da.[191] It is a water-soluble protein, isolated from bovine blood and commonly used as model protein in food research.[192–194] BSA is widely used in various applications due to its desired properties of binding, non-toxicity, biodegradability, low cost, easy to prepare and use.[195,196] Aqueous BSA solutions usually exhibit shear-thinning flow behaviour, particularly when small shear rates are applied. The protein molecules also tend to migrate to the interface between fluid and air, reducing the surface tension, which could be exhibited by the pork exudate.[197] The surface tension of BSA solutions can be as low as 51.1 mN/m.[198]

3.2.2.2 Formulation of Exudate Simulants

Exudate simulants were formulated to act as test liquids to assess the samples of developed packaging solutions against their liquid retention capacity. This included CMC simulants for liquid retention of capillary recesses, BSA simulant and surfactant simulants for liquid absorption of open-cell foam. Following a series of concentration trials and associated viscosity measures, the final concentrations of the simulants were determined to match the viscosity window of previously measured meat exudate.

3.2.2.2.1 CMC Simulants

CMC simulants were prepared to be used in liquid retention tests of capillary recesses. These simulant liquids had different surface tensions (high, medium, low). To prepare CMC simulants, sodium carboxymethyl cellulose (CMC) powder (Sigma Aldrich, UK) with a molecular weight of 90,000 g/mol was used to formulate aqueous CMC solutions with a concentration of 1 wt%. CMC powder was dissolved in DI water at temperature of 20 ± 1 °C. The CMC solutions were gently mixed with a magnetic stirrer at low rate

until the polymer was completely dissolved and any potentially trapped air was released. The CMC solutions were diluted as required to prepare CMC 1 wt% with varying surface tensions by adding varying amounts of 1 wt% solution of Triton X-100 surfactant (Sigma Aldrich, UK) and 1 wt% solution of E122 Azorubine dye (FastColours LLP, UK) for visualisation purposes.

3.2.2.2.2 BSA Simulant

BSA powder with a molecular weight of 66,000 g/mol (Sigma Aldrich, UK) was dissolved in DI water at temperature of 20 ± 1 °C. The BSA solution was then diluted with DI water and addition of 1 wt% solution (solid weight content: 0.01 wt%) of E122 Azorubine dye (FastColours LLP, UK) to prepare BSA solution with a concentration of 8 wt%.

3.2.2.2.3 Surfactant Simulants

DI water was used to prepare surfactant simulants with different surface tensions. The simulant liquids were DI water with added 1 wt% solution of Triton X-100 surfactant (Sigma Aldrich, UK) and 1 wt% solution of E122 Azorubine dye (FastColours LLP, UK). The resulting solutions were mixed with a magnetic stirrer at temperature of 20 ± 1 °C until homogeneous.

3.2.3 Characterisation of Pork Exudates and Simulants

Rheological characterisation, density and surface tension measurements were performed to adequately determine the rheological and physical properties of pork exudate and simulant liquids. This allows for defining the behaviour of the pork exudate and its simulants during retention and absorption tests. The rheological characterisation techniques included evaluation of shear viscosity and viscoelastic properties. All exudate simulants were characterised regarding surface tension and rheological properties. The formulation of CMC 1 wt% and surfactant simulants with varying surface tensions was to cover different wetting behaviours that may be exhibited by meat exudates.

3.2.3.1 Density Pycnometer

Density (ρ) measurement was carried out by gravity pycnometer with a glass bulb (nominal volume: 10 cm^3). Liquid density is the ratio of measured liquid mass to the

actual volume of pycnometer. The precise pycnometer volume was determined 5 times with DI water and the actual bulb volume was 10.2362 ± 0.0014 cm^3. The pycnometer stopper with a well-designed capillary channel allows accurate density measurement by releasing any excessive liquid in the glass bulb. The pycnometer was gently filled with liquid to prevent the formation of air bubbles. The mass of liquid was calculated by subtracting the weight of empty pycnometer from pycnometer filled with liquid. Density measurements were performed at temperature of 20 ± 1 °C.[199]

3.2.3.2 Shear Viscometry and Oscillatory Shear Viscometry

Flow behaviour was characterised by measuring the shear viscosity while viscoelastic properties by oscillatory shear measurements with AR-G2 rheometer (TA Instruments, UK) as shown in Figure 3.1. The rheometer was equipped with concentric cylinders (bob diameter: 28 mm, bob length: 42 mm, cup diameter: 30.4 mm and operating gap: 6 mm). The predetermined volumes of pork exudate/simulant liquid samples were precisely and consistently added to the cup by a pipette. The shear viscosity measurements were conducted within a range of shear rates of 0.1-100 s^{-1}. For oscillatory shear measurements, a stress amplitude sweep in the range of 0.01-5 Pa was applied to shear samples at oscillation frequency of 1 Hz. The linear region of storage and loss moduli (linear viscoelastic range) was identified for each fluid. A frequency sweep measurement was then carried out in the range of 0.1-1 Hz at a specific stress value obtained from the linear region of stress amplitude sweep. This allowed to measure the viscoelastic moduli (G' and G''), representing the elastic and viscous characteristics respectively, in addition to phase angle (δ).[200] The measurements were carried out at temperature of 16 ± 1 °C for pork exudates and 20 ± 1 °C for exudate simulants. The inner cylinder (bob) was used as internal flow geometry to minimise the artifact caused by the free semi-rigid surface film. Pork exudate and protein solutions are biological fluids with surface active properties, tending to form protein film on the fluid interface and leading to non-Newtonian behaviour artifact. Further, the artifacts created by low torque and secondary flows of pork exudate and simulant liquids were considered in all measurements.[201]

Figure 3.1: AR-G2 rotational rheometer (TA Instruments) used for rheological characterisation of pork exudate and simulant liquids.

3.2.3.3 Pendant Drop Method

Surface tension of liquid samples was measured by pendant drop technique that is based on the analysis of shape profile of hanging liquid drop. The gravity tends to elongate liquid drop while surface tension resists the gravity effect, tending to keep the spherical shape of liquid drop. Therefore, dimensional analysis of the resulting drop shape in equilibrium allows for determining the liquid surface tension.[202,203] Surface tension measurement was carried out by (First Ten Angstroms FTA1000c, First Ten Angstroms, Inc., UK) analyser system at temperature of 20 ± 1 °C as shown in Figure 3.2. Each liquid was filled in a vertically aligned syringe (volume: 1 mL) with needle G20 (external diameter: 0.9081 mm) and positioned on a hanger between a high-resolution camera and light source. The liquid drop was generated at the tip of needle and shape image of the elongated drop was taken by the camera. Drop shape profile was analysed by FTA32 shape analyser software to measure the equatorial diameter (d_e) and diameter (d_s) at distance of d_e from bottom drop tip as illustrated in Figure 3.3 to derive liquid surface tension (γ) value according to equation (3.1)[203]:

$$\gamma = \frac{g\rho d_e^2}{H} \qquad (3.1)$$

where g is gravity acceleration, ρ is liquid density as an average value of six repeated measurements by the calibrated pycnometer, H is physical quantity related to d_s/d_e.

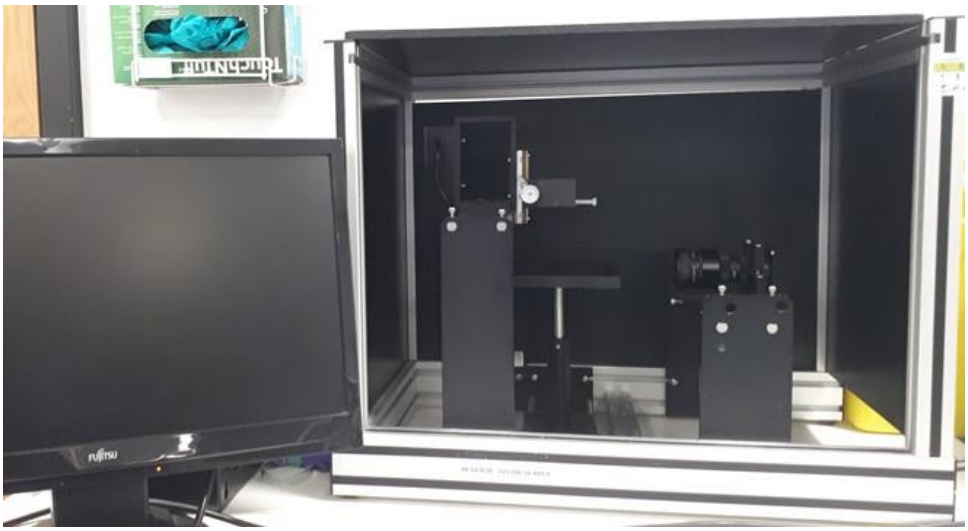

Figure 3.2: First Ten Angstroms FTA1000c analyser used to measure the surface tension of pork exudate and simulant liquids in addition to measure the liquid contact angle on surface of recess and foam samples.

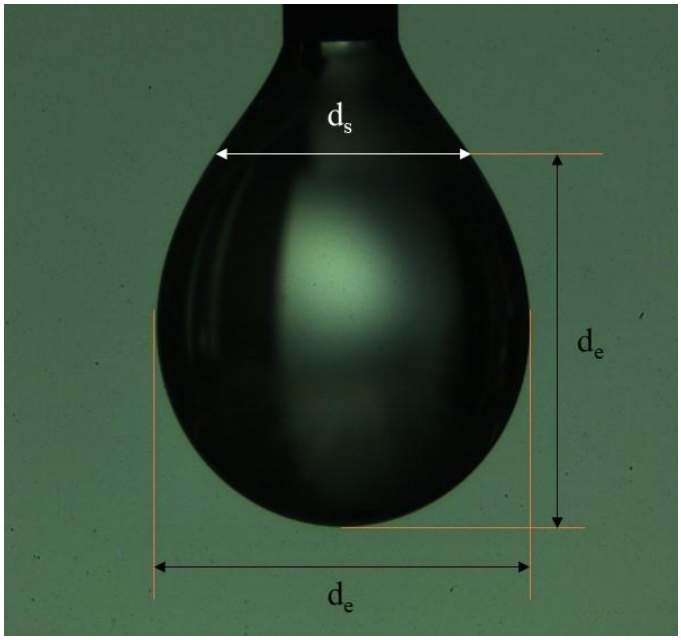

Figure 3.3: Liquid pendant drop profile for surface tension measurement.

3.3 Design and Preparation of Packaging Samples

3.3.1 Packaging Materials

The work explored both plastic film and foam products. Amorphous polyethylene terephthalate (PET) sheets were chosen as thermoforming substrates with capillary recesses. The PET sheets with nominal thickness of 0.5 mm were supplied and thermoformed in Klockner Pentaplast company, UK. PET polymer has various properties attractive for manufacturing of packaging, such as inertness, low cost, transparency, flexibility, strong mechanical strength, good barrier and thermal resistance characteristics.[182,204] Further, PET is the most common plastic material used in food and meat packaging, found in a variety of packaging designs and forms, such as shrinkable films, wrapping films and rigid trays.[205,206] For open-cell foam, white expanded polystyrene (PS) sheets with open-cell structure were supplied from Klockner Pentaplast company, UK. The PS foam sheets had nominal thickness of 5 mm with impermeable skin on top and bottom sides. Open-cell PS foam is widely used to manufacturing meat trays as soak-away for exudate scavenging.[9]

3.3.2 Design and Thermoforming of Capillary Recesses

3D prototype models of flat substrates with arrays of circular capillary recesses were designed to act as liquid-holding wells using SolidWorks designer software (Edition SP 4.0- 2016). This enables to sketch 3D models of capillary recesses with precise dimensions and visualise their shapes before executing the models into plastic capillary recesses.[207] Two substrate models were designed to assess the recesses with modified geometry. These included one substrate of recesses with no rims and the other substrate of recesses with peripheral rims raised from the substrate surface. The substrate models were both configured into 8-recess arrays of the same recess size with equal spacing distances. Other prototype models were sketched to design recesses with raised rims of different rim heights and widths. These prototype models were used to produce their thermoformed PET replicates as illustrated in Figure 3.4.

To assess the recesses for selective modification of their wall wettability, a substrate model was designed with recesses of varying sizes. The recesses were configured into 6-recess arrays of the same recess size with equal spacing distances. The mould manufacturing and vacuum thermoforming of PET sheets into substrates with recesses were carried out in Klockner Pentaplast company, UK.

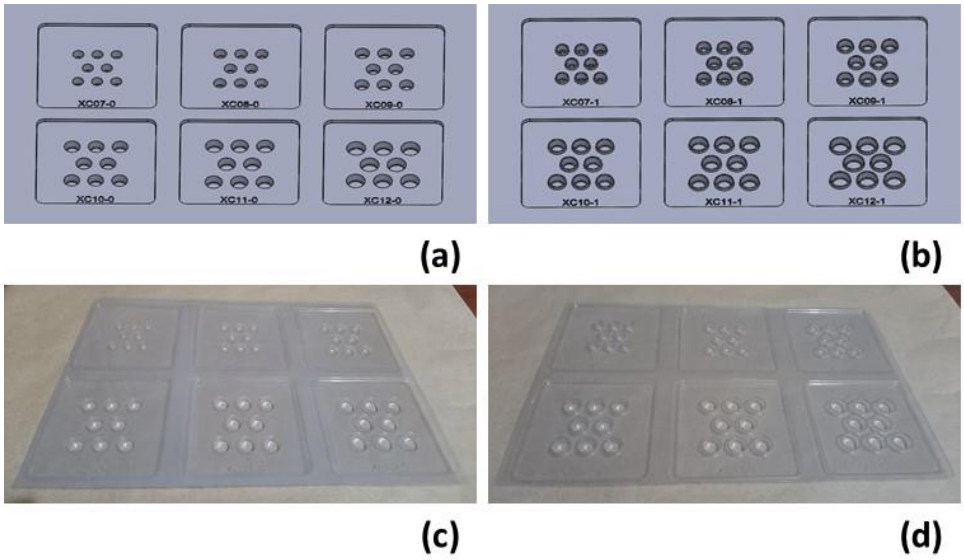

Figure 3.4: 3D prototype model of recess substrates; (a) no rim, (b) raised rim and photos of thermoformed PET recess substrates; (c) no rim, (d) raised rim.

3.3.3 Open-Cell Foam

Plain PS foam sheets with open-cell structure of large-scale industrial foam were obtained from Klockner Pentaplast company, UK. The foam sheets were cut into rectangle-shaped samples for structural, surface characterisation and liquid absorption tests.

3.4 Characterisation of Packaging Samples

3.4.1 Shape Profile, Dimensions and Volume Measurements of PET Capillary Recesses

3.4.1.1 Digital Smartzoom 5 Microscopy

The geometrical dimensions and shape profile of the formed PET recesses were determined by digital Smartzoom 5 microscope (Zeiss, UK) as illustrated in Figure 3.5. This light microscope allows for producing 2D shape profiles and accurate dimensional measurement using a camera with supplied motorised engine. The LED ring lighting provided helps eliminate any glare or excessive light reflection.[208,209] PET recesses were marked with a fine line over their centre axis and placed in the freezer at temperature of -80 ± 1 °C for 5 min. Each recess was cut directly after the removal from freezer by a sharp scalpel in its vertical plane through the marked line. The recesses were cut at low temperature to ensure a clean and uniform cut surface as the thermoformed polymers exhibit glassy properties at low temperatures.[210] The

resulting cross-sections of PET recesses were scanned by Smartzoom 5 microscope, and stitched 2D images were taken using FWD 36 mm lens to generate their shape profiles. A measurement tooling for dimensions in Smartzoom 5 software was used to measure the opening diameter, cavity depth and wall draft angle of each recess in addition to measuring the height and width of recess rims.

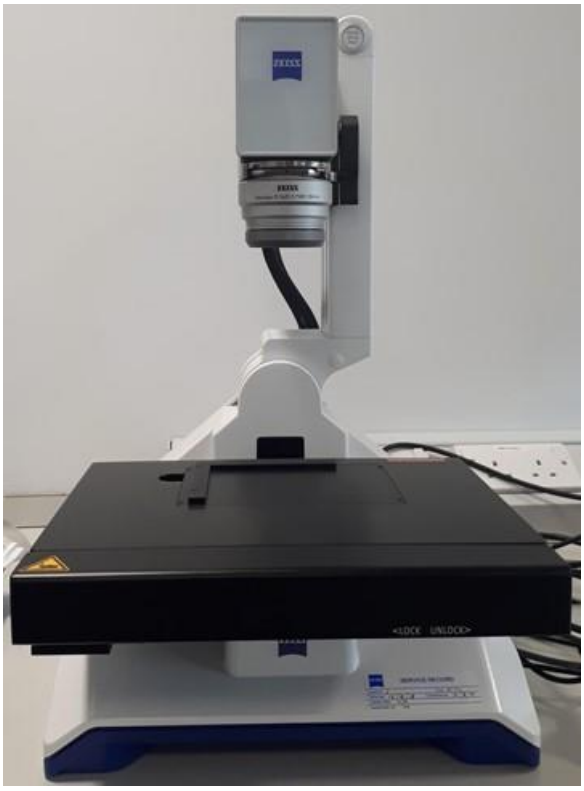

Figure 3.5: Digital Zeiss Smartzoom 5 microscope used to characterise the shape profile and measure the geometrical dimensions of capillary recesses.

3.4.1.2 Liquid Displacement Method

Cavity volume of PET recesses was determined by liquid displacement method. This involved measuring the mass of a liquid, with known density, occupying the recess cavities using analytical scale (Model: A200S, Sartorius Analytic, Germany) with resolution of 0.0001 g. A low surface tension 4-Hydroxy-4-methyl-2-pentanone liquid (Sigma Aldrich- boiling point: 166 °C, density: 0.931 g/mL, surface tension: 32.37 ± 0.59 mN/m) stained with methylene blue dye (Sigma Aldrich- M9140-25G) was used to give a better levelling with the recess edges. The liquid volume was then calculated by its known density and measured mass, representing the volume of the corresponding recess cavity.

3.4.2 Structural and Material Characterisation of Open-Cell PS Foam

3.4.2.1 Foam Density

Representative cubic samples were taken from PS foam sheets by a sharp scalpel. The geometrical dimensions of foam samples were measured by a digital calliper. The foam samples were weighed on analytical scale (Model: A200S, Sartorius Analytic, Germany) with resolution of 0.0001 g. The foam density (ρ_f) was determined by calculating the ratio of sample weight to its geometrical volume according to American Society for Testing and Materials (ASTM) standard D1622-14 and presented in kg/m^3.[211,212]

3.4.2.2 Expansion Ratio

Expansion ratio of PS foam was based on the measured density of PS foam (ρ_f) and PS solid polymer (ρ_s). This material property reflects the degree in the reduction of PS density and is associated to the open-cell content of foam. The expansion ration (ψ) of PS foam was represented by the ratio of solid polymer density to its corresponding foam density as shown in equation (3.2)[211]:

$$\psi = \frac{\rho_s}{\rho_f} \qquad (3.2)$$

3.4.2.3 Porosity

The porosity (n) is a characteristic property of foam that is associated with liquid uptake capacity of open-cell foam. The foam porosity is based on the ratio of gas volume (V_{gas}) occupying pore spaces to the geometrical volume of the foam sample (V_f). The volume of pore space was determined by subtracting the volume of solid polymer (V_s) from the geometrical volume of the foam sample (V_f). Therefore, the foam porosity was defined by compensating the volume with the corresponding mass and density as explained in equation (3.3)[62]:

$$n = \frac{V_f - V_s}{V_f} = \frac{\frac{m_f}{\rho_f} - \frac{m_f}{\rho_s}}{\frac{m_f}{\rho_f}} = 1 - \frac{\rho_f}{\rho_s} \qquad (3.3)$$

where m_f is mass of foam sample, ρ_f: density of foam sample, ρ_s: density of solid polymer.

3.4.2.4 Pore Size Distribution

The pore structure and pore size distribution of PS foam was characterised by scanning electron microscope (SEM, Zeiss Evo-LS25, UK) as shown in Figure 3.6. SEM allows for a high depth of focus through scanning foam cross-sections with electron beam. The secondary electrons emitted due to the interaction between the striking electrons and sample surfaces can be detected and analysed by SEM detector to be transformed into digital images.[213] This makes SEM an effective technique for imaging and analysis of morphology and dimensions of porous materials.[214] The cross-section surfaces of intact porous structure were prepared for imaging by scoring the foam samples with scalpel and immersing in liquid nitrogen. The scored samples were fractured and sputtered with platinum coating using Agar High Resolution Coater (Model: 208HR, Agar Scientific) to reduce the charging effect of the polymeric surface. Two adjacent surfaces of each PS foam sample were scanned and imaged in the SEM operating at 15 kV and within width of 2.287 mm. The SEM images were analysed by ImageJ 1.47v software to determine the pore size distribution. The pore size measurement was carried out by fitting a circle on each pore perimeter and measuring the corresponding diameter. The measured values of pore diameters were used to generate a histogram showing the distribution of pore sizes.[146]

Figure 3.6: Scanning electron microscope (Zeiss Evo-LS25, UK) used to analyse the pore structure and morphology of PS foam samples.

3.4.2.5 Open-Cell Content

Open-cell content of PS foam was measured to evaluate the portion of interconnected cells in the foam samples. The open cells form the accessible volume of foam matrix where liquid can flow, while the remaining portion consists of closed compartments and pore walls. The content of open cells was determined as the ratio of total open-cell volume to the geometrical volume of the foam sample. This was measured by a gas pycnometer (ULTRAPYC 1200e- Quantachrome Instruments, USA) using nitrogen gas as shown in Figure 3.7 and according to the standard measurement method ASTM D6226-10. The pycnometer is based on the gas displacement method to measure the volume of solid material occupying the sample chamber (pycnometer sample volume). Therefore, the open cell volume can be calculated from the difference between pycnometer sample volume and geometrical sample volume, providing the open-cell content as given by equation (3.4):

$$\text{Open-cell content \%} = \left[\frac{V_f - V_p}{V_f \text{ x } n}\right] \text{ x } 100 \qquad (3.4)$$

The content of cell walls and closed cells was determined as shown in equation (3.5) and (3.6) respectively:

$$\text{Cell wall content \%} = \left[\frac{m_f}{\rho_s \text{ x } V_f}\right] \text{ x } 100 \qquad (3.5)$$

$$\text{Closed-cell content \%} = 100 - (\text{Open-cell content \%} + \text{Cell wall content \%}) \qquad (3.6)$$

where V_f (m^3) is geometric volume of foam sample, V_p (m^3) is pycnometer volume, n is porosity, m_f (kg) is mass of foam sample, ρ_s (kg/m^3) is density of solid PS polymer. The measurements were carried out based on ASTM Standard D6226-10 as detailed in Appendix A.1.[211,215]

Figure 3.7: ULTRAPYC 1200e gas pycnometer (Quantachrome Instruments) used to measure the open-cell content of PS foam samples.

3.5 Oxygen Plasma Surface Treatment

Plasma treatments with oxygen as a working gas are commonly used in low pressure plasma units to increase the surface wettability of polymer materials. The plasma glow includes excited oxygen molecules, ions and electrons that introduce oxygen groups onto treated polymer surface, such as -OH and -COOH, leading to increased polarity and hydrophilicity of polymer surfaces. The plasma treatment under vacuum ensures a more uniform and consistent surface modification.[169]

A low pressure plasma unit (model: Nano, Diener Electronic, Germany) with a cylindrical chamber (diameter: 26.7 cm, length: 42 cm) was used for the surface treatment of samples as shown in Figure 3.8. The plasma unit was coupled with a frequency generator sourced with 230 V AC supply to provide a power source at 40 kHz. The distance between the powered electrode and sample-holding tray was 15 cm. The glow discharge was produced by oxygen gas supply with the vacuum pressure (base pressure: 0.1 mbar) in the plasma chamber as modified via the gas flow rate. The

O_2 plasma treatments were carried out at oxygen flow rate of 80 cm^3/min, working pressure of 0.14 mbar and power of 240 W. The plasma settings (power, pressure, flow rate) were defined through preliminary testing on plasma treatment to consistently give targeted surface wettability of samples, and in line with the equipment working range envelope.[216,217]

Figure 3.8: Low pressure plasma unit (Model: Nano, Diener Electronic, Germany) used for the surface modification of recess and foam samples.

3.6 Characterisation of Surface Properties of Packaging Samples

Surface properties of PET and PS foam samples were characterised in terms of surface wettability, surface chemical composition and surface topography. This helps explain the changes in surface properties induced by O_2 plasma surface treatments and the relationship between material surface properties and capillary liquid retention. The study involved the use of different techniques to determine these surface properties including contact angle measurement, X-ray photoelectron spectroscopy (XPS), atomic force microscopy (AFM) and drop absorption test.

3.6.1 Contact Angle

The wetting properties of polymer materials were characterised by measuring the static contact angle of DI water drops using sessile drop method. Small liquid drops deposited on a solid surface form contact angle at the triple contacting point of air, liquid and

solid phases. This contact angle in equilibrium (θ_e) reflects the surface wettability of solid surfaces as it depends on the competing cohesive and adhesive forces exhibited by the contacting interfaces. The equilibrium contact angle is related to the interfacial tensions of the air (vapour), liquid, solid interfaces as given by Young's relationship in equation (3.7):

$$\cos \theta_e = \frac{\gamma_{sv} - \gamma_{sl}}{\gamma_{lv}} \qquad (3.7)$$

where γ_{sv} is solid/vapour interfacial tension, γ_{sl} is solid/liquid interfacial tension, γ_{lv} is liquid/vapour interfacial tension.

Liquids present partial wetting properties on solid surface for $0° < \theta_e < 90°$ corresponding to hydrophilic surface regarding water, while de-wetting properties for $\theta_e > 90°$ corresponding to hydrophobic surface regarding water.[69,72] Therefore, DI water drops of 3 μL were deposited by a micropipette on clean sample surfaces and their contact angles were measured by (First Ten Angstroms FTA1000c) analyser system at temperature of 20 ± 1 °C and relative humidity of 54 ± 5%. The measured contact angle was an average of the left and right contact angles of DI water drops.[218] The sessile drop technique was also used to determine the surface energy (γ^{tot}) of sample surfaces with its polar (γ_s^p) and dispersive (γ_s^d) components. The surface energy measurement was based on Owens-Wendt method using DI water and diiodomethane (Sigma Aldrich, 158429- 25 ML, UK). This method is explained in Appendix A.2.[204]

3.6.2 X-ray photoelectron spectroscopy (XPS)

The surface chemistry of sample surfaces was quantitively and qualitatively analysed by the XPS technique. XPS is based on irradiating the solid surface with X-ray photons with high energy that result in emitting electrons (photoelectrons) with different kinetic energies. The electron intensities and corresponding binding energies can be determined by an electron analyser. This analyser is used to generate XPS spectrum of all elements and chemical bonds existed in 10 nm depth of the analysed surfaces.[219]

X-ray photoelectron spectroscopy (Kratos Analytical Ltd, UK) shown in Figure 3.9 was used to analyse the surface chemical composition of samples. The sample surfaces were exposed to an exciting X-ray source of monochromatic Al Kα (1486.6 eV) in the analysis chamber under low pressure. The XPS scans were carried out at take-off angle of 90° and the emitted photoelectrons were received and analysed by an encountering

hemispherical analyser. The surface charging was neutralised via the integral filament and magnetic lens system. The wide scan spectra were generated at pass energy of 160 eV and within a range of binding energy of 0–1400 eV. The high-resolution scans for C 1 s peaks were performed at pass energy of 20 eV. The peaks of all scan spectra were fitted on Shirley background and processed by CasaXPS software (Version 2.3.22PR1.0, Casa Software Ltd) and calibrated according to the reference position of carbon C 1s peak of 285.0 eV. Carbon peak components were deconvoluted and normalised with Gauss–Lorentz peak models to represent the different chemical groups in the carbon peak and calculate their concentrations.[220,221]

Figure 3.9: X-ray photoelectron spectroscopy (Kratos Analytical Ltd, UK) used for analysis of the surface chemistry of recess and foam samples.

3.6.3 Atomic Force Microscopy (AFM)

The surface topography of sample surfaces was characterised by AFM as a 3D imaging technique. AFM can scan solid surfaces with a resolution of sub-nanometre using a tip held on cantilever. This tip undergoes attractive and repulsive forces, causing cantilever deflections during probing sample surfaces. These deflections are captured and transformed into 3D topographical image with roughness values of the scanned surface.

Sample surfaces were scanned with atomic force microscopy (JPK NanoWizard 3) as shown in Figure 3.10. The scans were carried out in tapping mode with a resolution of 512 x 512 pixels. A silicon cantilever (nanoworld FM) was used to scan the sample surface and the tip was oscillating in resonance frequency of 75 kHz with force constant of 2.8 N/m. The scanning images were analysed by Gwyddion software (Version 2.55) to determine the surface roughness parameters.[222]

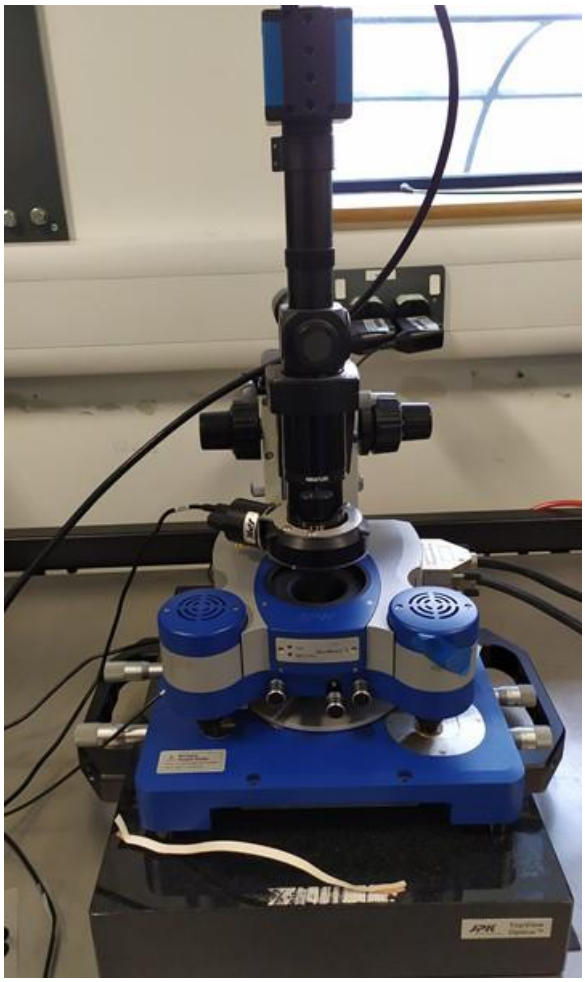

Figure 3.10: Atomic force microscopy (JPK NanoWizard 3) used to analyse the surface topography of PET recess samples.

3.6.4 Drop Absorption Test

The effect of O_2 plasma surface treatment on the increase in surface wettability and capillary liquid absorption of PS foam was assessed by drop absorption test. DI water drops (10 μL) were placed on the cut sides of foam samples with exposed porous structure (no skin). For foam pores with sufficient wettability towards water, DI water drops can be wicked into the foam matrix by capillary action. The time for the water drops to be fully wicked into the porous PS structure was measured by high-speed

camera (Fastcam Mini, Model: UX100, Photron). A photograph was also taken for the water drops on the porous structure of untreated and plasma-treated foam samples to compare their surface wettability.[92]

3.7 Liquid Retention Tests

The liquid retention capacity of PET recesses and liquid absorption capacity of PS foam were assessed with test liquids under normal gravity. Samples were tested with liquids as exudate simulants of different surface tensions to cover a wide range of surface tensions that might be exhibited by meat exudates. All retention tests were carried out at temperature of 20 ± 1 °C.

3.7.1 Liquid Retention Capacity of PET Recesses

Liquid retention capacity of PET recess samples was determined by retention tests. These tests involved evaluation of the effects of localised plasma treatment and raised recess rim on recess retention capacity. Therefore, the liquid retention capacity of recesses was assessed for various combinations of recess size and rim presence, and combinations of recess size and plasma treatment. The retention tests included tilting the recess samples on purpose-built tilting board (horizontal to downward facing) for an angle of 180° over 5 s, after filling with simulant liquids as illustrated in Figure 3.11. The weight of simulant liquid in full recess sample was measured before tilting. The recess sample was then mounted on a sticky tape on the board. The weight of trapped liquid in the tilted sample was then measured representing the liquid retention capacity (g).[127] For practicality of using the recesses in food packaging, the retention capacity of recesses with best liquid retention performance was calculated in mL/m^2. This was based on the liquid volume retained in recesses with a hexagonal packing per square metre of PET substrate with spacing of 1 mm between the neighbouring recesses.[223]

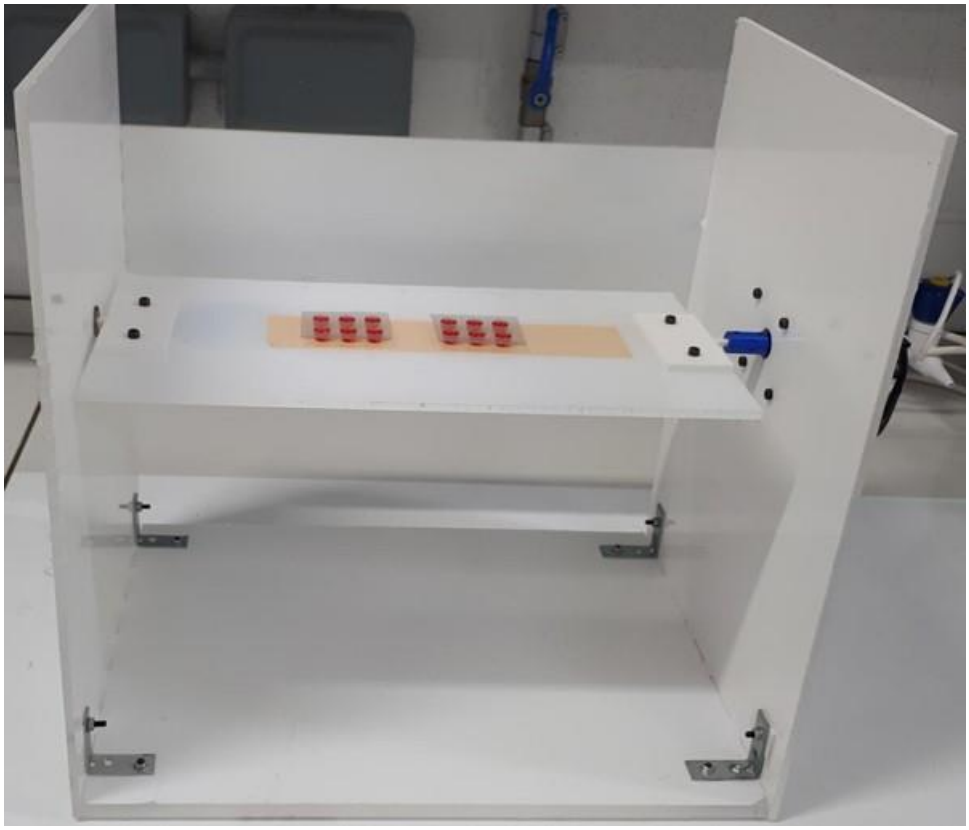

Figure 3.11: Purpose-built tilting board for liquid retention test of PET recesses. The board has a sticky tape to fix recess samples and can be turned freely around its axis.

3.7.2 Liquid Absorption Capacity of PS Foam

The absorption capacity of PS foam was determined for rectangular foam samples of dimensions (L x W x T: 40 mm x 10 mm x 5 mm). The foam samples were treated with O_2 plasma with samples oriented to focus the plasma on one cut side (L x T). The absorption test was performed by freely placing the cross-sections (L x T) of untreated and plasma-treated samples on the simulant liquid within a plastic plate. The measurements of absorption capacity were estimated by the liquid weight in grams absorbed per gram of dry foam sample in equilibrium. The dry foam samples were weighed before the absorption test (W_d) and after their saturation with test liquid (W_s). The foam samples were removed from the liquid for 30 s to allow any excess liquid to drain before weighing. The resulting absorption capacity (R) was given by equation (3.8)[133]:

$$R = \frac{W_s - W_d}{W_d} \qquad (3.8)$$

Chapter 4

Characterisation of Rheological and Physical Properties of Pork Meat Exudate and Formulation of Meat Exudate Simulants

4.1 Introduction

The rheological and physical properties of meat exudate are important to understand the exudate behaviour during liquid retention tests. These are also required to formulate artificial exudate simulants with comparable properties. This chapter investigates methods to characterise the rheological and surface tension properties of pork exudate. Based on the measured properties of pork exudate, simulant liquids are prepared and characterised to ensure these liquids exhibit similar flow behaviour and wetting properties of the pork exudate. These simulant liquids will be used in Chapter 5, 6, 7 to assess liquid retention technologies that are based on capillarity and interface phenomena so that effective packaging solutions can be designed and developed to trap meat exudate.

4.2 Materials and Experimental Methodology

4.2.1 Materials

Pork exudate (PE) was collected from packaged fresh pork meat purchased from four major retailers in the UK (Sainsburys, TESCO, Aldi, Lidl), corresponding to retailer 1, retailer 2, retailer 3 and retailer 4 respectively. The pork exudate accumulated in the pork meat packaging trays from each retailer was decanted into a separate plastic bottle (Section 3.2.1). Sodium carboxymethyl cellulose (CMC) (Sigma Aldrich, UK) was used as a rheology modifier. Bovine serum albumin (BSA) (Sigma Aldrich, UK) was used in simulant liquid formulation to mimic the presence of proteins in the meat exudate (Section 3.2.2.1). Triton X-100 surfactant (Sigma Aldrich, UK) was used to make simulant liquids of varying surface tensions. E122 Azorubine dye (FastColours LLP, UK) was used to stain simulant liquids to improve the visualisation of these liquids during liquid retention tests.

4.2.2 Formulation of Exudate Simulants

Simulant liquids were formulated to be used as alternative test liquids of real meat exudate in liquid retention tests. These included three sets of aqueous simulant liquids

(CMC simulants, BSA simulant, surfactant simulants) as presented in Table 4.1. CMC simulants were prepared from aqueous CMC 1 wt% solutions and BSA simulant from aqueous BSA 8 wt% solution. Surfactant simulants were prepared from DI water with added surfactant. The simulant liquids were formulated with small amounts of surfactant (Triton X-100) and red dye (E122 Azorubine), for easy visualisation, to prepare simulant liquids of varying surface tensions (Section 3.2.2.2).

Table 4.1: Solid weight contents of simulant liquids.

CMC Simulant	CMC (wt%)	Surfactant (wt%)	Dye (wt%)
High Surface Tension	1	0	0.01
Medium Surface Tension	1	0.0025	0.01
Low Surface Tension	1	0.1	0.01
BSA Simulant	BSA (wt%)	Surfactant (wt%)	Dye (wt%)
	8	0	0.01
Surfactant Simulant	-	Surfactant (wt%)	Dye (wt%)
High Surface Tension		0	0.01
Medium Surface Tension		0.0025	0.01
Low Surface Tension		0.1	0.01

4.2.3 Characterisation of Pork Exudates and Simulant Liquids

4.2.3.1 Shear Viscosity and Oscillatory Shear Measurement

The flow behaviour and viscoelastic properties of pork exudate and simulant liquids were characterised by carrying out measurements of shear viscosity and shear oscillatory (Section 3.2.3.2). The measurements were performed by AR-G2 rheometer (TA Instruments) equipped with concentric cylinders (bob diameter: 28 mm, bob length: 42 mm, cup diameter: 30.4 mm and operating gap: 6 mm). The concentric cylinders (bob and cub) geometry was chosen to adequately characterise liquids with low viscosity and minimise their surface tension effects. The predetermined volumes of liquid samples were added to the cup by a pipette. The shear viscosity measurements were carried out within a range of shear rates of 0.1-100 s^{-1}.

For oscillatory shear measurements, a stress amplitude sweep in the range of 0.01-5 Pa was applied to shear samples at oscillation frequency of 1 Hz. The linear region of storage (G') and loss (G'') moduli (linear viscoelastic range) was identified for each fluid. A frequency sweep measurement was then carried out in the range of 0.1-1 Hz at a stress value of the linear region of stress amplitude sweep. This allowed to measure the viscoelastic moduli (G' and G''), representing the elastic and viscous characteristics respectively, in addition to phase angle (δ). The measurements were carried out at temperature of 16 ± 1 °C for pork exudate and 20 ± 1 °C for simulant liquids.

4.2.3.2 Density Measurement

Density (ρ) measurement of pork exudate and simulant liquids were carried out by gravity pycnometer with a glass bulb (nominal volume: 10 cm^3). The measured density was based on the ratio of measured liquid mass to the actual volume of pycnometer. The precise pycnometer volume was determined 5 times with DI water and the actual bulb volume was 10.2362 ± 0.0014 cm^3. The pycnometer was gently filled with liquid to prevent the formation of air bubbles. The mass of liquid was calculated by subtracting the weight of empty pycnometer from pycnometer filled with liquid. Density measurements were repeated 6 times at temperature of 20 ± 1 °C (Section 3.2.3.1).

4.2.3.3 Surface Tension Measurement

The surface tension of pork exudate and simulant liquids was measured by pendant drop technique. A pendant drop was produced at the tip of needle G20 (external diameter: 0.9081 mm) and the drop shape profile was produced by a high-resolution camera. The analysis of drop shape profile was caried out in (First Ten Angstroms FTA1000c) analyser system to calculate the liquid surface tension at temperature of 20 ± 1 °C (Section 3.2.3.3).

4.3 Experimental Results

4.3.1 Flow Behaviour Properties of Pork Exudate and Simulant Liquids

The measured apparent shear viscosity of all four pork exudates and water are shown in Figure 4.1. The pork exudates exhibited nearly constant shear viscosities within the range of shear rates between 1 and 100 s^{-1}. These measured viscosities were higher than the viscosity of pure water, showing low viscosities in the range of 4-10 mPa.s. Both pork exudates and water exhibited apparent viscosities that were variable at shear rates

< 1 s^{-1}, while most measured viscosities were within low torque limit of the rheometer. The low torque and secondary flow limits were calculated and plotted to determine the reliable experimental window of viscosity measurements. The measured exudate viscosities were within the determined experimental window of measurements. Comparable flow behaviour of simulant liquids was observed through their apparent shear viscosities in Figure 4.2. The CMC 1 wt% and BSA 8 wt% simulants exhibited constant and low apparent shear viscosities. BSA 8 wt% simulant had viscosity nearly twice higher than water, while CMC 1 wt% had viscosity of around 5 mPa.s. Similarly to pork exudates, the simulant liquids showed variability in their measured viscosities at shear rates < 1 s^{-1} as the measured viscosities approached the low torque limit of the rheometer. The experimental window of viscosity measurements also proved the validity of the measured viscosities of simulant liquids as illustrated in Figure 4.2.

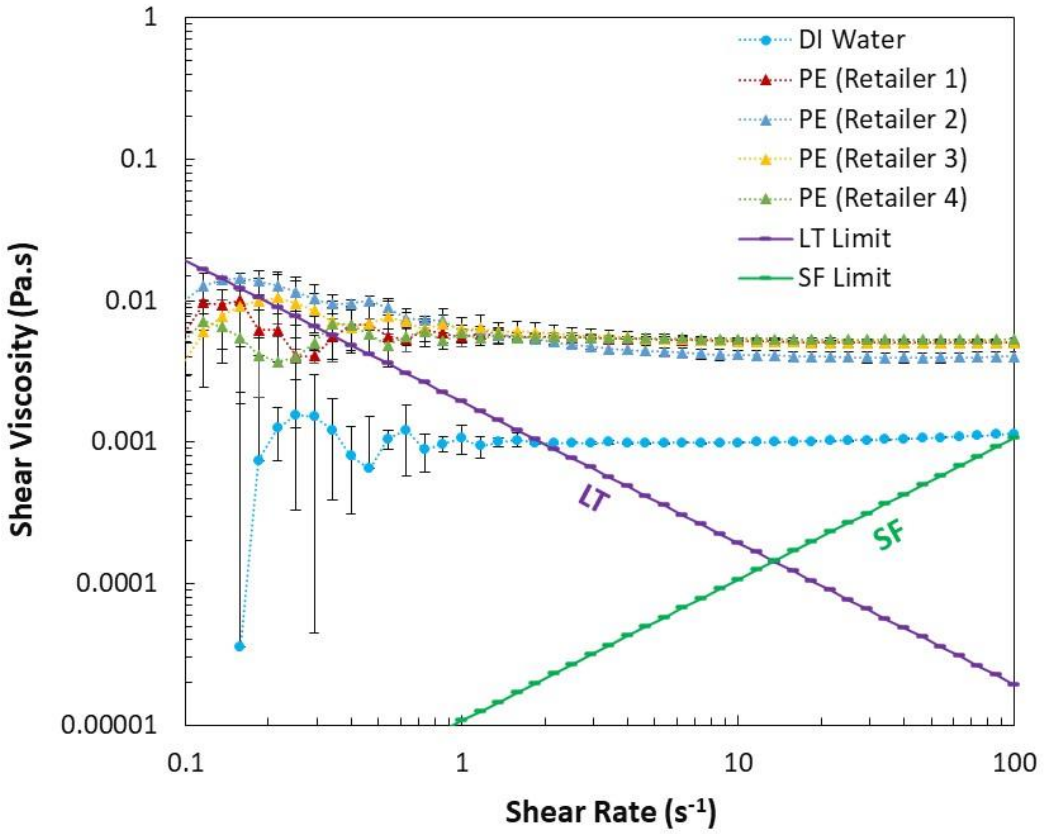

Figure 4.1: Apparent shear viscosity vs shear rate (0.1-100 s^{-1}) of DI water and pork exudate (PE) from different retailers. Low torque (LT) and secondary flow (SF) limits highlight the experimental window of shear viscosity measurements.

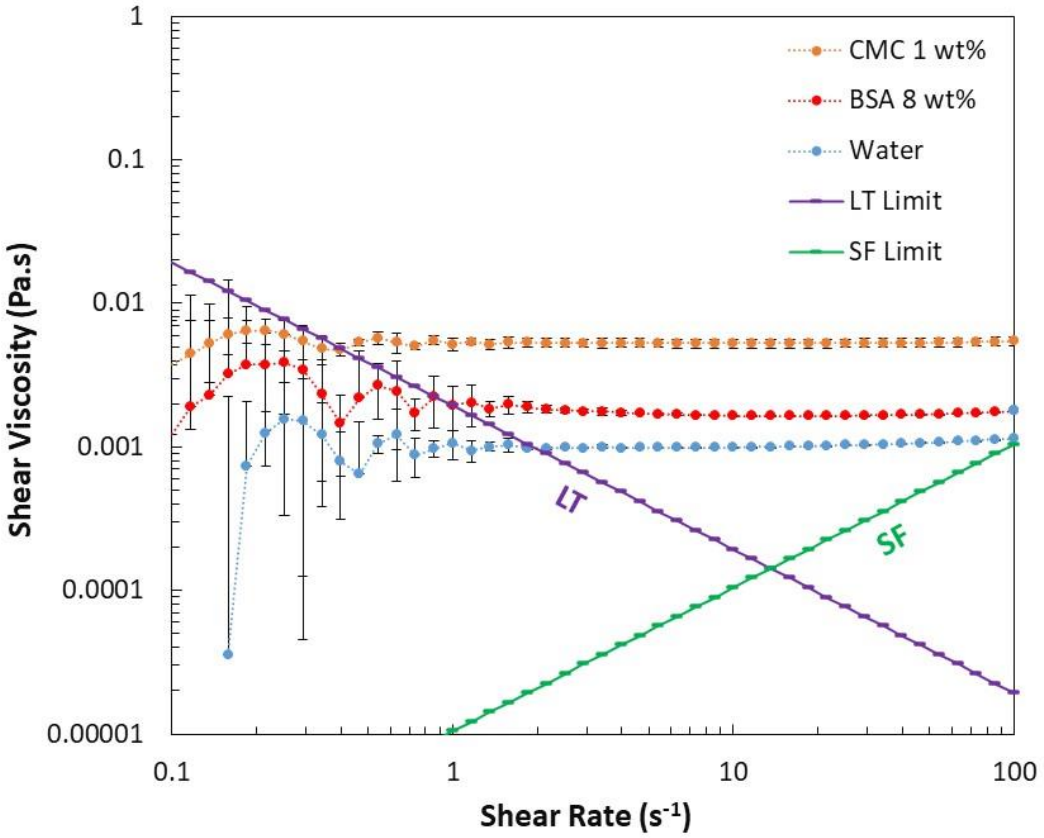

Figure 4.2: Apparent shear viscosity vs shear rate (0.1-100 s^{-1}) of simulant liquids; CMC 1 wt%, BSA 8 wt% and DI water. Low torque (LT) and secondary flow (SF) limits highlight the experimental window of shear viscosity measurements.

4.3.2 Viscoelastic Properties of Pork Exudate and Simulant Liquids

The viscoelastic properties as represented by storage modulus (G'), loss modulus (G'') and phase angle (δ) during frequency sweeps are illustrated in Figure 4.3 for pork exudates and Figure 4.4 for simulant liquids. The frequency sweeps were conducted at stress value of 0.02 Pa. For all four exudates, although elastic and viscous moduli (G', G'') increased with the applied frequency, it was difficult to accurately detect the very low values of storage modulus (G') due to the low exudate viscosities. The loss (viscous) modulus was higher than storage (elastic) modulus for pork exudates over most frequency range. However, the two moduli were crossed and a slight increase in magnitude of storage modulus over loss modulus was shown at high frequency oscillation. This corresponded to phase angle $\delta > 80°$ at low frequency, which decreased for higher frequencies. For CMC 1 wt% and BSA 8 wt% simulants, the measured stresses representing viscoelastic moduli (G', G'') were also very low. The loss modulus was higher than storage modulus at low frequencies. These moduli were crossed with an increase in the storage modulus over the loss modulus at higher frequencies. The

moduli crossing for BSA 8 wt% occurred at lower frequencies in comparison with CMC 1 wt%.

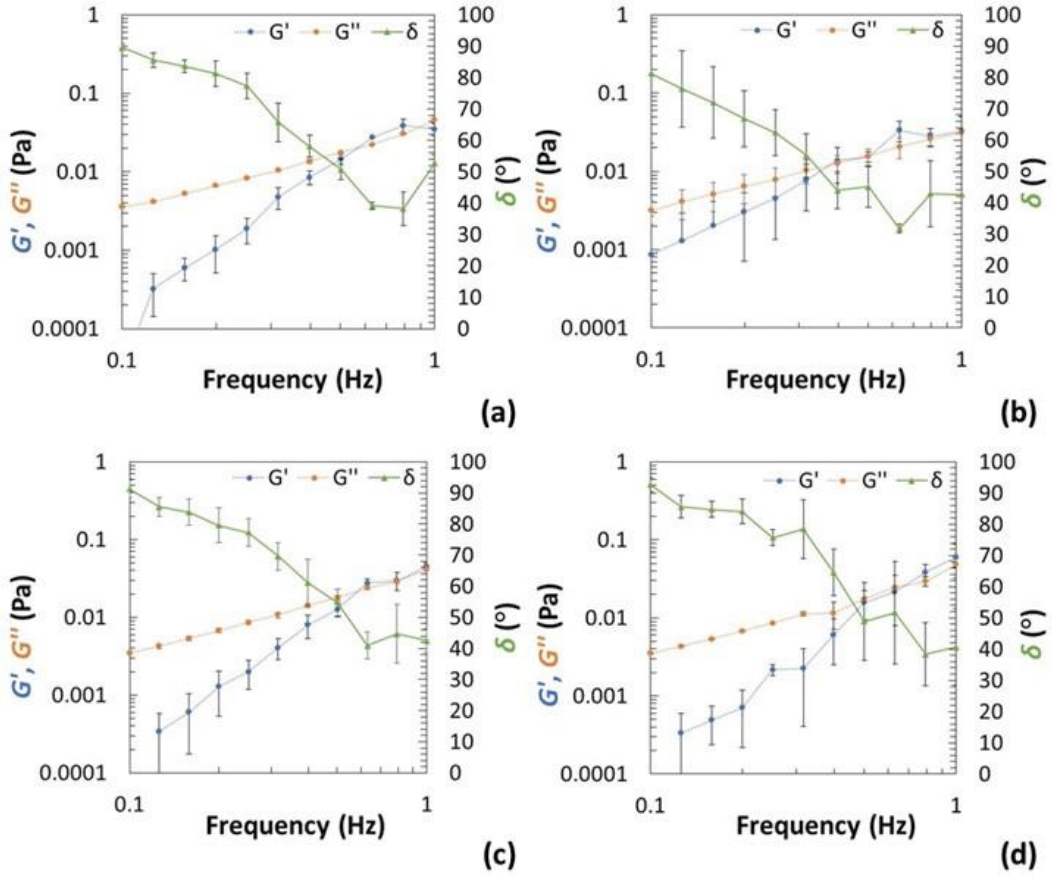

Figure 4.3: Storage modulus G' (blue symbol), loss modulus G'' (amber symbol), phase angle δ (green symbol) from frequency oscillatory sweeps of pork exudates; (a) retailer 1, (b) retailer 2, (c) retailer 3, (d) retailer 4.

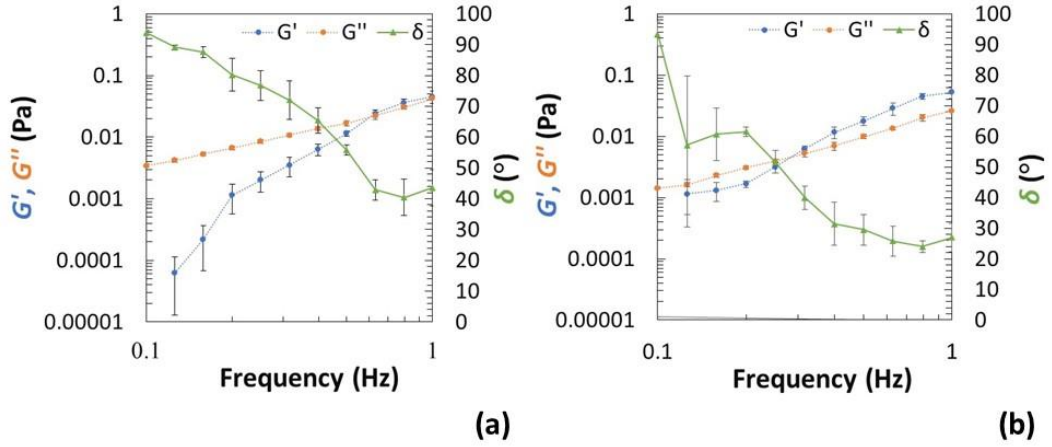

Figure 4.4: Storage modulus G' (blue symbol), loss modulus G'' (amber symbol), phase angle δ (green symbol) from frequency oscillatory sweeps of simulant liquids; (a) CMC 1 wt% and (b) BSA 8 wt%.

4.3.3 Density and Surface Tension of Pork Exudate and Simulant Liquids

The measured surface tension and density values are presented in Table 4.2 for pork exudates and Table 4.3 for simulant liquids. The pork exudates exhibited reduced surface tensions with varying values in the mid-range of 52-59 mN/m. The exudate surface tensions were based on the measured exudate densities that are necessary to calculate the surface tension values. The simulant liquids had different surface tensions, depending on their content of surfactant as shown in Table 4.3. The presence of CMC alone with concentration of 1 wt% showed no significant effect on the surface tension of the solution. However, BSA with concentration of 8 wt% resulted in a reduced surface tension of BSA simulant to 52.03 ± 0.52 mN/m. The surface tension of simulant liquids decreased for higher concentrations of the surfactant.

Table 4.2: Surface tension (γ) and density (ρ) of pork exudate purchased from different retailers.

Pork Exudate	γ (mN/m) ± SD	ρ (g/mL) ± SD
Retailer 1	54.84 ± 0.82	1.0334 ± 0.0027
Retailer 2	55.31 ± 1.33	1.0356 ± 0.0015
Retailer 3	52.40 ± 1.11	1.0463 ± 0.0007
Retailer 4	59.18 ± 1.86	1.0417 ± 0.0026

Table 4.3: Surface tension (γ) and density (ρ) of simulant liquids.

Exudate Simulant	γ (mN/m) ± SD	ρ (g/mL) ± SD[a]
CMC (High Surface Tension)	72.55 ± 0.34	
CMC (Medium Surface Tension)	52.33 ± 0.52	1.0017 ± 0.0005
CMC (Low Surface Tension)	31.52 ± 0.09	
Surfactant Simulant (High Surface Tension)	72.63 ± 0.16	
Surfactant Simulant (Medium Surface Tension)	52.28 ± 0.31	0.9982
Surfactant Simulant (Low Surface Tension)	31.54 ± 0.28	
BSA	52.03 ± 0.52	1.0229 ± 0.0017

[a)] Density of water was taken as standard value of 0.9982 g/mL at temperature of 20 °C.

4.4 Discussion

Pork exudates collected from the plastic packaging trays of fresh pork meat showed essentially Newtonian-like shear flow behaviour. This was demonstrated in their nearly constant low viscosity against the shear rates. Previous work reported comparable low viscosities of pork exudate within the range of 3-10 mPa.s.[43] Work reported previously showed that exudate from other meat types, such as beef exudate also had low viscosities between 3 and 4 mPa.s.[47] The measured low viscosity of all pork exudates was, however, higher than pure water which can be due to the presence of soluble proteins in exudates.[46] The concentration and composition of exudate proteins can vary according to the meat ageing and exudate amount released from meat,[37,40] but protein concentration of meat exudate can be as high as 112 mg/mL. This might have led to the variations in viscosity of pork exudates from different sources.

For simulant liquids of meat exudate, CMC 1 wt% and BSA 8 wt% solutions exhibited flow performance comparable to the pork exudates. The measured viscosities of the simulant liquids were closely matching the viscosity range of pork exudates. The use of CMC as a rheology modifier allows for formulating aqueous solutions with low viscosities at low CMC concentrations.[187] The Newtonian-like flow and constant shear viscosity are usually observed for BSA solutions when characterised by geometry with small liquid/air interface as the case of concentric cylinders. This was observed in the viscosity measurements of BSA solutions with capillary viscometer in previous work.[224] The observed variations in the measured viscosities of pork exudates and simulants at shear rates $< 1\ s^{-1}$ might arise from approaching the low torque limit of rheometer instrument. On the other hand, the oscillatory frequency sweeps of pork exudates reflected their very weakly viscoelastic properties with low levels of elastic stresses. Comparable weak viscoelastic properties were observed for simulant liquids, more notable in BSA simulant than CMC simulant. This indicates that the pork exudates and simulant liquids were very weakly structured, with essentially low shear viscosities and very weak elastic stresses.[225]

The presence of soluble proteins in pork exudates had also role in reducing their surface tensions (52 to 59 mN/m). Other work on pork exudate showed reduced surface tension to 50 mN/m.[43] Similar decrease in surface tension of aqueous BSA simulant

was found due to the BSA protein molecules. The protein solutions experience migration of the protein molecules to the air-liquid interface, leading to a reduction in the liquid surface tension.[197] Surface tension of BSA solutions can be as low as 51.1 mN/m.[198] The addition of surfactant to the simulant liquids allowed for solutions with reduced surface tension, covering the range of surface tensions of pork exudates. Therefore, all simulant liquids had rheological and surface tension properties that could cover the range of the pork exudates, hence these liquids can be used as alternative to the real meat exudate. This is important in designing and developing food packaging solution for exudate retention that are based on the interface and capillary phenomena.

4.5 Closure

The rheological and surface tension properties of exudate are of great importance to capillary liquid retention and transport as described in Chapter 2. Based on the measured exudate properties, the formulated simulant liquids showed a good match with pork exudate regarding the surface tensions, essentially low and constant apparent shear viscosities and weak elastic stresses. This enabled capturing the range of exudate behaviours during liquid retention and absorption tests by using controlled and stable simulant liquids. The obtained exudate simulants are used in liquid retention and absorption tests of the developed plastic packaging solutions demonstrated in Chapter 5, 6 and 7.

Chapter 5

Improved Liquid Retention in Capillary Recesses with Raised Rims for Food Packaging Applications

5.1 Introduction

Having developed suitable simulated exudate materials (Section 4.2.2), this chapter and the following experiment chapters investigate methods for improving the retention of these liquids in the packaging. The specific focus of this chapter is the development of methods to trap liquid based exclusively on modifying the geometry of the thermoformed meat packaging containers.

Liquid trapping in capillary tubes can be increased by a stronger pinning effect and increased stability of the liquid menisci, assuming the tube openings act as capillary valves. The increase in the expansion angle of capillary valves is critical for enhancing their liquid pinning effect and pressure barrier. This technique can be exploited to design capillary liquid-holding recesses with enhanced pinning effects. Thus, larger capillary recesses with improved liquid retention capacity can be integrated into plastic meat trays to develop a packaging solution for isolation of meat exudate (as described in Section 2.5). This chapter, therefore, details an investigation into the use of capillary recesses with a range of diameters, integrated with raised peripheral rims, as a means of improving liquid retention in plastic trays. The recess rims are proposed to improve the liquid pinning effects, hence liquid retention capacity of the recesses. Polyethylene terephthalate (PET) sheets were thermoformed to produce substrates with arrays of capillary recesses. These recesses were then investigated for their ability to retain liquid.

5.2 Materials and Experimental Methodology

5.2.1 Materials

Polyethylene terephthalate (PET) sheets (nominal thickness: 0.5 mm) were supplied and thermoformed in Klockner Pentaplast company (UK) to produce substrates with capillary recesses for liquid retention tests (Section 3.3.1). The recesses were dipped and rinsed with Isopropyl alcohol (IPA) (Propan-2-ol ≥ 99.5%, Fisher Scientific, UK) to remove any organic contaminants prior to testing. Aqueous test liquids were prepared

to mimic meat exudate using sodium carboxymethyl cellulose (CMC) (Molecular weight: 90,000 g/mol, Sigma Aldrich, UK) as a rheology modifier and Triton X-100 surfactant (Sigma Aldrich, UK) to prepare test liquids of different surface tensions (Section 3.2.2.2.1). Exudate collected from plastic packaging of fresh meat pork (Section 3.2.1) was used in retention tests. 4-Hydroxy-4-methyl-2-pentanone (Density: 0.931 g/mL, surface tension: 32.37 mN/m, Sigma Aldrich, UK) was stained with methylene blue dye (M9140-25G, Sigma Aldrich, UK) to measure cavity volume of the thermoformed recesses. Red azorubine colorant- E122 (FastColours LLP, UK) was added to stain the test liquids in retention tests.

5.2.2 Prototype and Thermoforming of Substrates with Capillary Recesses

3D prototype models of two flat substrates with arrays of circle-shaped recesses were designed to act as liquid-holding wells using SolidWorks designer software (Edition SP 4.0- 2016). One design included recesses with no rim and the other had recesses with peripheral rims raised above the substrate surface (rim height: 2 mm, rim width: 0.5 mm). The substrates were both configured into arrays of 8-recesses each with the same recess size and equally spaced. The recesses had circular-peripheral shapes with cavity depths of 5 mm. The recess walls had a draft angle of 10° and the recess opening diameters were 7, 8, 9, 10, 11, 12 mm. Other 3D models were designed with different combinations of rim height and width. These models were used to produce thermoformed PET parts (Section 3.3.2) as shown in Figure 5.1.

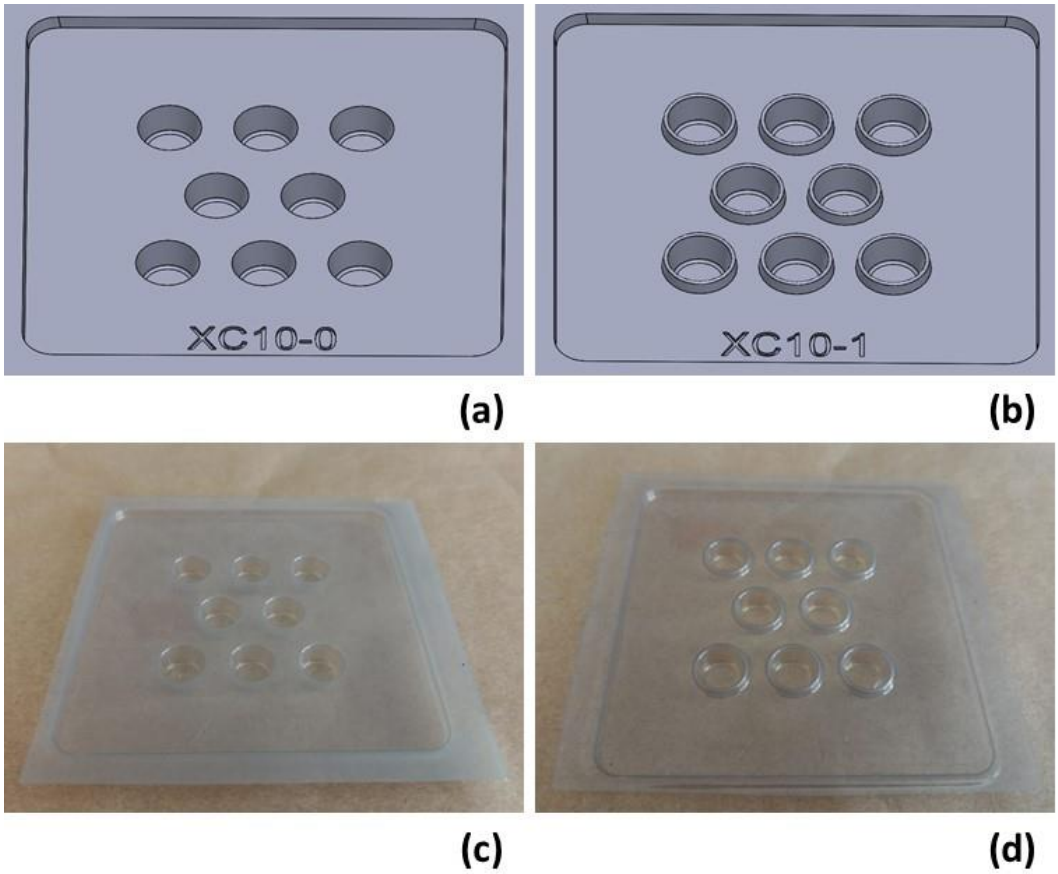

Figure 5.1: 3D prototype model of recess sample; (a) no rim, (b) raised rim and photos of resulting thermoformed PET recess sample; (c) no rim, (d) raised rim (nominal recess diameter: 10 mm).

5.2.3 Dimensions and Volume Measurement of Thermoformed PET Recesses

The geometrical dimensions (opening diameter, cavity depth, draft angle, rim height, rim width) were determined for the formed PET recesses. Stitched 2D images of the recess cross-sections were acquired using Smartzoom 5 microscopy (Zeiss, UK) (Section 3.4.1.1). The resulting cross-section profiles were used to measure the dimensions of the recesses with nominal diameters of 7, 8, 9, 10, 11, 12 mm. The volume measurement of the recess cavities was based on the mass of a liquid filling the recess cavity. The recesses of the studied sizes were filled with 4-Hydroxy-4-methyl-2-pentanone coloured with methylene blue dye, and the corresponding liquid masses were then measured. This liquid had a specific density and low surface tension to provide a good liquid levelling with the recess openings. The recess volume was defined as the volume of the liquid occupying the recess cavity and determined by the measured liquid mass and density (Section 3.4.1.2).

5.2.4 Wettability and Surface Energy of PET Recesses

The wettability of PET samples (recess and substrate surfaces) was characterised by the sessile drop technique (Section 3.6.1). Small drops (3 µL) of deionised (DI) water were placed on clean flat PET surface and the measurement of their static contact angles were carried out in a goniometer (First Ten Angstroms FTA1000c analyser). The surface energy of the PET sample surfaces was measured using polar and non-polar liquids represented by DI water and diiodomethane (Sigma Aldrich, 158429- 25 ML, UK) respectively. The surface energy values were determined by Owens-Wendt method (Section 3.6.1). The contact angle measurements were performed 6 times at temperature of 20 ± 1 °C and relative humidity of 54 ± 5%.

5.2.5 Test liquids Used for Retention Capacity Tests

Test liquids were prepared as meat exudate simulants from CMC 1 wt% solutions with varying amounts of Triton X-100 surfactant (Section 3.2.2.2.1) and as detailed in Chapter 4. The test liquids had different surface tension values (γ: 72.55, 52.33 and 31.52 mN/m) to cover a broad range of surface tensions that could be found in exudate as well as mimicking the rheological characteristics. The test liquids were also stained with food red colorant (azorubine- E122, FastColours LLP) to improve their visualisation in the retention tests.

5.2.6 Retention Test of PET Recesses

Retention tests were conducted to assess liquid holding capacity of the PET recesses for combinations of varying recess sizes and rim presence. The recess samples (8-recess arrays) were placed horizontally, filled with test liquids and then tilted upside down on a rotating board over a period of 5 s (Section 3.7.1). The weight of test liquid in the recess samples was determined before and after tilting. The liquid retention capacity (g) was defined by the weight of liquid retained in recesses after tilting. The retention tests were also performed for recess samples with combinations of varying rim heights and widths. For practicality of using the recesses in food packaging, the retention capacity of recesses with best liquid retention performance was calculated in mL/m^2. This corresponded to the liquid volume retained in recesses with hexagonal packing (recess spacing: 1 mm) on square metre of PET substrate.

5.3 Experimental Results

5.3.1 Analysis of Geometrical Dimensions, Volume and Surface Properties of PET Recesses

The thermoformed PET recess samples revealed a comparable replication of their 3D prototype models as shown in Figure 5.1. This was also demonstrated in the cross-section profiles and geometrical dimensions of the PET recesses in comparison with their prototype models. The shape profile and key dimensional measurements of PET recess and its prototype model (nominal diameter: 10 mm) are illustrated in Figure 5.2. Table 5.1 shows the recess volumes for the various nominal diameters of recess openings. Capacities increased with nominal diameter and there was close agreement between capacities with rims and no rims (error < 0.007 mL). Table 5.2 and 5.3 show the geometrical dimensions of the PET recesses with nominal opening diameters of 7, 8, 9, 10, 11, 12 mm. All recesses showed wall thinning and uneven thickness distribution in the recess walls. The recess openings formed round edges, therefore, the opening diameter was defined as the distance between the bottoms of opposing round edges on the recess cross-section profiles. The measured dimensions of PET recesses were consistent with their prototype models as shown in Table 5.2 and 5.3. The opening diameters of the recesses with raised rim and with no rim had errors < 0.211 mm and < 0.156 mm respectively in comparison with their nominal diameters. The cavity depths of the corresponding PET recesses had also small errors < 0.178 mm and < 0.137 mm respectively. Although the geometrical dimensions of PET recess rims slightly deviated from their nominal dimensions (height and width), these rims were dimensionally consistent for the studied recess sizes. For PET recesses with different rim heights and widths, the recess geometrical dimensions were also consistent as presented in Appendix A.3.

The wetting properties of the PET recesses were characterised by the measured water contact angles on the PET sample surface. The cleaned PET surface showed water contact angle of 75.23 ± 0.74° with consistent measured values on the recess and substrate surfaces. This lack of hydrophilicity corresponded to the measured low surface energy of 48.14 mJ/m^2.

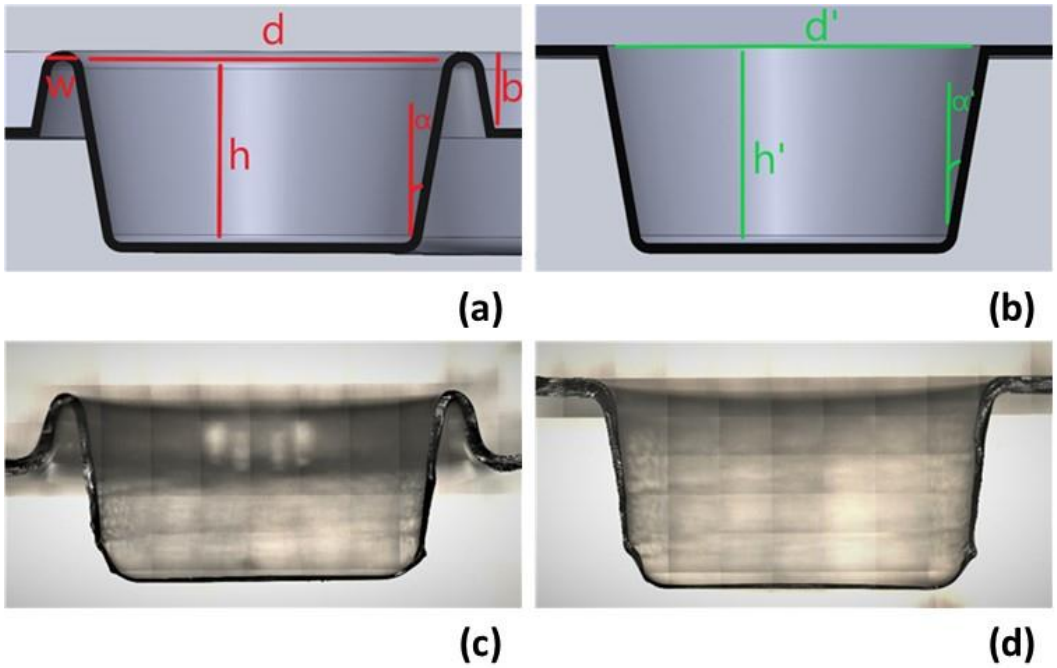

Figure 5.2: Cross-section profiles of recess model; (a) raised rim, (b) no rim and thermoformed PET recess; (c) raised rim, (d) no rim (nominal diameter: 10 mm).

Table 5.1: Average cavity volumes of thermoformed PET recesses.

Nominal diameter (mm)	Recess volume (mL)	
	Raised rim	No rim
7	0.148 ± 0.003	0.151 ± 0.003
8	0.202 ± 0.002	0.208 ± 0.002
9	0.262 ± 0.003	0.266 ± 0.002
10	0.329 ± 0.009	0.331 ± 0.001
11	0.409 ± 0.003	0.412 ± 0.002
12	0.478 ± 0.011	0.485 ± 0.004

Table 5.2: Average geometrical dimensions of PET recesses integrated with raised rims.

Measured dimensions (mm) of PET recesses with raised rims					
Nominal diameter	Diameter (*d*)	Depth (*h*)	Draft angle (*α*, °)	Rim height (*b*)	Rim width (*w*)
7	6.789 ± 0.097	4.885 ± 0.032	5.433 ± 0.416	1.666 ± 0.023	0.652 ± 0.081
8	7.947 ± 0.017	4.951 ± 0.032	7.267 ± 0.115	1.839 ± 0.032	0.610 ± 0.082
9	8.987 ± 0.058	4.933 ± 0.022	6.767 ± 0.231	1.791 ± 0.042	0.578 ± 0.065
10	9.939 ± 0.025	4.913 ± 0.018	7.267 ± 0.252	1.704 ± 0.067	0.565 ± 0.031
11	10.911 ± 0.049	4.822 ± 0.018	7.467 ± 0.493	1.671 ± 0.051	0.559 ± 0.059
12	11.889 ± 0.112	4.985 ± 0.071	6.233 ± 0.814	1.753 ± 0.057	0.520 ± 0.035

Table 5.3: Average geometrical dimensions of PET recesses with no rims.

Measured dimensions (mm) PET recesses with no rims			
Nominal Diameter	Diameter (*d'*)	Depth (*h'*)	Draft Angle (*α'*, °)
7	7.037 ± 0.048	5.061 ± 0.068	6.067 ± 0.115
8	8.025 ± 0.051	5.137 ± 0.014	6.367 ± 0.987
9	8.918 ± 0.046	5.043 ± 0.092	6.233 ± 0.416
10	10.094 ± 0.043	5.118 ± 0.030	6.633 ± 0.306
11	11.156 ± 0.211	5.036 ± 0.021	7.033 ± 0.451
12	12.017 ± 0.067	5.089 ± 0.028	6.700 ± 0.624

5.3.2 Analysis of Liquid Retention of PET Recesses

The liquid retention capacity of thermoformed PET recesses was evaluated with test liquids of different surface tensions (solutions A, B, C) and real pork exudate (solution D) as shown in Table 5.4.

Table 5.4: Composition and surface tension of liquids used in retention tests.

Test liquid	Composition	Surface tension (mN/m)
Solution A	CMC 1 wt%	72.55 ± 0.34
Solution B	CMC 1 wt% + surfactant 0.0025 wt%	52.33 ± 0.52
Solution C	CMC 1 wt% + surfactant 0.1 wt%	31.52 ± 0.09
Solution D	Real pork exudate	60.04 ± 1.22

5.3.2.1 Recesses with Rims vs Recesses with No Rims

The effect of incorporating rims on liquid retention capability of PET recesses was evaluated by comparing recess samples (8-recess arrays) with raised rims (rim height: 2 mm and rim width: 0.5 mm) against their corresponding samples with no rims. The retention capacity was estimated in grams for a combination of various recess sizes and liquid surface tensions under normal gravity. Figure 5.3 illustrates the relative retention capacities with nominal recess diameter of 10 mm with solution A (without surfactant). The test liquid in the tilted recess sample with no rim notably drained, while the liquid remained trapped in the tilted sample with the raised rim. Comparisons of liquid retention capacity of recess samples (nominal recess diameter: 7, 8, 9, 10, 11, 12 mm) with solutions A, B, C, and D are shown in Figure 5.4. Retention capacity of recess samples was affected by nominal diameter, the absence of rims and the surface tension of the test liquid. The presence of integrated recess rims considerably improved the liquid retention capacity of the PET recesses with all test liquids including the real pork exudate. This was most strongly observed for samples with recess diameter of 10 mm with solution A (without surfactant), and samples with recess diameter of 9 mm with solutions B and D (intermediate surface tension liquid and pork exudate respectively) as shown in Figure 5.4a, b, and d. This corresponded to retention capacities of 2.53 g, 2.02 g and 2.12 g for rim-integrated recess samples respectively. On the other hand, the retention capacities of the corresponding samples with no rims were only 0.79 g, 0.53 g and 0.79 g respectively. The beneficial effect of recess rim was diminished with the increase in recess sizes as the liquid in the tilted recesses drained more readily. This occurred for the samples of recess diameters > 10 mm with solution A and > 9 mm with solutions B and D. For samples with small recess diameters, such as 7 mm and 8 mm,

the tilted recesses with solutions A and B maintained full capacity regardless the presence of raised recess rims.

The liquid surface tension had a significant effect on the liquid retention of the recess samples as their retention capacity improved with increasing surface tension of test liquids. The increase in liquid surface tension also magnified the effect of recess rim on enhancing the retention capacity. However, at very low surface tensions, with solution C, the recess samples lost their retention capacity. This very low surface tension of the test liquid facilitated liquid drainage for the recesses of all sizes with only slight improvement in the retention capacity for samples with raised rims as shown in Figure 5.4c. The liquid retention was also evaluated in terms of the liquid volume (mL) that can be trapped per square metre of PET substrate with recesses. Therefore, the retention capacity (mL/m^2) was estimated for hexagon-packed recesses (recess diameter: 9 mm) with even spacing distance of 1 mm. The retention capacity of the rim-integrated recesses with solutions B and D (intermediate surface tension liquid and pork exudate respectively) was 2898 ± 66 and 2921 ± 63 mL/m^2 respectively, while the corresponding recesses with no rims had retention capacities of 763 ± 288 and 1059 ± 126 mL/m^2 respectively. This can validate the practicality of introducing recesses with raised rims to the plastic meat packaging considering the limited draw ratios that can be achieved for plastic packaging trays.

5.3.2.2 Effect of Rim Height and Width

The effects of the geometrical dimensions of the recess rim on liquid retention capacity were studied for rim-integrated recess samples of mid-range surface tension (solution B). The liquid retention capacities of recess samples (nominal recess diameter: 9 mm) with different rim heights and widths are shown in Figure 5.5a and 5.5b respectively. For recess samples with nominal rim width of 0.5 mm, rim heights of 0.2 mm were sufficient to give the full retention capacity, with no benefit in increasing the rim height further. The recess samples showed partial liquid drainage with a decrease in the retention capacity from 2.02 g to 1.18 g for rim height of 0.1 mm. On the other hand, recess samples with nominal rim height of 2 mm and varied rim widths (0.2-5 mm) in Figure 5.5b showed that the recess samples with rim widths of 0.2 to 0.5 mm maintained their full liquid retention capacity, but that further increases in rim width reduced the capacity so that the retention capacity was partially lost from 2.02 g to 1.23 g for rim

width of 1 mm. The retention capacity then further decreased for wider rims until the recess samples were comparable with samples with no rim.

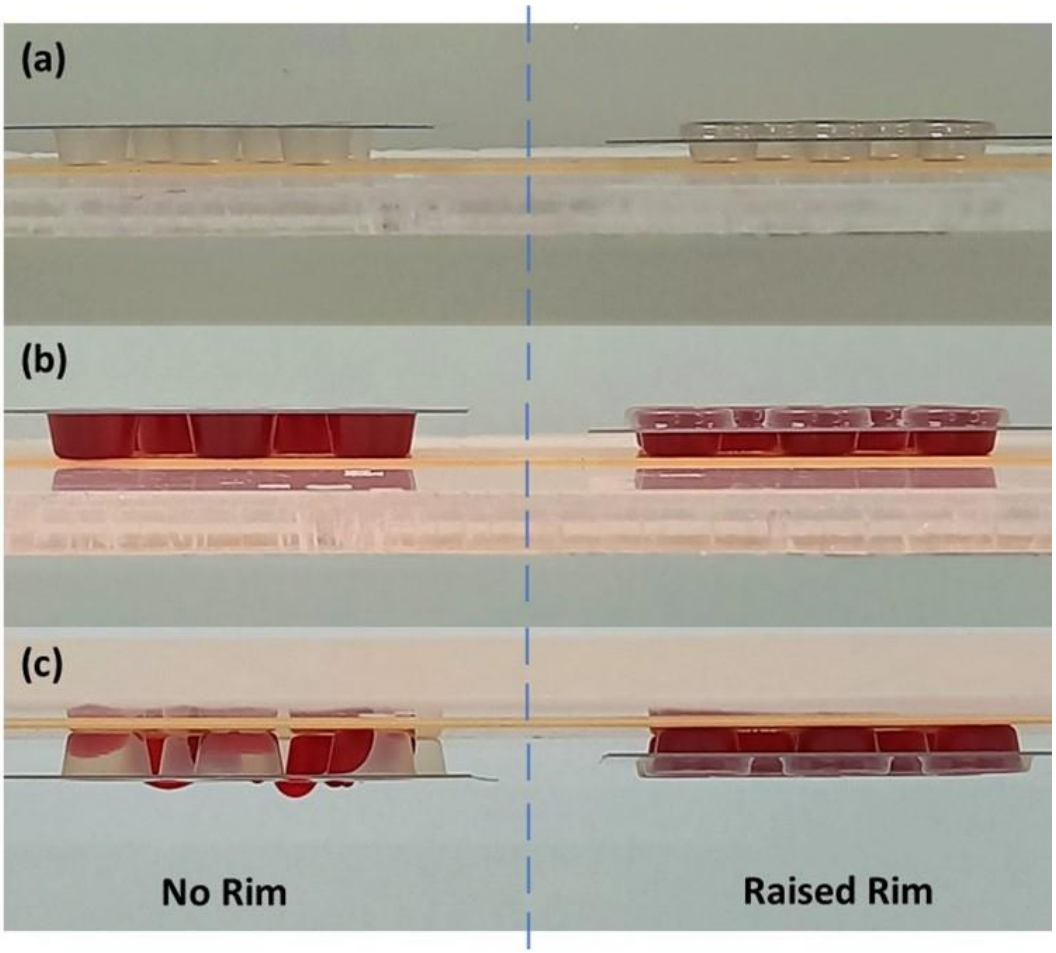

Figure 5.3: Retention test of PET recess samples (8-recess arrays) with nominal recess diameter of 10 mm (left: no rim, right: raised rim) with solution A (γ: 72.55 mN/m); (a) empty recesses, (b) before tilting, (c) after tilting.

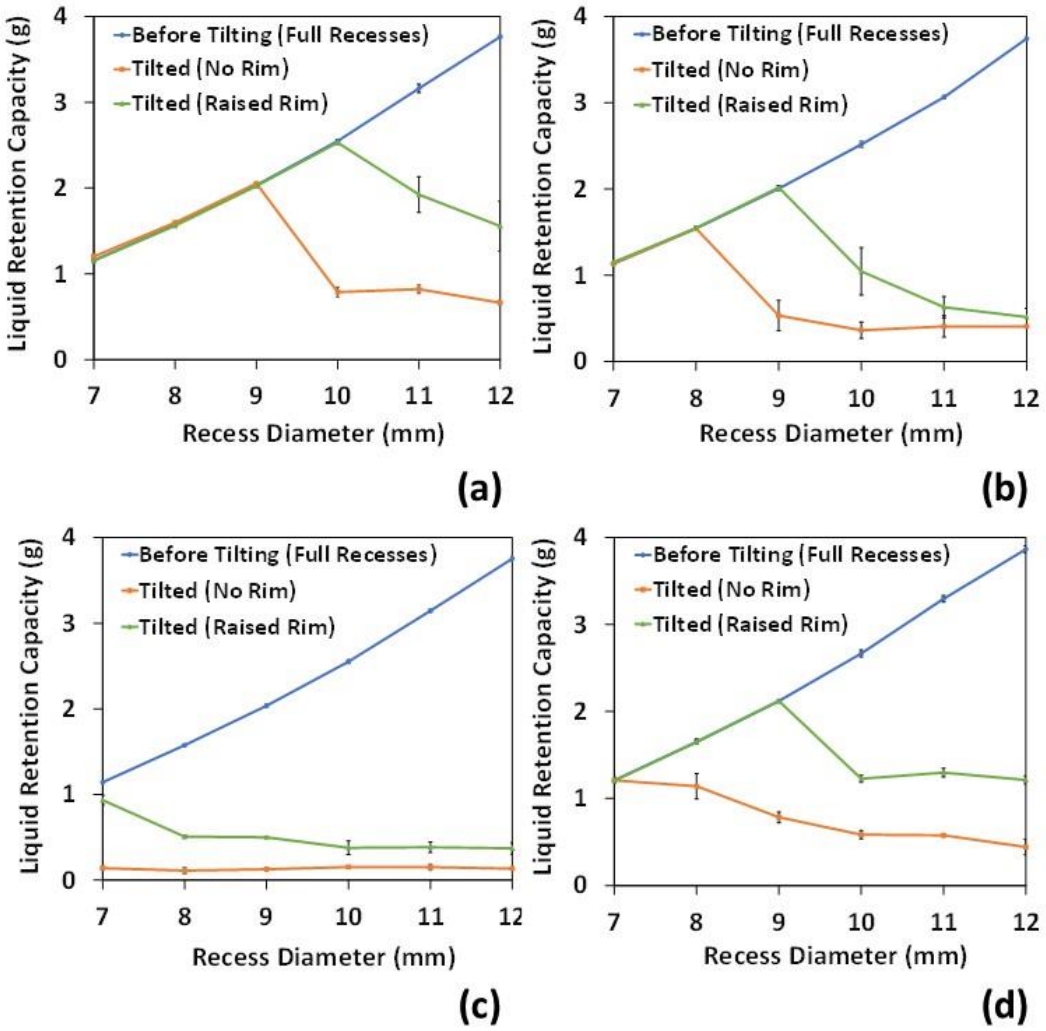

Figure 5.4: Liquid retention capacity of tilted PET recess samples (8-recess arrays) with raised rim and with no rim; (a) solution A (γ: 72.55 mN/m), (b) solution B (γ: 52.33 mN/m), (c) solution C (γ: 31.52 mN/m), (d) solution D (γ: 60.04 mN/m).

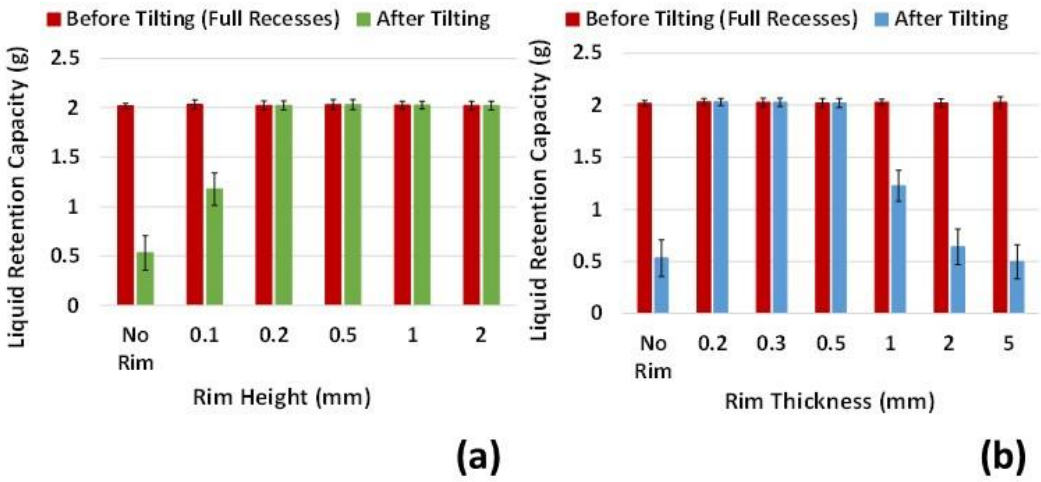

Figure 5.5: Liquid retention capacity of tilted PET recess samples (8-recess arrays, nominal recess diameter: 9 mm) with solution B (γ: 52.33 mN/m); (a) different rim heights, (b) different rim widths.

5.4 Discussion

5.4.1 Characteristics of Recess Geometry and Dimensions

The thermoforming process of the PET substrates allowed consistent replication of the recesses with respect to their 3D prototype models. The thermoforming technology is widely used in the food packaging industry and performs effectively for both simple and relatively complex-shaped plastic packaging products.[226] The variations in wall thickness distribution of the PET recesses occurred as the heated polymeric sheet deforms on the mould during the thermoforming process. This is usually observed in thermoformed plastic products, such as food trays.[227] The relaxation and release of residual stress experienced by thermoformed plastic products might also play role in the small scale variation of the recess dimensions.[228–230] Therefore, the current thermoforming technology, used for the manufacture of conventional plastic food trays, is fit for the intended purpose giving sufficient accuracy to produce a range of recess sizes at scale.

5.4.2 Liquid Retention Capacity of PET Recesses

The low polarity and surface energy of PET surface resulted in low surface wettability of the recess surfaces.[76,204] The raised rims introduced to the PET recesses with this consistent low surface wettability increased their liquid retention capacity. This enables design and thermoforming of plastic meat trays with capillary rim-integrated recesses

for improved liquid self-isolation. These trays can trap the exudate released from packaged meat products during their shelf lifetime.

The mechanism of the capillary liquid retention fundamentally depends on the effects of liquid pinning and dominant pressures on the liquid menisci. This was described in studies conducted by Extrand[125,127] on the capillary liquid trapping and draining in tubes and enclosures with small orifices. A liquid in inclined tube or capillarity forms air-liquid interface on its open bottom end that undergoes capillary, hydrostatic and atmospheric pressures.[125] While the atmospheric pressure upwardly pushes the liquid into the capillarity cavity against the encountering hydrostatic pressure, it introduces air fingers into the liquid bulk for unstable liquid menisci as illustrated within capillary recess in Figure 5.6a. This phenomenon is called Taylor finger, which can propagate into the liquid leading to liquid draining out from the capillarity opening.[124–126] However, geometrical valves usually introduced to capillary systems improve the liquid pinning on their expanded walls leading to increases in the pressure barrier. The PET recesses have a capillarity structure with recess openings acting as geometrical valves. These openings allow the liquid to be pinned on their edges, and hence the capillary pressure generates a local pressure barrier to prevent liquid drainage.[120] This results in more stable menisci and improved resistance to air finger formation that causes the liquid drainage.[126] The capillary pressure and stability of the liquid menisci significantly improved with the decrease in recess sizes. Therefore, liquid menisci in the tilted small recesses were stable with a sufficient pressure barrier to restrict Taylor finger development. This allowed atmospheric pressure to prevent the liquid drainage from the recess cavities as described by Extrand.[125] This was manifested as full liquid retention in inclined recesses with diameter of 7 mm regardless the presence of raised rim. However, the liquid curvature and capillary pressure decreased for larger recesses.[125] This could reduce the menisci stability and undermine the liquid pinning on the recess openings. Thus, the air finger was initiated since the pressure barrier was not sufficient to resist the growing local hydrostatic pressure during the recess inclination.[125–127] This resulted in liquid drainage of the recess cavities as manifested in the reduced liquid retention of larger sized recesses, notably for recesses with no rim.

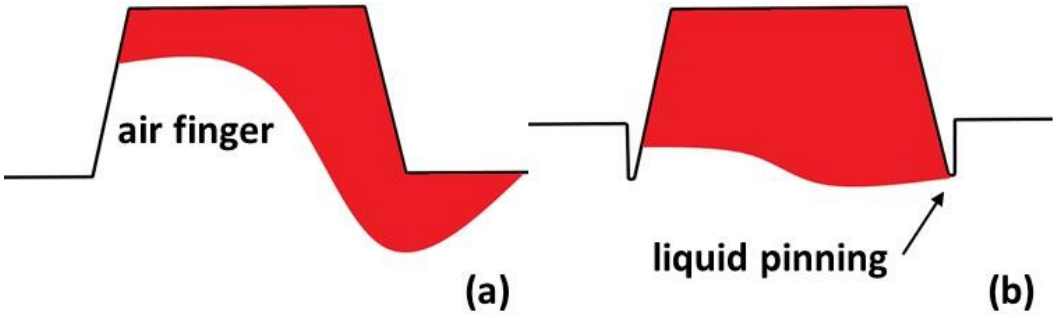

Figure 5.6: Capillary action and liquid behaviour in tilted recesses; (a) no raised rim (underlining unstable meniscus and liquid drainage), (b) with raised rim (underlining stable meniscus and liquid retention).

The presence of thin recess rims above the substrate surface enhanced the valving functionality of the recess openings. The raised rim introduced a larger expansion angle to the recess opening, which improved their liquid pinning effect and the capillary pressure barrier,[111,113] with the proposed action illustrated in Figure 5.6b. The increased expansion angle of the recess openings leads to an increase in maximal contact angle that liquid menisci form on the rim edges of the recesses. The resulting liquid menisci were more stable with stronger pinning on the recess rims as explained by Wang et al.[120] This improved the resistance of the liquid menisci to air finger development and liquid drainage, especially for larger recesses in comparison with their corresponding recesses with no rims. Therefore, the introduced recess rims led to considerable increases in liquid retention capacity of the capillary recesses. The liquid retention of the rim-integrated recesses was also enhanced with real pork exudate, demonstrating the real-world application of this technology. This reveals that the improved valving functionality by recess rims was insensitive to the presence of proteins in the liquid. However, the liquid retention capacity decreased for lower liquid surface tensions as the liquid menisci exhibited less stability and pressure barrier. The reduction in liquid surface tension reduced the resistance to the liquid drainage by facilitating the propagation of air finger as explained by Kumar et al.[126]. The PET recesses with the very low surface tension liquid (γ: 31.52 mN/m) lacked retention capabilities. This could be attributed to the lost pinning effect as the PET substrate had surface energy (48.14 mJ/m^2), higher than the surface tension of the test liquid. Therefore, the liquid fully wetted the recess edges resulting in liquid drainage out of the recess cavities. Although the raised recess rim improved the liquid pinning effect, it only led to slight increases in the retention capacity with the very low surface tension

liquid for the studied recess sizes. However, meat exudates are unlikely to have such low surface tension.[43]

The geometrical dimensions of the recess rims determined the effectiveness of their valving functionality in enhancing the liquid retention capacity. A minimum rim height (0.2 mm) was required for the full liquid pinning effect, while the recesses with rims of lower height (0.1 mm) showed decreased capacity for enhanced liquid retention. The rim width also governed the improvement in liquid retention capacity by influencing the liquid pinning and pressure barrier. Larger rim widths reduced the sharpness of the raised rim, diminishing the effectiveness of the increased expansion angle. This was comparable with the study findings about liquid trapping on capillarity tips as reported by Agonafer et al.[121]

This work demonstrates that recesses integrated with thin rims can be an effective technology to isolate the exudate in plastic meat packaging. For pork exudate, rim-integrated PET recesses with opening diameter of 9 mm had retention capacity of 2921 ± 63 mL/m^2 reflecting an increase of 2.76 times when compared with recesses with no rims. This improved retention capacity is comparable to the absorbent pads used in plastic meat trays, which typically have a liquid absorption capacity of ~3000 mL/m^2 (2949 mL/m^2 based on experimental testing with a simulant liquid). The recesses with raised rims have a permanent effect with low manufacturing cost as the recess production takes place during the normal forming stage. Further, meat exudate trapped in the PET recesses with raised rims can be readily removed by washing the recesses with water to be ready for the recycling process. This allows the manufacture of fully recyclable meat trays, and replaces the use of the non-recyclable absorbent pads that restrict the recycling process of plastic trays and have additional material cost and associated labour.[64] It can also reduce the footprint of the overall plastic packaging waste.

5.5 Closure

The integration of raised thin rims on to PET capillary recesses with extended sizes was an effective technology to substantially enhance their capacity to retain liquids. The PET recesses with raised rims exhibited increases in liquid retention capacity (by 2.76 times for recess diameter of 9 mm, γ: 60.04 mN/m) in comparison to the recesses with no rims, with a potential capacity of around 2900 mL/m^2 which is comparable with

current absorbent pads. The introduced thin rims improved the valving functionality of the recess openings throughout increasing their expansion angles. The liquid menisci on the recess openings were more stable and resistant to liquid drainage. As well as polyethylene terephthalate, these plastic trays can also be made from other single polymeric materials, such as, polypropylene and polyethylene to produce fully recyclable trays, while the design of the recesses allows used trays to be rinsed and cleaned to directly enter closed loop recycling. Having demonstrated that the capacity of thermoformed recesses can be substantially increased by modifying their geometry, the next chapter will explore the use of localised surface treatment as a further method of improving retention capacity of thermoformed recesses.

Chapter 6

Improved Liquid Retention of Capillary Recesses by Localised Plasma Surface Treatment for Food Packaging Applications

6.1 Introduction

The previous chapter demonstrated that the capacity of thermoformed recesses for food packaging can be substantially increased solely by modifying their geometry so that their ability to retain liquid is comparable to current absorbent pad systems. This chapter reports the development of an alternative method to trap liquid in plastic food packaging through the selective surface modification of liquid-holding recesses via plasma treatment, and without employing the raised recesses reported previously. Localised plasma surface treatment of only the internal walls of the recesses is intended to improve their surface wettability and free energy. This generates a contrast in the wetting properties between the recess walls and recess edges. It is proposed that this can induce valve functionality based on surface wettability variation, and thus may improve stability of the liquid menisci and liquid retention capacity. This work used a combined approach of varying both size and surface wettability of capillary recesses. This was carried out through developing a 3D design of a substrate with capillary recesses of different sizes. This design model was then used to produce thermoformed polyethylene terephthalate (PET) substrate with capillary recesses as liquid holding wells. For comparison, the recess samples underwent both localised (recess only) and full plasma treatments to investigate the effect on their liquid retention capacity, using a similar approach as detailed in the previous chapter. Prior to this, the surface properties of PET recesses were characterised by measuring the surface wettability, surface energy, surface chemical composition and topography of the PET surface before and after the plasma treatment. Such treatment may be transient but if it is to be a practical solution it must retain effectiveness during the anticipated lifetime of the packaging product, therefore the longevity of the plasma treatment effect was investigated in terms of the aforementioned properties and crucially in terms of the liquid retention of recesses over extended storage times.

6.2 Materials and Experimental Methodology

6.2.1 Materials

Amorphous polyethylene terephthalate (PET) sheets with thickness of 0.50 mm (Klockner Pentaplast Group, UK) were used to thermoform substrates with capillary recesses (Section 3.3.1). Isopropyl alcohol (IPA) (Propan-2-ol ≥ 99.5 %, Fisher Scientific, UK) was used to clean the recess surfaces by dipping and rinsing the samples in IPA solvent. 4-Hydroxy-4-methyl-2-pentanone (Sigma Aldrich- boiling point: 166 °C, density: 0.931 g/mL, surface tension: 32.37 mN/m) with methylene blue dye (Sigma Aldrich) were used for volume measurement of recess cavities. Test liquids formulated with aqueous solutions of sodium carboxymethyl cellulose (CMC) powder with different surface tensions were prepared as simulant liquids of the meat exudate for retention tests (Section 3.2.2.2.1) as shown in Table 6.1. Red azorubine colorant- E122 (FastColours LLP, UK) was used to dye the simulant liquids for retention tests.

Table 6.1: Test liquids and their surface tensions used in retention tests.

Test liquid	Surface Tension (mN/m)
CMC 1 wt% (High Surface Tension)	72.55 ± 0.34
CMC 1 wt% (Medium Surface Tension)	52.33 ± 0.52
CMC 1 wt% (Low Surface Tension)	31.52 ± 0.09

6.2.2 Design and Thermoforming of Substrates with Capillary Recesses

The 3D model design of a substrate with arrays of capillary recesses of different sizes was generated by computer-aided design (CAD) SolidWorks software (Edition SP 4.0-2016). The recesses had truncated cone shape with internal depth of 6 mm, draft angle of 10°. The opening diameters of the recesses were in the range of (4-12 mm). The substrate was configured with arrays of 6 even-spaced recesses of the same diameter (Section 3.3.2) as shown in Figure 6.1. The 3D design of the substrate was used for mould designing and thermoforming process to produce PET replicates of the substrate with capillary recesses that were carried out in Klockner Pentaplast Company, UK.

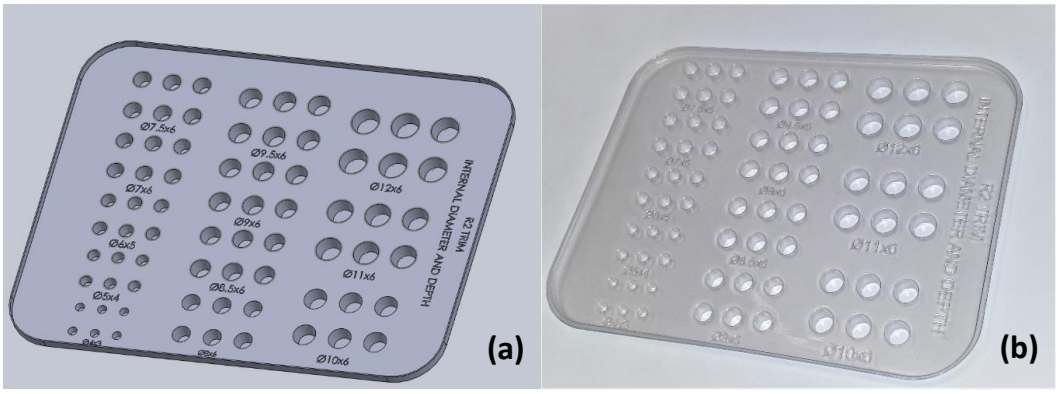

Figure 6.1: (a) 3D model design, (b) photo of thermoformed PET replicate of substrate with capillary recesses.

6.2.3 Shape Profile and Volume of Capillary Recesses

The dimensions and shape profile of the formed PET recesses were determined by digital Smartzoom 5 microscopy (Zeiss, UK) for recesses with nominal diameters of 7, 8, 9, 9.5, 10, 11 mm. The shape profiling with measurement of the geometrical dimensions and cavity volume of PET recesses were described previously in Section 5.2.3.

6.2.4 Oxygen Plasma Treatment of Capillary Recesses

The formed PET substrate was trimmed to separate each 6-recess array of the same recess size in one sample. The recess samples were cleaned to eliminate any organic contaminants by rinsing with Isopropyl alcohol.[180] A low pressure plasma unit (model: Nano, Diener Electronic, Germany) with a cylindrical chamber was used for the surface treatment (Section 3.5). The glow discharge was produced by oxygen gas supply with the vacuum pressure (base pressure: 0.1 mbar). Based on application of plasma treatment, the recess samples were separated into groups (no treatment, localised plasma treatment of recess walls, plasma treatment of recess walls and edges) as illustrated in Figure 6.2. The plasma treatments were carried out at oxygen flow rate of 80 cm^3/min, working pressure of 0.14 mbar and power of 240 W. The recesses were treated for two exposure times of 6 and 18 s to obtain the target levels of surface hydrophilicity. For localised plasma treatments of the recess walls, the selective plasma treatments of only internal surface of recess walls were conducted by placing an electrostatic film mask (made from polypropylene, PP) on the sample face surface as shown in Figure 6.3. The mask had holes for each recess, while it formed a barrier

between PET surface and excited plasma species preventing the treatment of masked areas. The PP film mask was prepared via laser cutting (Epilog Laser) and discarded after the plasma treatment.

Figure 6.2: Illustrative sketch of plasma-treated areas of PET recesses based on oxygen plasma application; (from left to right) untreated, treated walls only, treated walls and edges.

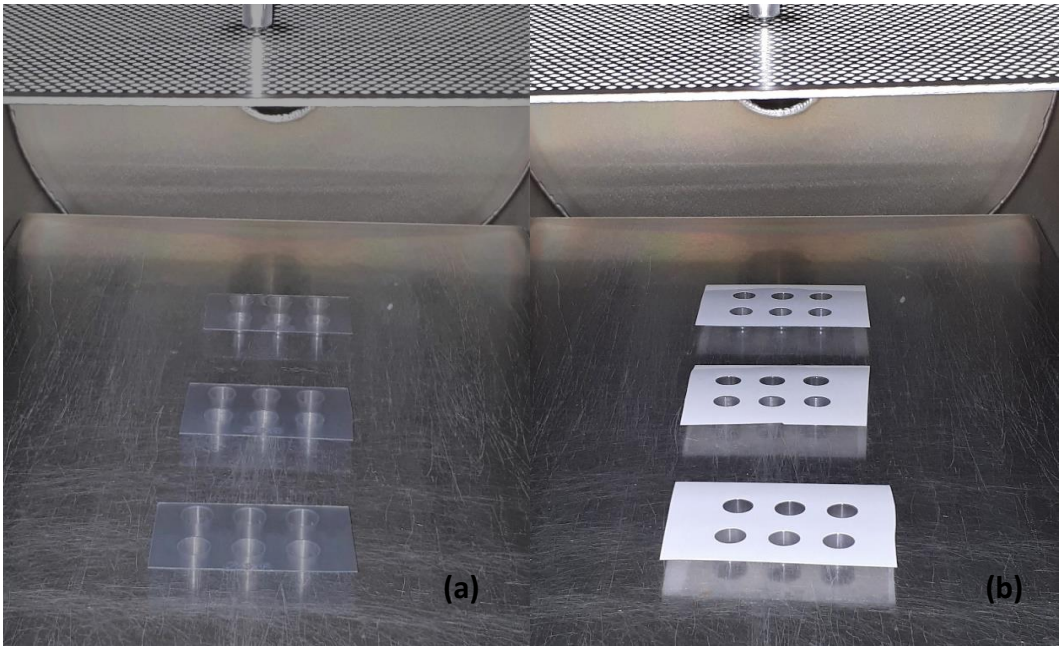

Figure 6.3: Oxygen plasma treatment of (a) unmasked and (b) masked (with perforated PP film) PET recess samples.

6.2.5 Characterisation of PET Surface Properties

6.2.5.1 Wettability and Surface Energy Measurements

Static contact angle measurements were carried out by sessile drop technique to characterise the surface wettability of the PET recesses. The contact angle of 3 µL DI water drops was measured on flat surface of the untreated and plasma-treated recesses. The measurements were conducted in (First Ten Angstroms FTA1000c) analyser system and repeated 6 times at temperature of 20 ± 1 °C and relative humidity of 54 ±

5%. The contact angle values were obtained within 2 h after plasma treatment as a mean of measured values for 6 samples. Surface energy (γ_s^{tot}) with the polar (γ_s^{p}) and dispersive (γ_s^{d}) components were also determined for the recess surfaces. The surface energy measurement was based on Owens-Wendt method (Section 3.6.1).

6.2.5.2 Surface Chemical Composition by X-ray Photoelectron Spectroscopy (XPS)

X-ray photoelectron spectroscopy (Kratos Analytical Ltd, UK) was used to analyse the surface chemistry of pristine and O_2 plasma-treated PET recess samples (Section 3.6.2). The chemical composition of the PET surfaces was characterised (5 min after the plasma treatment) in the analysis chamber under pressure in order of 10^{-8} Torr. The sample surfaces were exposed to an exciting X-ray source of monochromatic Al Kα (1486.6 eV). The photoelectrons emitted from each analysis location area were analysed by hemispherical analyser. The charge effect of the polymer surfaces was neutralised by magnetic neutralisation lens. Each sample was scanned at pass energy of 160 eV in five analysis locations. The same analysis locations were also analysed with large area scan at pass energy of 20 eV. The resulting peaks were processed with CasaXPS software (Version 2.3.22PR1.0, Casa Software Ltd). The element peaks were fitted on Shirley background and calibrated according to the reference position of carbon C 1s peak of 285.0 eV.

6.2.5.3 Surface Topography by Atomic Force Microscopy (AFM)

The effect of oxygen plasma on surface roughness of capillary recesses was evaluated by scanning their surface topography with atomic force microscopy (JPK NanoWizard 3). Cut samples in the size of 1 cm × 1 cm were taken from pristine and O_2 plasma-treated PET recesses and scanned by the AFM over areas of 1 µm × 1 µm in tapping mode (Section 3.6.3). The scanning images were analysed by Gwyddion software (Version 2.55) to determine the surface roughness parameters. The average roughness (Ra) and root mean squared roughness (RMS) values were averaged from scans of 3 different areas.

6.2.6 Liquid Retention Test of Capillary Recesses

Liquid retention capacity of the recesses was evaluated for various combinations of recess size and plasma treatment by retention test under normal gravity. The test

included tilting the recess samples (diameter: 7, 8, 9, 9.5, 10, 11 mm) for an angle of 180° over 5 s, after filling with simulant liquids as shown in Figure 6.4 (Section 3.7.1). The weight of simulant liquid in full sample (6-recess array) was measured before tilting and mounted on a sticky tape on a built-in tilting board. The weight of trapped liquid in the tilted sample was then measured representing the liquid retention capacity (g). The retention capacity was also estimated in mL/m^2 with simulant liquid (CMC 1 wt%, density: 1.0017 g/mL) for recesses of optimised retention capacity. This was based on a hexagonal packing of recesses per square metre with spacing of 1 mm between the neighbouring recesses.[223]

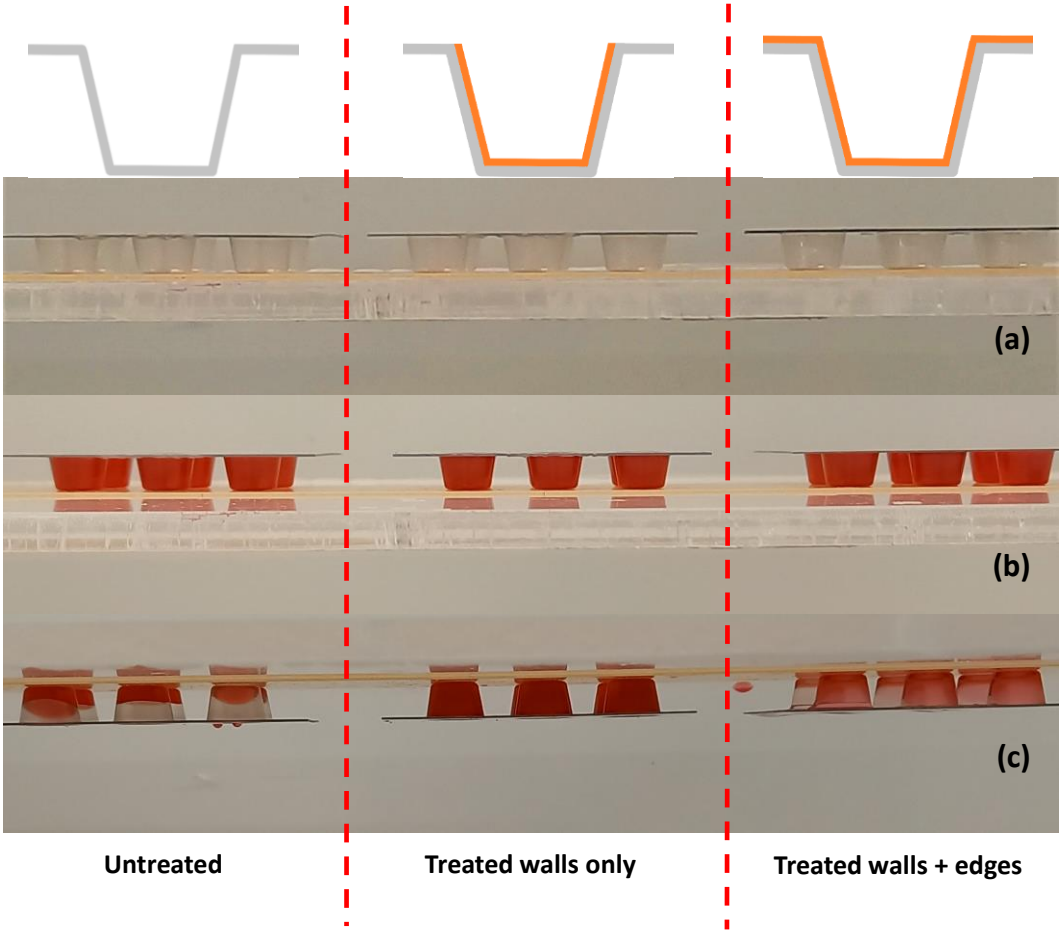

Figure 6.4: Retention test with simulant liquid (CMC 1 wt%, γ: 72.55 mN/m) of PET recesses (untreated, plasma-treated walls, plasma-treated walls and edges) with nominal diameter of 10 mm; (a) empty recesses, (b) before tilting, (c) after tilting.

6.2.7 Ageing Effect on Plasma-treated Capillary Recesses

The effect of hydrophobic recovery on surface properties and liquid retention capacity of the plasma-treated recesses (diameter: 8 and 9 mm) was assessed for different storage periods. The PET recess samples were treated with O_2 plasma for 18 s and stored in

clean plastic boxes at controlled temperature of 20 ± 1 °C (humidity 40-60 % *RH*). The degradation of wettability and surface energy was evaluated by measuring the contact angles of the test liquids on PET surfaces over storage times of 0, 1, 2, 3, 7, 14, 21, 28, 60 days. The chemical composition of the aged PET recess surfaces was analysed by XPS technique, and the liquid retention capacity was evaluated with CMC 1 wt% (γ: 52.33 mN/m) under normal gravity.

6.3 Experimental Results

6.3.1 Shape Profile and Size of Model and PET Recesses

Geometrical characterisation of the PET recesses showed consistent wells in line with nominal dimensions. Figure 6.5 shows cross-section profiles of recess model and corresponding thermoformed PET recess with diameter of 9 mm. All thickness, dimension and volume values were measured for recesses with nominal diameters of 7, 8, 9, 9.5, 10, 11 mm and presented in Table 6.2. The PET recesses had a comparable replication of geometrical dimensions of their models with error less than 0.04 mm for opening diameters, 0.08 mm for cavity depths and 3.17° for draft angles. The wall thickness profiles exhibited wall thinning towards the bottom corners. This is due to deformation and stretching during thermoforming process.[227] The opening of the PET recesses had round corners due to irregular wall thickness resulting in a variation of their opening diameters. Therefore, the bottom of the round corners was a reference point to measure the opening diameters. The measured recess volumes were proportional with recess sizes. Recesses with diameters of 7 mm and 11 mm had the smallest and largest cavity volumes of 0.208 mL and 0.521 mL respectively.

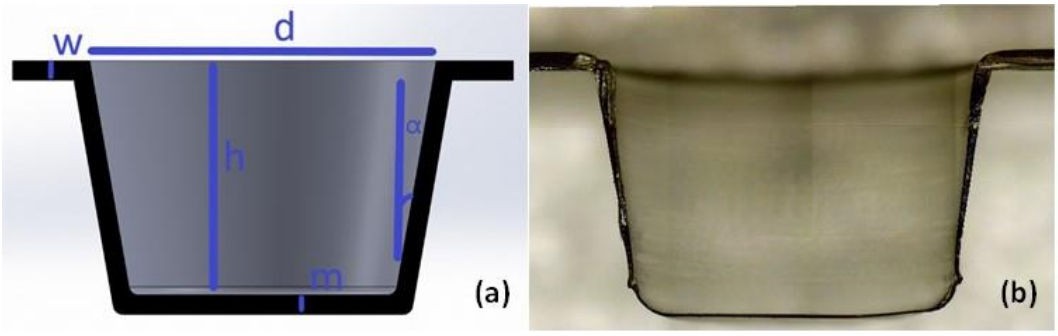

Figure 6.5: 2D cross-section profile of (a) recess model and (b) thermoformed PET recess with nominal diameter of 9 mm. The wall thickness measurements are taken for the substrate (w) and recess base (m). The geometrical dimensions of the recesses are measured for opening diameter (d), cavity depth (h) and wall draft angle (α).

Table 6.2: Average recess cavity volume, geometrical dimensions, and wall thickness of thermoformed PET recesses.

Recess Model	Thermoformed PET Recess					
	Geometrical Dimensions (mm)			Wall Thickness (mm)		Recess Volume (mL)
Diameter	Diameter (d)	Depth (h)	Draft Angle (α)	Substrate (w)	Base (m)	
7	6.992 ± 0.009	5.975 ± 0.028	7.010 ± 0.605	0.496 ± 0.041	0.043 ± 0.011	0.208 ± 0.003
8	8.004 ± 0.004	5.982 ± 0.032	7.078 ± 0.402	0.464 ± 0.037	0.059 ± 0.019	0.270 ± 0.005
9	8.961 ± 0.023	5.974 ± 0.060	6.867 ± 0.252	0.478 ± 0.008	0.077 ± 0.004	0.346 ± 0.006
9.5	9.470 ± 0.035	5.923 ± 0.085	6.833 ± 0.379	0.456 ± 0.027	0.087 ± 0.007	0.389 ± 0.008
10	9.965 ± 0.046	5.952 ± 0.074	6.900 ± 0.400	0.495 ± 0.015	0.104 ± 0.003	0.440 ± 0.008
11	10.970 ± 0.023	5.929 ± 0.072	6.967 ± 0.208	0.483 ± 0.047	0.121 ± 0.005	0.521 ± 0.004

6.3.2 Wettability and Surface Energy Analyses for Plasma-treated PET

The surface wettability of untreated and plasma-treated PET recesses is represented by measured WCA in Figure 6.6a. The untreated PET surface exhibited a WCA of 77.6 ± 0.6°. The O_2 plasma treatment resulted in a dramatic increase in surface wettability reflected in the decrease of WCA to 46.5 ± 0.5° and 15.3 ± 0.4° for treatment times of 6 s and 18 s respectively. The PET surfaces will be identified by their characteristic WCA due to the consistency in their wettability results. Figure 6.6b illustrates the effect of O_2 plasma treatment on surface energy of PET recesses. The total surface energy of untreated PET was 47.7 ± 0.5 mJ/m^2 with a dispersive component of 44.3 ± 0.7 mJ/m^2 and a polar component of 3.4 ± 0.4 mJ/m^2. The surface energy of plasma-treated PET considerably increased and was proportional with the treatment time. The total surface energy reached 76.5 ± 0.5 mJ/m^2 after O_2 plasma treatment for 18 s. This corresponded to an increase in polar component by a factor of approximately 9 times, while dispersive component showed no significant changes.

6.3.3 Chemical Composition of Plasma-treated PET

The chemical composition of untreated PET and plasma-treated PET was characterised through XPS survey spectra as shown in (c) and (d) of Figure 6.6. Both untreated and plasma-treated PET surfaces had distinct peaks for carbon C 1s and oxygen O 1s. Small peak of Si 2p for silicon was also detected as it was potentially originated from the silicon oil used in food packaging production as a de-nesting agent. The wide spectrum of plasma-treated PET surface showed an increase in O 1s peak intensity and decrease in C 1s peak intensity with appearance of additional small peak of nitrogen N 1s. Table 6.3 presents the O/C ratio and atomic concentration of the elements detected on untreated and plasma-treated PET surfaces. The O/C ratio of untreated PET was 27.07 % corresponding to O% of 21.28 % and C% of 78.63 %. The O_2 plasma treatment increased O/C ratio to reach 40.12 % and 44.29 % for PET surface treated for 6 s and 18 s respectively. This corresponded to an increase in the oxygen concentration and reduction of carbon concentration as shown in the Table 6.3. The nitrogen element was present after plasma treatment in small concentrations of 0.11 % and 0.20 % for treatment times of 6 s and 18 s respectively. The C 1s peak was deconvoluted into different components to characterise the functional groups on the PET surface as shown in Figure 6.7. The analysed C 1s peak of untreated and plasma-treated PET showed four peak components at binding energies of 285.0, 286.6, 289.0 and 291.5 eV accounting for C-C/C-H, C-O, O-C=O and pi-pi* shake-up bonds respectively. Functional group of C=O bond was formed at a binding energy of 287.5 eV after the plasma treatments. Concentrations of the functional groups are presented in Table 6.4. The C=O bond was emerged with concentrations of 2.95 % and 5.09 % for plasma treatments of 6 and 18 s respectively.

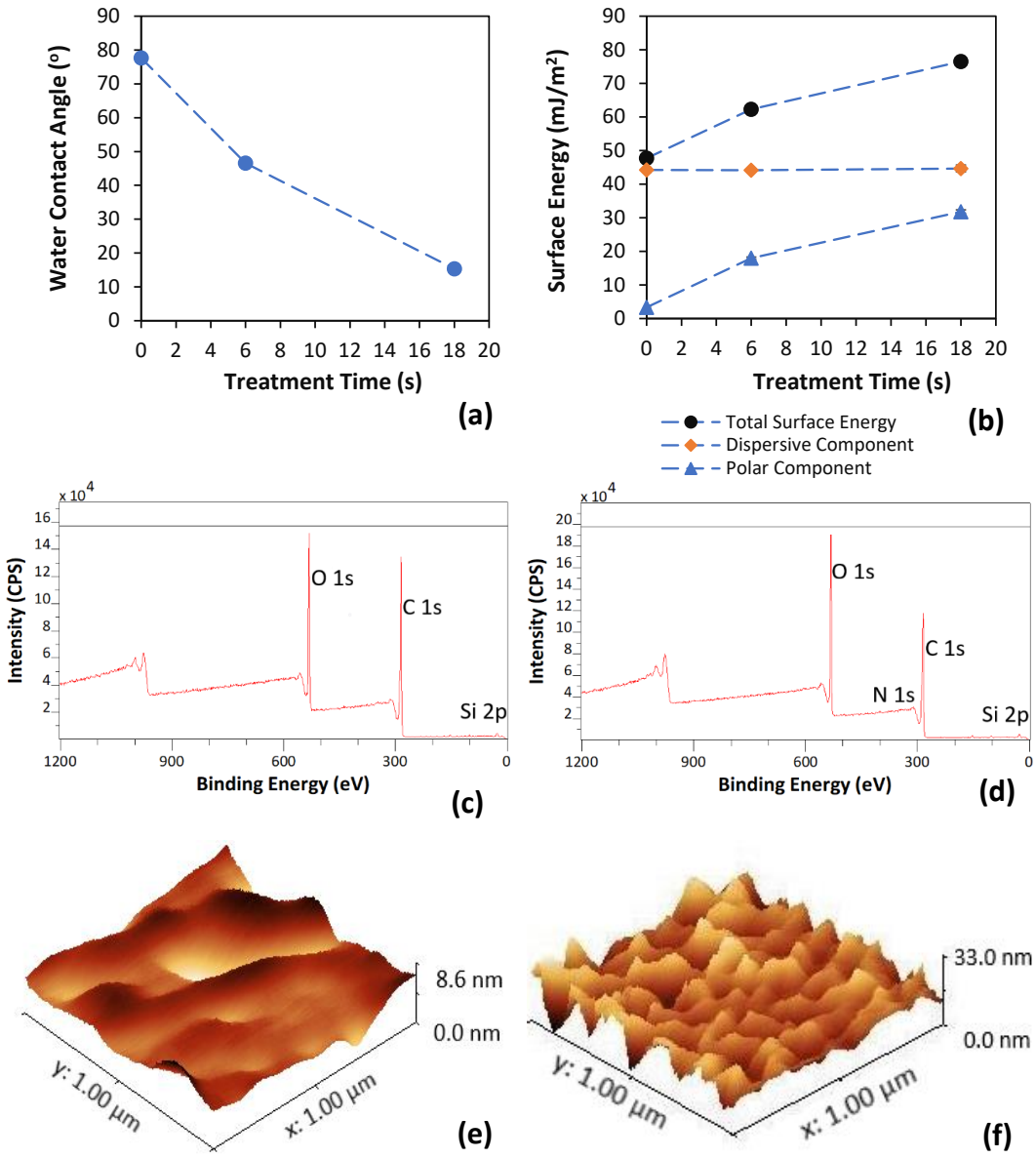

Figure 6.6: Changes in surface properties of PET recesses over O_2 plasma treatments; (a) water contact angle, (b) surface energy, (c) wide XPS spectrum of untreated PET, (d) wide XPS spectrum of plasma-treated PET for 18 s, (e) 3D AFM image of untreated PET, (f) 3D AFM image of plasma-treated PET for 18 s.

Table 6.3: Elemental composition and O/C ratio of PET recess surfaces.

Atomic Concentrations of Surface Elements on the PET surface					
PET Recess Surface	C%	O%	Si%	N%	O/C
Untreated	78.63 ± 0.13	21.28 ± 0.16	0.09 ± 0.06	-	27.07 ± 0.25
Plasma-treated for 6 s	71.17 ± 0.14	28.55 ± 0.12	0.17 ± 0.06	0.11 ± 0.06	40.12 ± 0.21
Plasma-treated for 18 s	69.11 ± 0.36	30.61 ± 0.18	0.08 ± 0.04	0.20 ± 0.13	44.29 ± 0.22

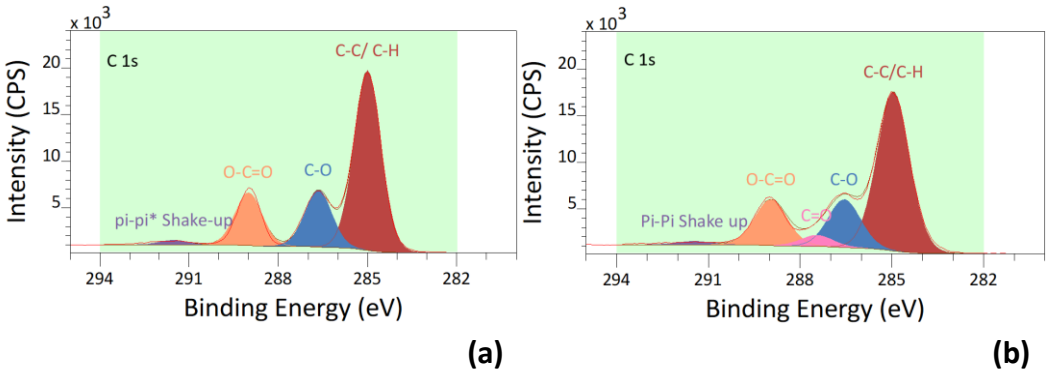

Figure 6.7: Functional groups deconvoluted from high-resolution C 1s peak for (a) untreated PET and (b) plasma-treated PET for 18 s.

Table 6.4: Atomic concentrations of functional groups of C 1s for PET recess surface before and after O_2 plasma treatment for 18 s.

Atomic Concentration (%) of C 1s Components					
	C-C, C-H	C-O	C=O	O-C=O	Pi-Pi*
Binding Energy (eV)	285.0	286.6	287.5	289.0	291.5
Untreated	63.89 ± 0.18	18.46 ± 0.18	-	16.44 ± 0.22	1.22 ± 0.14
Plasma-treated for 6 s	54.61 ± 0.65	21.65 ± 0.45	2.95 ± 0.13	19.37 ± 0.26	1.41 ± 0.12
Plasma-treated for 18 s	60.22 ± 0.50	16.68 ± 0.38	5.09 ± 0.43	17.21 ± 0.28	0.80 ± 0.31

6.3.4 Nanoscale Surface Topography of Plasma-treated PET

The surface texture of PET recesses was studied at nanoscale using AFM for scanned areas of 1 µm × 1 µm. The surface topography before and after plasma treatment were characterised by surface roughness parameters of RMS and Ra as presented in Table

6.5. The RMS and Ra before plasma treatment were 1.44 nm and 1.12 nm respectively. The PET recesses had rougher surface after 18 s of the plasma treatment attributed to RMS of 6.73 nm and Ra of 4.84 nm. The topological features are visualised in the 3D AFM images for untreated PET (e) and plasma-treated PET (f) in Figure 6.6. The untreated PET had nearly smooth surface, while it showed rougher surface with small spike-like features after the plasma treatment.

Table 6.5: Root mean squared roughness (RMS) and average roughness (Ra) parameters of PET recess surfaces.

PET Recess Sample	RMS (nm)	Ra (nm)
Untreated	1.44 ± 0.29	1.12 ± 0.25
Plasma-treated	6.73 ± 1.68	4.84 ± 2.12

6.3.5 Liquid Retention Test of PET Recesses

6.3.5.1 Effect of Recess Size and Surface Wettability

Retention capacity of PET recess samples (6-recess arrays) of each size (nominal diameter: 7, 8, 9, 9.5, 10, 11 mm) was investigated after mild plasma treatment for 6 s and strong treatment for 18 s. The corresponding surface wettability of the plasma-treated recesses was represented by the characteristic WCA of 46.5° and 15.3° respectively. Figure 6.8 shows retention capacity of the recess samples before, after non-localised and localised O_2 plasma treatments of their inner walls. The retention capacity value was average of 6 repeated measurements with simulant liquid (CMC 1 wt%, γ: 52.33 mN/m). The samples with recess diameter of 7 mm maintained full (retention capacity: 1.214 g) before and after localised plasma treatments. The retention capacity of all recesses with diameter > 8 mm decreased with the increase of their sizes. The recess samples treated with localised O_2 plasma exhibited higher retention capacity than untreated samples. The selective improvement in wall surface wettability increased recess capacity to trap the simulant liquid. In contrast, wettability improvement of the combined recess edges and walls (non-localised treatment) diminished their retention capacity to even lower than untreated samples. For example, the retention capacity of untreated sample (recess diameter: 9 mm) increased from 0.696 g to 1.500 g after localised plasma treatment for 18 s. However, the corresponding non-localised plasma decreased the retention capacity to 0.392 g. The retention capacity

was proportionate to the wall surface wettability of PET recesses as it was higher for WCA of 15.3° than WCA of 46.5°.

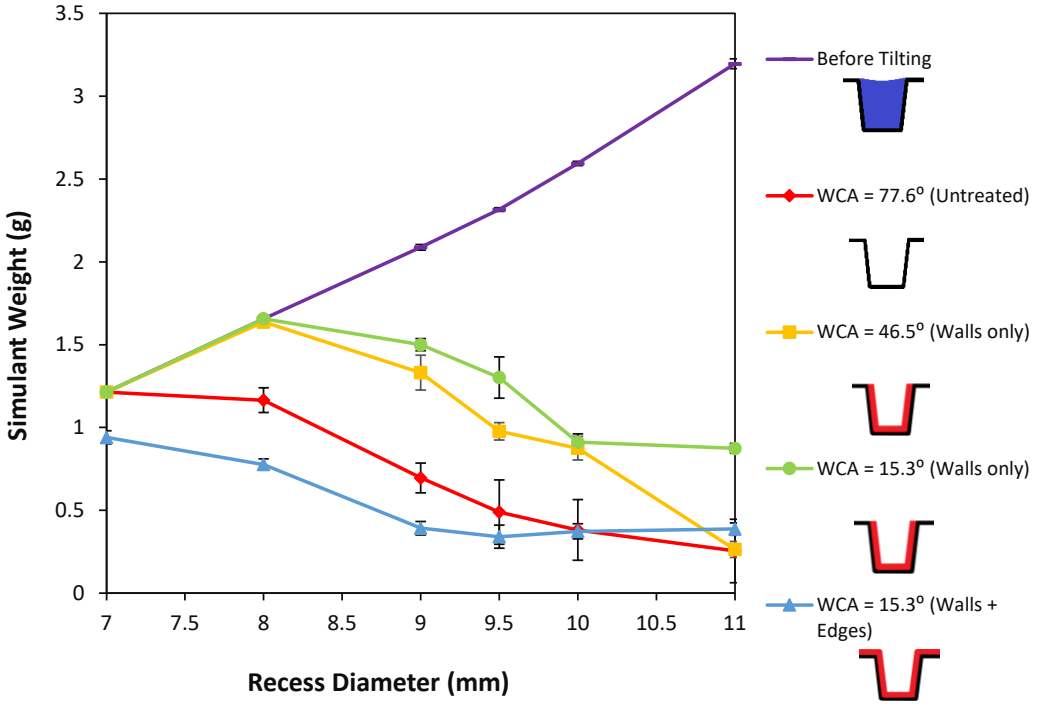

Figure 6.8: Retention capacity of tilted PET recess samples (6-recess arrays) with CMC 1 wt% (γ: 52.33 mN/m) after oxygen plasma treatments; untreated, mild localised treatment (6 s, WCA: 46.5°, recess walls only), strong localised treatment (18 s, WCA: 15.3°, recess walls only), strong full-area treatment (18 s, WCA: 15.3°, recess walls + edges).

6.3.5.2 Effect of Liquid Surface Tension and Recess Surface Wettability

Simulant liquids (CMC 1 wt%) with surface tension values of 72.55, 52.33, 31.52 mN/m were used for retention test of the recess samples. Figure 6.9 illustrates the effect of liquid surface tension on retention capacity of untreated samples (a) and samples with localised plasma treatment of 18 s (b). The recess walls treated with O_2 plasma had WCA of 15.3° while the outer edge surface had WCA of 77.6°. For both untreated and plasma-treated samples, the retention capacity was proportionate with the liquid surface tension. For the simulant liquid with surface tension of 72.55 mN/m, the untreated samples maintained full after tilting until recess diameter of 9 mm while plasma-treated samples until recess diameter of 10 mm with retention capacity of 2.594 g. The corresponding untreated sample (recess diameter: 10 mm) had only retention capacity of 0.783 g. The increase in liquid surface tension notably magnified the plasma treatment effect (wall surface wettability) on improving liquid retention of recess

samples. Lower surface tension of 52.33 mN/m led to a sharp decrease in retention capacity of untreated recess samples. This had less impact on the retention capacity of the plasma-treated samples as shown in Figure 6.9. However, both untreated and plasma-treated samples for all recess sizes could not retain the lowest surface tension liquid (31.52 mN/m).

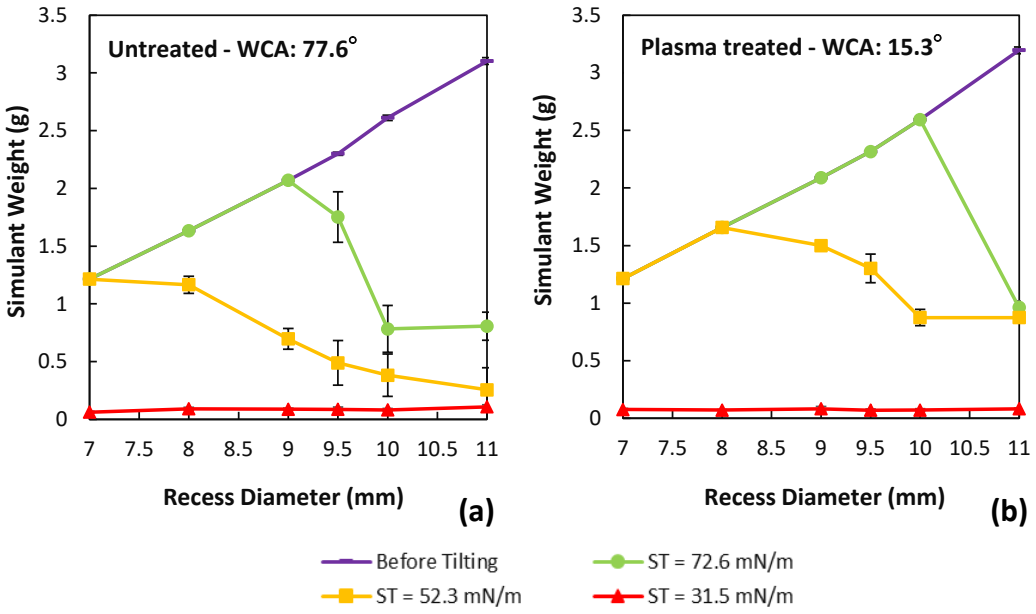

Figure 6.9: Retention capacity of PET recess samples (6-recess arrays) with CMC 1 wt% (γ: 72.55, 52.33, 31.52 mN/m) before (a) and after (b) localised O_2 plasma of internal recess walls.

6.3.6 Ageing Effect Analysis

6.3.6.1 Ageing Effect on Surface Properties of Plasma-treated PET Recesses

The surface hydrophobic recovery of plasma-treated PET recesses was investigated for their wettability, surface energy and chemical composition over different ageing times. The recess samples treated with O_2 plasma for 18 s were stored in air. WCA, surface energy and XPS measurements were performed for the aged samples during storage periods of 0, 1, 2, 3, 7, 14, 21, 28, 60 days. Figure 6.10 shows WCA (a) and surface energy (b) developed on plasma-treated PET over the storage times. The WCA sharply increased from 15.3° to 34.6° in the first three storage days as the ageing rate of treated PET surface was high. It was then increased gradually to reach 54.8° after 28 days. The WCA was almost stable between 28 and 60 days. The surface energy of plasma-treated PET substantially decreased in the first three days from 76.5 mJ/m^2 to 66.1 mJ/m^2. It then decreased gradually forming a plateau after 28 days. This corresponded to a similar

decrease in the polar component of surface energy while the dispersive component was constant. The reduced wettability and surface energy of the aged PET reflected its tendency to return to its original surface properties before the plasma treatment.

The elemental composition of aged PET surface after O_2 plasma treatment showed a decrease in oxygen concentration over the storage periods as shown in Table 6.6. This revealed a loss of functional polar oxygen groups on the aged PET surface. The highest ageing rate was observed in the first day with a reduction in oxygen concentration from 30.61 % to 28.30 % corresponding to a decrease in O/C ratio from 44.29% to 39.65%. The oxygen concentration then slightly decreased over the ageing time. After 60 days, the oxygen concentration was 27.23 % and O/C ratio was 37.90 %, which are still higher than the corresponded values of untreated PET with O% of 21.28 % and O/C of 27.07 %. Therefore, part of oxygen groups introduced by the plasma treatment remains on PET surface for relatively long ageing time. The nitrogen content showed a slight increase over time, while the silicon element showed no significant changes in its concentrations.

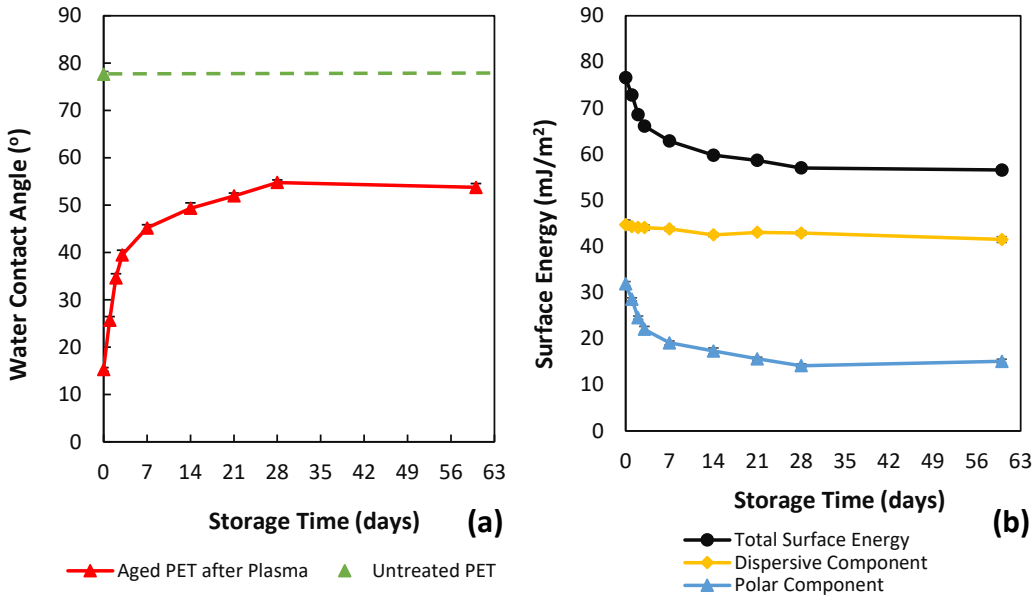

Figure 6.10: Changes of surface properties of PET recess surface treated with plasma for 18 s over different storage times; (a) water contact angle, (b) surface energy.

Table 6.6: Changes in elemental composition and O/C ratio of O_2 plasma-treated PET surface over ageing times.

Atomic concentrations of surface elements on the aged PET surface					
Ageing Time (days)	C%	O%	Si%	N%	O/C
0	69.11 ± 0.36	30.61 ± 0.18	0.08 ± 0.04	0.20 ± 0.13	44.29 ± 0.22
1	71.38 ± 0.10	28.30 ± 0.09	0.13 ± 0.02	0.18 ± 0.06	39.65 ± 0.17
2	71.45 ± 0.11	28.08 ± 0.08	0.15 ± 0.03	0.32 ± 0.08	39.30 ± 0.15
3	71.59 ± 0.15	27.93 ± 0.09	0.14 ± 0.02	0.34 ± 0.06	39.01 ± 0.21
7	71.73 ± 0.13	27.87 ± 0.07	0.14 ± 0.03	0.26 ± 0.04	38.85 ± 0.16
14	71.69 ± 0.07	27.60 ± 0.04	0.45 ± 0.01	0.27 ± 0.05	38.50 ± 0.08
21	71.84 ± 0.09	27.63 ± 0.09	0.24 ± 0.03	0.29 ± 0.10	38.46 ± 0.14
28	71.87 ± 0.06	27.54 ± 0.08	0.27 ± 0.07	0.31 ± 0.07	38.32 ± 0.13
60	71.84 ± 0.21	27.23 ± 0.15	0.37 ± 0.05	0.57 ± 0.05	37.90 ± 0.32
Untreated	78.63 ± 0.13	21.28 ± 0.16	0.09 ± 0.06	-	27.07 ± 0.25

6.3.6.2 Ageing Effect on Retention Capacity of Plasma-treated PET Recesses

Liquid retention capacity of recess samples after localised O_2 plasma treatment was investigated for storage times of 0, 1, 3, 7, 14, 21, 28, 60 days. This was illustrated in Figure 6.11 for samples with recess diameter of 8 mm (a) and 9 mm (b) with simulant liquid (CMC 1 wt%, γ: 52.33 mN/m). The plasma-treated samples with recess diameters of 8 and 9 mm maintained constant retention capacity of 1.664 g and 1.558 g respectively over the storage times. However, the corresponding untreated samples had retention capacity of 1.165 g and 0.696 g respectively as shown in Figure 6.11. For practical application of liquid-holding recesses within food packaging, the retention capacity is also assessed by the liquid volume (mL) retained in a square metre. This capacity can be optimised by hexagonal packing with spacing distance of 1 mm between the circular recesses in 0.9 m^2 taking limited draw ratio of thermoforming process into consideration.[223] Therefore, the retention capacity of plasma-treated

recesses with diameter of 8 and 9 mm was 3901 ± 22 and 2972 ± 62 mL/m^2 respectively after 60-day ageing period.

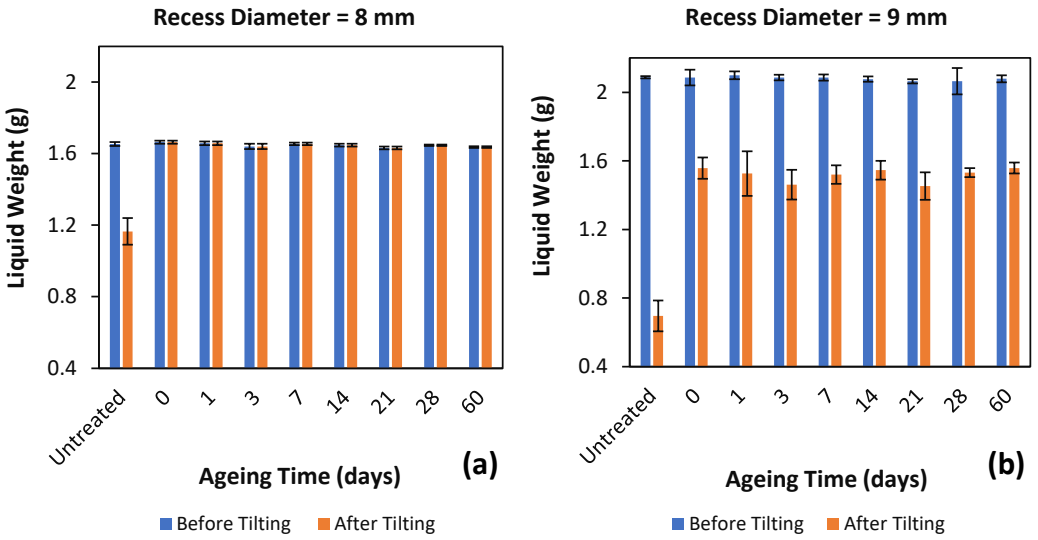

Figure 6.11: Liquid retention capacity of plasma-treated PET samples with nominal recess diameters of 8 mm (a) and 9 mm (b) over different storage times.

6.4 Discussion

6.4.1 Shape Profile and Dimensions of Recesses

The thermoformed PET recesses were dimensionally very consistent and similar to the designed models with only very small deviations as observed in their cross-section visualisation. These deviations may occur due to irregular distribution of wall thickness during vacuum thermoforming with high draw ratios. The elastic shrinkage and release of residual stress of the formed PET recesses can also contribute to these small scale dimensional deviations.[228–230]

6.4.2 Plasma Impact on Recess Surface Properties

The O_2 plasma treatment of PET recesses increased their surface hydrophilicity and therefore their wettability for water-based liquids.[68,169,176] It functionalised the untreated PET surface with hydrophilic oxygen groups, such as C-OH and COOH causing a decrease in WCA. The prolonged plasma treatment further decreased the WCA to 15.3° as more hydrophilic groups were attached on the treated surface.[179,222] The modification treatment is initiated with scission of C-C bonds in the polymer chains and hydrogen abstraction. This is carried out by the highly reactive plasma species, such as radical oxygen and hydroxyl groups forming radical sites. The

excited oxygen in plasma glow reacts with the radical sites to generate different oxygen groups including C-OH, C=O and COOH.[169,204] A comparable decrease in WCA from 72° to 19° on PET surface was found after O_2 plasma in work of Junkar et al.[222] The polar oxygen groups also contributed to the substantial increase in polar component of surface energy by 28.5 mJ/m^2 (3.4 to 31.9 mJ/m^2), which primarily accounted for the increase in total surface energy of 28.8 mJ/m^2. A comparable increase in surface energy of plasma-treated PET was found by Yang et al.[204]

Oxygen plasma treatment resulted in increasing oxygen concentration and hence O/C.[169,222] This was manifested as additional oxygen groups, such as C=O were introduced to the treated recess surface.[204] The O/C was also proportionate with treatment time as high number of active sites are ready to incorporate oxygen groups for prolonged treatments.[179] Therefore, the increase in oxygen concentration can explain the increased wettability and surface energy of the plasma-treated PET. Similar effects of plasma treatments have been reported by different studies.[182,204,222] The C 1s peak analysis (Table 6.4) showed that under the plasma treatment new C=O was formed, while absent from the untreated samples. This has been observed to significantly improve the surface polarity and wettability in literature.[179,231] As well as an increase in oxygen to carbon ratio, small amounts of nitrogen were detected in the plasma-treated samples. This element might be present due to post-plasma reaction between the activated surface and the nitrogen in air.[217] The peak of pi-pi satellite appeared due to the emitted photoelectrons of excited aromatic phenyl groups.[220]

Etching effect of the plasma treatment led a substantial increase in nanoscale surface roughness of the PET recesses. The excited plasma particles have more predominating etching and eroding impact on the amorphous areas of the PET surface than crystalline areas. The varied etching rate over the treated surface may have resulted in rougher PET surface with larger projected area.[180] This could contribute to long-lasting improvement in wettability of PET recesses even after ageing due to increased interface between the PET surface and contacting liquid,[180,232] based on Wenzel law.[87]

6.4.3 Liquid Retention Capacity of PET Recesses

The localised increase in wettability and surface energy was an effective means of enhancing liquid retention of the PET recesses. This allows manufacturing of food

plastic trays incorporated with recesses of increased liquid-holding capacity. Therefore, food exudate released from even very exudative food products can be isolated and retained in the designated recesses during the product shelf life. The liquid trapping functionality gained by the capillary recesses can be explained by the liquid pinning phenomenon and pressures acting on liquid interface. This was investigated by Extrand[125,127] for capillary tubes and orifices in vertical and inclined positions. Liquid in a capillarity with closed-top end is subject to encountering atmospheric and hydrostatic pressures. A capillary pressure also acts on the liquid to form a meniscus on the recess walls.[125] Liquid drainage in a tilted large capillarity such as a recess is induced by propagation of air finger (Taylor finger) into the liquid-air interface due to instability in the liquid meniscus. This results in replacing the liquid with air as the liquid forms a film on the capillarity walls and drains out of the open end.[124,126]

The recess opening has a geometrical valving functionality where the capillary pressure induces liquid pinning effects and forms valving pressure barrier.[120] This enhances stability of the liquid menisci and prevent liquid drainage due to phenomenon of Taylor finger.[126] This was manifested in stable menisci on recess openings of small sizes as the capillary pressure and pinning effects are large enough to restrict initiation of the air finger. The atmospheric pressure upwardly acting on liquid meniscus, therefore, was able to retain the liquid in the tilted small recesses as explained by Extrand.[125] For example, the recesses with diameter of 7 mm were maintained full during and after tilting even without plasma treatment. However, the liquid interface had smaller curvature for untreated recesses with larger sizes as the capillary pressure decreased.[125] The recess inclination during tilting resulted in local change in the hydrostatic pressure acting on the liquid interface.[233] This resulted in liquid advancing on one recess wall and receding on the other wall as described by work of Extrand.[127] The low capillary pressure of untreated large recesses resulted in unstable meniscus and diminished pining effect against the advanced meniscus. This facilitated air finger propagation leading to liquid drainage of the recesses.[125–127]

On the other hand, the localised plasma treatment of internal recess walls improved the pinning effect and pressure barrier on the recess opening. The low surface energy of PET recesses allowed localised plasma treatment to induce a considerable variation in wetting properties between the inner walls and outer edges of the treated recesses.[76] This introduced additional pinning effect due to the wettability variation,

which acts as capillary burst valve. Therefore, the recess openings gained improved liquid pinning from combined valving effects of geometrical and wettability changes.[113,114] This provided the liquid menisci with more resistance to the air finger propagation and liquid drainage, particularly for larger recesses in comparison with corresponding untreated recesses. Consequently, the stability of liquid menisci and pinning effects were enhanced for the plasma-treated recesses leading to higher liquid retention capacity. The retention capacity was also proportionate with wall surface wettability as the wetting properties between the walls and outer edges were further magnified.[113,125,234] However, the decrease in liquid surface tension resulted in less stable liquid interfaces and lower capillary pressure barriers. Therefore, the recess resistance to drainage was undermined causing reduced retention capacity. This was also found by Kumar et al[126] in liquid drainage from closed tubes.

For liquid with the lowest surface tension (31.52 mN/m), there was a lack of retention capacity as the liquid surface tension was lower than the surface energy of the untreated substrate (47.7 mJ/m^2). This caused a complete wetting of the recess edges leading to evacuation of the liquid from recess cavities in all conditions (both untreated and locally treated). Non-localised plasma treatment increased hydrophilicity (WCA: 15.3°) on both wall and edge surfaces. The highly hydrophilic outer edges led to enhancing adhesive forces on the edges surface. These forces compete with cohesive forces of the liquid and prevent pinning of liquid menisci. This was reported by Kazemzadeh et al[119] for highly hydrophilic capillary valves. The retention capacity of samples (recess diameter: 9 mm) with localised and non-localised O_2 plasma treatment (WCA: 15.3°) was 1.500 g and 0.392 g respectively, but retention capacity of the corresponding untreated samples was 0.696 g. This provides the conclusion that the liquid retention improvement requires a distinct difference in wetting characteristics between the recess walls and their outer edges.

6.4.4 Longevity and Practicality of Plasma Treatment

The improved retention capacity and surface properties of PET recesses gained by the O_2 plasma treatment were subject to ageing during the storage periods. This was manifested in increasing WCA and decreasing surface energy over 60 days. It also corresponded to the decrease in oxygen concentration and O/C ratio over the ageing time. Ageing phenomenon is observed in polymer surfaces after plasma treatments as

the aged surfaces exhibit tendency to lose their polar groups and become more hydrophobic surfaces.[179] This includes migration of non-polar groups from the polymer matrix to the treated surface. The polymer chains may also experience reorientation resulting in burying the functional groups inside deeper layers of the polymer surface.[180,235] However, WCA on the aged PET after 60 days was still substantially lower than untreated PET (53.7° vs 77.6°), and surface energy remained higher than the untreated PET (see Figure 6.10). This suggests that plasma treatment induced a permanent increase in the surface wettability and energy.[182] A comparable recovery behaviour was reported by Kostov et al[180] and Homola et al.[182] Despite the apparent reduction in surface wettability and oxygen to carbon ratio, the partial hydrophobic recovery still allowed the wettability transition between the recess walls and outer edges to be maintained. This contributed to improved pinning effect and retention capacity of the treated recesses during ageing times.[234] Even after 60 days, the treated recess cavity was fully functional, allowing similar high retention, with no drop in performance.

For liquids with comparable surface tension value of meat exudate, retention capacity of aged PET recesses with diameter of 9 mm was 2972 ± 62 mL/m^2 as an increase of 2.24 times after the localised plasma treatment. This showed a comparable retention capacity with conventional absorbent meat pads. These absorbent pads are typically used in meat packaging industry with retention capacity of 3000 mL/m^2 (2949 mL/m^2 as assessed in laboratory by simulant liquid on a sample). The enhanced liquid retention lasts long enough for practical use by packaging companies, and realistically a plasma unit could easily be incorporated to the production line.[171]

6.5 Closure

This work has demonstrated that localised increases in surface wettability of capillary recess walls by plasma treatment is an effective method to increase their liquid retention capacity. Plasma-treated PET recesses of extended sizes demonstrated a considerable and long-lasting increase in their liquid retention capacity (2.24 times) when compared with untreated PET samples. The localised oxygen plasma treatment introduced polar oxygen groups onto the PET recess surface resulting in an increase in surface wettability and energy. These surface energy increases were partially diminished over time due to ageing effects. However, this was not at the expense of liquid retention

capacity as the plasma-treated inner walls maintained wetting characteristics different to the untreated outer edges. The treated recesses were able to exploit the capillary valving functionalities, even after 60 days of ageing, to form more stable menisci and prevent liquid drainage. This resulted in a potential capacity of around 2900 mL/m^2. This liquid retention capacity, and the relative improvement offered by the modification vs standard recesses were very similar to the benefits provided by the capillary recesses reported previously (Chapter 5) and both were comparable with current absorbent pads.

Having demonstrated that the capacity of thermoformed recesses can be substantially and similarly increased by either modifying their geometry or via selective plasma treatment, the next chapter will explore modifications that can be made to foam packaging so that it may also act as a reservoir for exudate.

Chapter 7

Improvement in Liquid Absorption of Open-Cell Polymeric Foam by Plasma Treatment for Food Packaging Applications

7.1 Introduction

In the previous two chapters, substantial increases in the liquid retention within food packaging could be achieved via thermoformed plastic recesses with either modified geometry of the recesses or selective plasma treatment. This chapter describes an innovative approach in scavenging meat exudate within commercial plastic packaging by surface modification of the porous structure of plastic foam packaging. This involves improving the liquid absorption capabilities of open-cell polystyrene (PS) foam through the application of oxygen plasma treatment rather than chemical wetting agents. The excited plasma species diffuse into the porous foam structure introducing polar oxygen groups onto the pore walls and improves their surface hydrophilicity. Hence, the foam pores, with enhanced wettability towards water-based liquids, are proposed to have a larger sucking capillary pressure thus increasing the absorption capacity of the porous PS foam. Open-cell PS foam sheets were extruded and cut into cubic samples. Oxygen plasma was used to treat the foam samples and the impact of this treatment on their liquid absorption capacity and surface properties was evaluated. The longevity of the plasma treatment was investigated by carrying out liquid absorption tests after different post-treatment times.

7.2 Materials and Experimental Methodology

7.2.1 Materials

Open-cell PS foam was supplied as plain sheets with thickness of 5 mm from large-scale industrial foam (Klockner Pentaplast Group, UK) as shown in Figure 7.1. The foam sheet had impermeable skin on top and bottom sides (Section 3.3.1), and it was cut into rectangle-shaped samples for surface characterization and absorption tests. DI water and Triton X100 surfactant (Sigma Aldrich, UK) were used to prepare test liquids (surfactant simulants) with different surface tension values to cover a range of wetting behaviours of meat exudate (Section 3.2.2.2.3). BSA simulant was also prepared to mimic the presence of proteins in meat exudate and assess their effect on the liquid absorption capacity of PS foam (Section 3.2.2.2.2). Red azorubine colorant- E122

(FastColours LLP, UK) was added to stain the test liquids in absorption tests. The test liquids and their surface tensions are presented in Table 7.1.

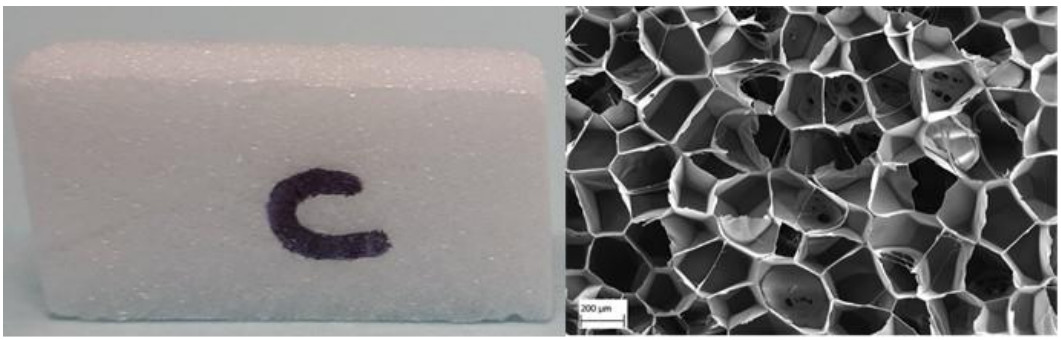

Figure 7.1: (a) Photo of white open-cell PS foam, (b) SEM micrograph of cross-section of open-cell PS foam. The letter "C" is the label of control sample.

Table 7.1: Test liquids and their surface tensions used in absorption tests.

Test liquid	Surface Tension (mN/m)
Surfactant Simulant (High Surface Tension)	72.63 ± 0.16
Surfactant Simulant (Medium Surface Tension)	52.28 ± 0.31
Surfactant Simulant (Low Surface Tension)	31.54 ± 0.28
BSA 8 wt%	52.03 ± 0.52

7.2.2 Structural Characterisation of PS Foam Materials

7.2.2.1 Foam Density and Expansion Ratio

Representative cubic samples were taken from PS foam by a sharp scalpel. The foam samples had dimensions (L x W x T: 20 mm x 20 mm x 5 mm) and were weighed on analytical scale (Model: A200S, Sartorius Analytic, Germany) with resolution of 0.0001 g. The density of PS foam was based on ratio of the mass of the foam samples to their geometric volumes (Section 3.4.2.1). Expansion ratio (ψ) measurement was based on the ratio of solid PS polymer density (ρ_s) to the measured density of PS foam sample (ρ_f) (Section 3.4.2.2) as shown in equation (7.1):

$$\psi = \frac{\rho_s}{\rho_f} \qquad (7.1)$$

7.2.2.2 Porosity and Pore Size Distribution

The porosity (n) of PS foam represents the ratio of gas volume (V_{gas}) occupying pore spaces to the geometric volume of the foam sample (V_f) (Section 3.4.2.3). The volume of pore space was calculated by subtracting the volume of solid polymer (V_s) from the geometric volume of the foam sample (V_f) with dimensions (L x W x T: 20 mm x 20 mm x 5 mm). Therefore, the porosity is presented in equation (7.2):

$$n = \frac{V_f - V_s}{V_f} = \frac{\frac{m_f}{\rho_f} - \frac{m_f}{\rho_s}}{\frac{m_f}{\rho_f}} = 1 - \frac{\rho_f}{\rho_s} \qquad (7.2)$$

where m_f is the mass of the foam sample, ρ_f is the density of the foam sample, ρ_s is the density of the solid polymer.

The pore structure and pore size distribution of PS foam was characterised by scanning electron microscope (SEM, Zeiss Evo-LS25, UK) (Section 3.4.2.4). The cross-sections of intact foam samples were prepared for imaging by scoring the foam samples with a scalpel and immersing in liquid nitrogen (30 min). The scored samples were then fractured and sputtered with a layer of platinum coating (approximately 10 nm) using Agar High Resolution Coater (Model: 208HR, Agar Scientific, UK). The foam samples were scanned and imaged by SEM operating at (15 kV) and within width of 2.287 mm. The SEM images were analysed by ImageJ software (Version: 1.47v) to determine the pore size distribution. The pore size measurement was carried out by fitting a circle on each pore perimeter and measuring the corresponding diameter. The measured values of pore diameters were used to generate a histogram showing the distribution of pore sizes.

7.2.2.3 Open-Cell Content

Open-cell content of PS foam was measured to evaluate the portion of interconnected cells in the foam samples. The content of open cells was based on the ratio of total open-cell volume to the geometric volume of the foam sample (Section 3.4.2.5). This was measured by a gas pycnometer (ULTRAPYC 1200e- Quantachrome Instruments, USA). The open cell content was calculated from the difference between the pycnometer volume and geometric volume of foam samples as given by equation (7.3):

$$\text{Open-cell content \%} = [\frac{V_f - V_p}{V_f \text{ x } n}] \text{ x } 100 \quad (7.3)$$

The content of cell walls and closed cells was determined as shown in equation (7.4) and (7.5) respectively:

$$\text{Cell wall content \%} = [\frac{m_f}{\rho_s \text{ x } V_f}] \text{ x } 100 \quad (7.4)$$

$$\text{Closed-cell content \%} = 100 - (\text{Open-cell content \%} + \text{Cell wall content \%}) \quad (7.5)$$

where V_f is geometric volume of foam sample, V_p is pycnometer volume, n is porosity, m_f is mass of foam sample, ρ_s is density of solid PS polymer.

7.2.3 Oxygen Plasma Surface Treatment of PS Foam

Samples for plasma treatment were taken from PS foam sheets of 5 mm thickness, with skin on the top and bottom faces of the sheet. Cut foam sections were treated with low pressure plasma (Diener Electronic, Germany), with samples oriented to focus the plasma on the skin or edges as required. The plasma discharge was generated using supplied oxygen gas under an electric field of 40 kHz (Section 3.5). The loaded samples were outgassed as the unit chamber was pumped to low pressure (0.12 mbar). The O_2 plasma treatments were conducted for exposure time of 27 s at power of 240 W to achieving a target wettability (WCA: ~ 15°) on foam skin. The treated foam samples were then put in clean plastic containers to minimize any accidental contamination.

7.2.4 Surface Characterisation of the PS Foam

7.2.4.1 Surface Chemical Composition by XPS Analysis

The surface composition and functional groups of PS foam surface were analysed by X-ray photoelectron spectroscopy provided with Axis supra system (Kratos Analytical Ltd, UK). Survey scans were carried out to determine the surface elements on untreated and O_2 plasma-treated PS samples. The foam samples were irradiated at 1486.6 eV from an X-ray source of monochromatic Al Kα. The XPS scans were carried out at take-off angle of 90° and the resulting photoelectrons were received and analysed by an encountering hemispherical analyser. The surface charging was neutralized via the integral filament and magnetic lens system. The wide scan spectra were generated at pass energy of 160 eV and within a range of binding energy of 0-1400 eV. The high-resolution scans for C 1s peaks were performed at pass energy of 20 eV. The peaks of

all scan spectra were fitted on Shirley background and processed by CasaXPS software (Version 2.3.22PR1.0, Casa Software Ltd). Carbon peak components were deconvoluted and normalized with Gauss–Lorentz peak models to represent the different chemical groups in the carbon peak and calculate their concentrations (Section 3.6.2) The surface chemical analysis was carried out for three PS foam samples.

7.2.4.2 Contact Angle Measurement

Static contact angles were measured on PS foam skin of untreated and plasma-treated samples using the sessile drop method. A micro-pipette was used to produce drops of DI water (3 µL) on the sample skin to evaluate the surface wettability. The measurements of the contact angles were carried out by goniometer (FTA1000c, First Ten Angstroms, USA) and the resulting drop profiles were analysed by FTA32 shape analyser software. All contact angle measurements were conducted 6 times at a room temperature of 20 ± 1 °C (Section 3.6.1).

7.2.4.3 Water Drop Absorption Test

DI water drops (10 µL) were placed on the cut sides of the foam samples with exposed porous structure (no skin) before and after plasma treatment. The time for the water drops to be fully wicked into the porous PS structure was measured by high-speed camera (Fastcam Mini, Model: UX100, Photron, Japan). The recorded wicking times were averaged for 6 water drops in different locations of the foam samples. A photograph was also taken for the water drops on the porous structure of the untreated and plasma-treated foam samples to compare their surface hydrophilicity (Section 3.6.4).

7.2.5 Liquid Absorption Capacity

The absorption capacity of PS foam was determined for foam samples of dimensions (*L* x *W* x *T*: 40 mm x 10 mm x 5 mm). The liquid absorption capacity was assessed against liquids with different surface tensions as described in Table 7.1. The foam samples were treated with O_2 plasma for 27 s with samples oriented to focus the plasma on one cut side (*L* x *T*). The absorption test was performed by freely placing the cross-sections (*L* x *T*) of the untreated and plasma-treated samples on the test liquid within a plastic plate. The measurements of absorption capacity were repeated three times at room temperature of 20 ± 1 °C, and estimated by the liquid weight in grams absorbed

per gram of dry foam sample in equilibrium. The dry foam samples were weighed before the absorption test (W_d) and after their saturation with test liquid for 15 min (W_s). The foam samples were removed from the liquid for 30 s to allow any excess liquid to drain before weighing (Section 3.7.2). The resulting absorption capacity (R) was given by equation (7.6):

$$R = \frac{W_s - W_d}{W_d} \qquad (7.6)$$

7.2.6 Ageing Effect

The changes in surface characteristics and absorption capacity due to ageing phenomena were studied for plasma-treated PS foam after various storage times. All samples were stored in sealed plastic boxes at room temperature of 20 ± 1 °C as normal storage conditions after oxygen plasma treatment of 27 s. The surface wettability and chemical composition of the aged foam samples were characterised by WCA and XPS techniques respectively. The absorption capacity (R) was measured for the foam samples with BSA 8 wt% (γ: 52.03 mN/m). The surface wettability, chemical composition, and absorption capacity were determined with 3 repeats per measurement in different durations over 60 days. For practicality of using PS foam as a soak-away in food packaging, the liquid absorption capacity was also estimated in kilograms of absorbed liquid per cubic meter of the PS foam.

7.3 Experimental Results

7.3.1 Porous Structure Properties of PS Foam

Table 7.2 shows the material characteristics of PS foam samples. The PS foam had low density (41.61 kg/m^3) and large expansion ratio (25.24). The gaseous void content of the foam structure was represented by a porosity of 96%. This high porosity included closed and open cells, which are determined by the ratio of gaseous volume to the foam matrix volume. The open cells presented the interconnected foam pores showing high connectivity and open-cell content (90.91%).[63] The closed-cell content was only (4.24%) and solid PS material was estimated by the cell wall content (4.86%).

The morphology of the cellular PS structure was characterised by the SEM micrographs as shown in Figure 7.2a. The foam structure primarily exhibited open cells (pores) with irregular shapes. The open cells were interconnected with smaller pores on

their cellular walls (Figure 7.2a). This can provide the porous foam matrix with tortuous paths. Each pore size was determined by diameter of the fitted circle on its perimeter. The measured diameters of foam pores on the sample cross-section are dependent on the fracture position and will therefore not be reflective of the maximum pore diameters of all cells. The cross-section plane formed during the sample fracturing may not cross the centre of symmetry of individual foam cells leading to errors in the diameter measurements. However, the pore diameter measurements were performed on two adjacent cross-sections of six foam samples, with a total of 738 pores measured. This improves the representation of actual diameters of foam pores and reduces any directional skews of the results.

The frequency of the measured pore diameters is presented in a histogram shown in Figure 7.2b. The reticulated PS foam showed a wide pore size distribution with (93.8%) of the pores with diameters in range of (120-280 μm). However, a substantial portion of the pore diameters (36.6%) was distributed in the narrower range of (180-220 μm). Large pores with diameter (> 280 μm) formed (3.9%) with pore diameters reaching (340 μm).

Table 7.2: Material properties of open-cell PS foam.

Material Property	Measured Value
Density [kg/m^3]	41.61 (± 0.94)
Expansion ratio	25.24 (± 0.58)
Porosity %	96% (± 0)
Open-cell content %	90.91 (± 0.21)
Closed-cell content %	4.24 (± 0.28)
Cell wall content %	4.86 (± 0.11)

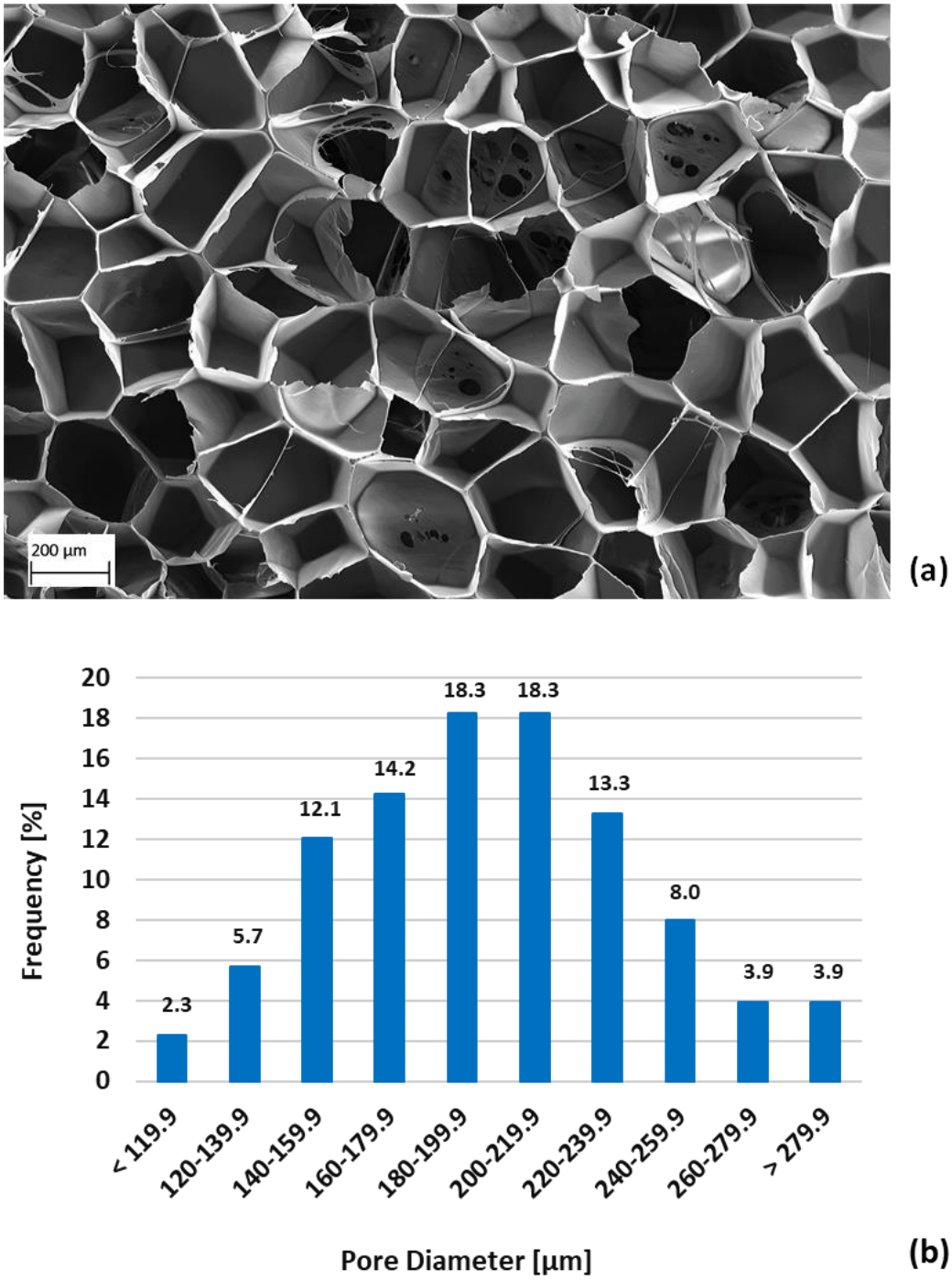

Figure 7.2: (a) SEM micrograph of open-cell PS foam with view width of 2.287 mm, (b) histogram of pore size distribution.

7.3.2 Chemical Composition of PS Foam

The elemental composition of PS foam before and after plasma treatment is illustrated in the XPS survey spectra in Figure 7.3a and b. The atomic concentrations of the detected surface elements are presented in Table 7.3. The spectrum of untreated PS showed a distinct C 1s peak for carbon and small O 1s peak for oxygen as the major

elements of the PS surface. This revealed the predominantly carbon-based composition of pristine PS with C% of 99.49% and O% of 0.47%. The plasma-treated PS spectrum exhibited a very small new peak for nitrogen N 1s with a more distinct O 1s peak as shown in Figure 7.3b. The O_2 plasma treatment introduced more oxygen to the PS surface resulting in a higher relative oxygen concentration of 18.38%, while the carbon concentration decreased to 81.17%. The corresponding Oxygen/Carbon ratio (O/C) of untreated and plasma-treated PS was 0.47% and 22.64% respectively. The nitrogen element was incorporated to the plasma-treated PS accounting for small concentration of 0.32%, and traces of silicon element < 0.20% was also found on PS foam surface as presented in Table 7.3.

The high-resolution C 1s peak was deconvoluted to its components to identify the bonds and functional groups on the PS surface. Figure 7.3c and d show the sub-peaks of the deconvoluted C 1s peak before and after plasma treatment. The analysed C 1s peak revealed three peak components for untreated PS defined at binding energy of 284.6, 286.2, and 291.2 eV. This corresponded to bonds of C=C/C-C/C-H, C-O, and π-π* shake-up respectively. The plasma treatment led to emerging new functional groups of C=O, O-C=O, and O-C(=O)-O at binding energies of 287.3, 288.4, and 289.5 eV respectively. The C=C, C-C, C-H bonds were defined at binding energy of 284.6 eV, lower than their normal binding energy (285.0 eV) due to the presence of aromatic rings in the PS structure.[221] The untreated PS showed prevalence of C=C, C-C and C-H bonds with concentration of 92.74% as presented in Table 7.4. C-O and shake-up bonds were detected with small concentrations of 2.73 and 4.54% respectively. On the other hand, the plasma treatment resulted in a substantial decrease in the C=C, C-C, and C-H bonds to reach 80.56% with increasing concentration of C-O bond to 10.67%. The shake-up (π-π*) bond concentration notably decreased to 0.89% after the plasma treatment and the new polar functional groups of C=O, O-C=O and O-C(=O)-O had small concentrations of 4.38, 1.57 and 1.94% respectively.

Table 7.3: Analysis of elemental composition and O/C ratio of PS foam surface.

PS foam surface	C%	O%	N%	O/C[a)]
Untreated	99.49	0.47	-	0.47
Plasma-treated for 27 s	81.17	18.38	0.32	22.64

[a)]Traces of Si < 0.20%

Table 7.4: Analysis of C 1s components of PS foam surface.

Bond	C=C, C-C, C-H	C-O	C=O	O-C=O	O-C(=O)-O	π-π*
Binding Energy (eV)	284.6	286.2	287.3	288.4	289.5	291.2
Untreated	92.74	2.73	-	-	-	4.54
Plasma-treated for 27 s	80.56	10.67	4.38	1.57	1.94	0.89

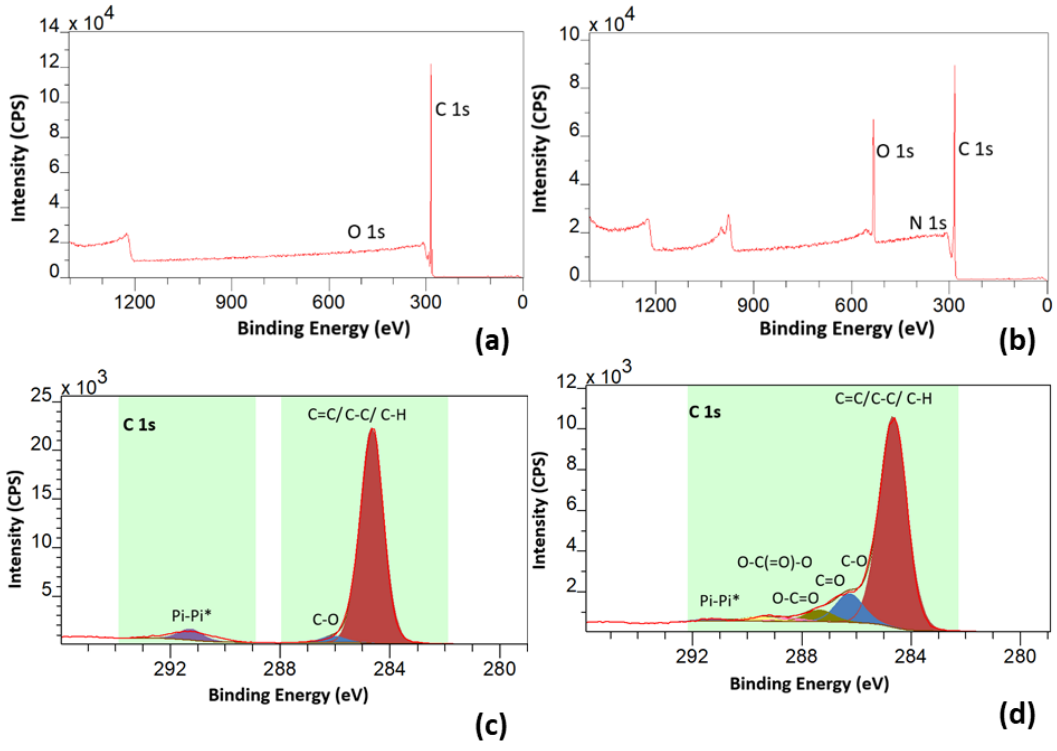

Figure 7.3: Wide XPS spectra of (a) untreated and (b) plasma-treated PS foam for 27 s, and functional groups of deconvoluted C 1s peak for (c) untreated and (d) plasma-treated PS foam for 27 s.

7.3.3 Surface Wettability of PS Foam

The surface wettability of PS foam was determined by measuring the apparent contact angle of DI water drops on the foam skin. The measured WCA of PS foam decreased from 86.01 ± 0.86° for untreated samples to 15.13 ± 0.70° for plasma-treated samples, indicating a substantial increase in surface hydrophilicity. The enhanced surface wettability was also observed in the drop absorption test on the foam cross-section with exposed porous structure. The red-dyed water drops on untreated PS foam showed high contact angle value of 100.15 ± 4.74°, while the high-speed camera (500 frame/s) showed instantaneous wicking of water drops into the bulk structure of plasma-treated PS foam within a time of 0.062 ± 0.020 s. This is illustrated in photograph of the instant absorption of water drop on the plasma-treated foam sample in comparison with large water drop on the untreated sample as shown in Figure 7.4.

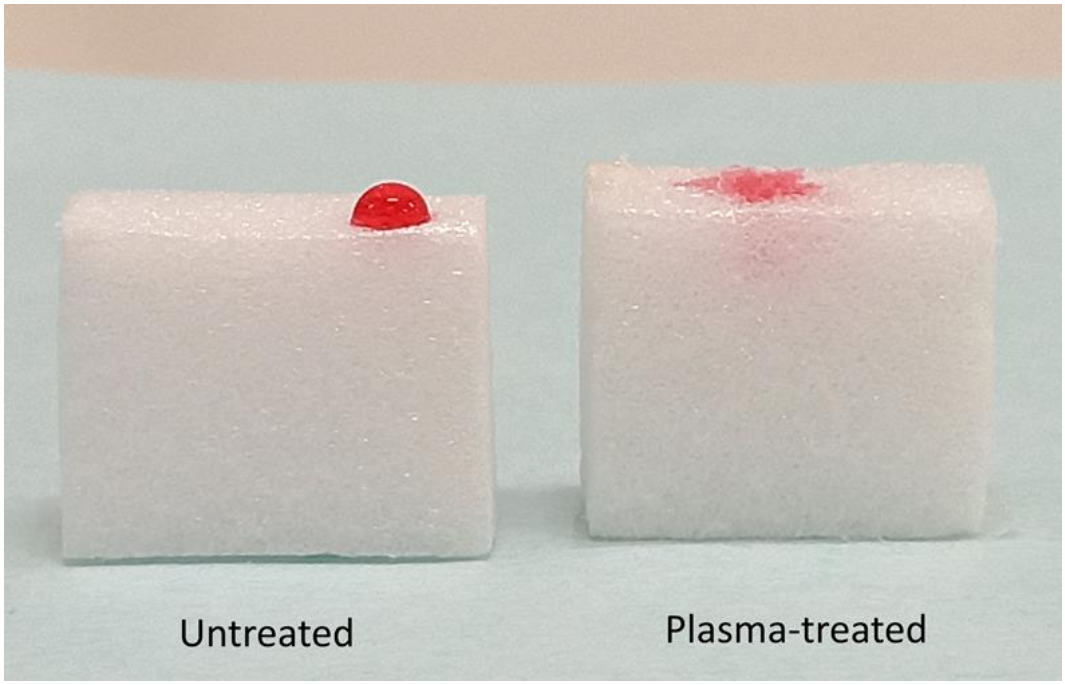

Figure 7.4: Photograph of red-dyed water drops on untreated and plasma-treated cross-sections of PS foam samples with dimensions (*L* x *W* x *T*: 20 mm x 20 mm x 5 mm).

7.3.4 Liquid Absorption Capacity

The liquid uptake of PS foam samples was evaluated in terms of their capacity to absorb and retain the test liquids. Figure 7.5 compares the retention capacity of untreated and plasma-treated PS foam with liquids of different surface tensions. The untreated PS foam exhibited low retention capacity < 1.60 g/g with test liquids of BSA 8 wt% (γ: 52.03 mN/m), pure water (γ: 72.63 mN/m), and water with surfactant (γ: 52.28 mN/m)

and for these liquids, the plasma treatment of the foam samples considerably improved their surface wettability and liquid uptake capacity. This resulted in increases in absorption capacity by 4 to 8 times depending on the liquid. However, in the case of the water with surfactant at the lowest surface tension (γ: 31.54 mN/m), the liquid highly wetted the foam pores resulting in substantial retention capacity of 8.93 ± 0.32 g/g even in the absence of plasma treatment. Therefore, the plasma treatment had no additional effect as it is assumed that the sample was fully saturated.

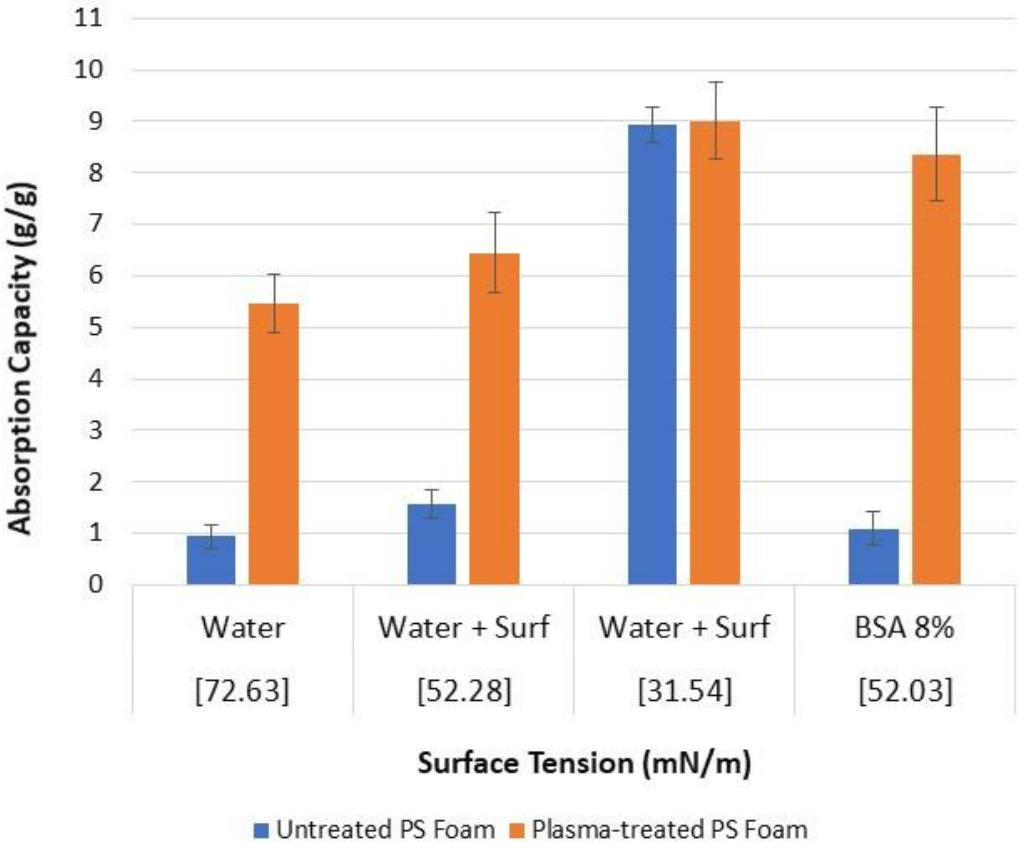

Figure 7.5: Liquid absorption capacity of open-cell PS foam before and after O_2 plasma treatment with different test liquids.

7.3.5 Analysis of Ageing Effect of Plasma Treatment

The hydrophobic recovery of the aged plasma-treated PS foam was studied through the changes in the wettability and surface chemical composition over time. The ageing study was carried out for PS foam samples up to 60 days post plasma treatment. Figure 7.6 illustrates the WCA developed on PS foam skin over different storage periods. The ageing rate was relatively high in the first three days post treatment, leading to an increase in the WCA from 15.13° to 29.70°. The PS foam then exhibited a slower rate of ageing with a small increase in the WCA showing stable wettability after 28 days of

the storage time. This corresponded to WCA of 41.55°, which is still considerably lower than WCA of 86.01° for untreated PS. The chemical composition of the aged PS foam samples also changed with a considerable decrease in the oxygen concentration and O/C ratio, particularly in the first day as shown in Table 7.5. This corresponded to a drop in O% and O/C ratio from 18.38% and 22.64% respectively at day 0 to 15.63% and 18.68% respectively at day 1. However, the oxygen concentration after 60 days remained relatively high at 13.12% in comparison with O% of 0.47% for the untreated PS samples. The nitrogen concentration was almost unchanged during the storage times.

The effect of aging on liquid absorption capacity of the PS foam was assessed during these same ageing times. Figure 7.7 shows the absorption capacity with BSA 8 wt% (γ: 52.03 mN/m) before and after the plasma treatment for storage periods of 0, 7, 14, 21, 28 and 60 days. The PS foam samples had a nearly constant enhanced liquid capacity of about 8 times that of the untreated samples, with no deterioration during the 60 days of ageing. For practicality of using PS foam as a liquid absorber, the liquid absorption capacity was also normalized in terms of kilograms (liquid) absorbed per cubic metre (foam). This revealed an estimated increase in the absorption capacity of PS foam sheet (nominal thickness: 5 mm) from 45.35 ± 6.53 kg/m^3 before plasma treatment to 365.34 ± 19.80 kg/m^3 after 60 days of the O_2 plasma treatment.

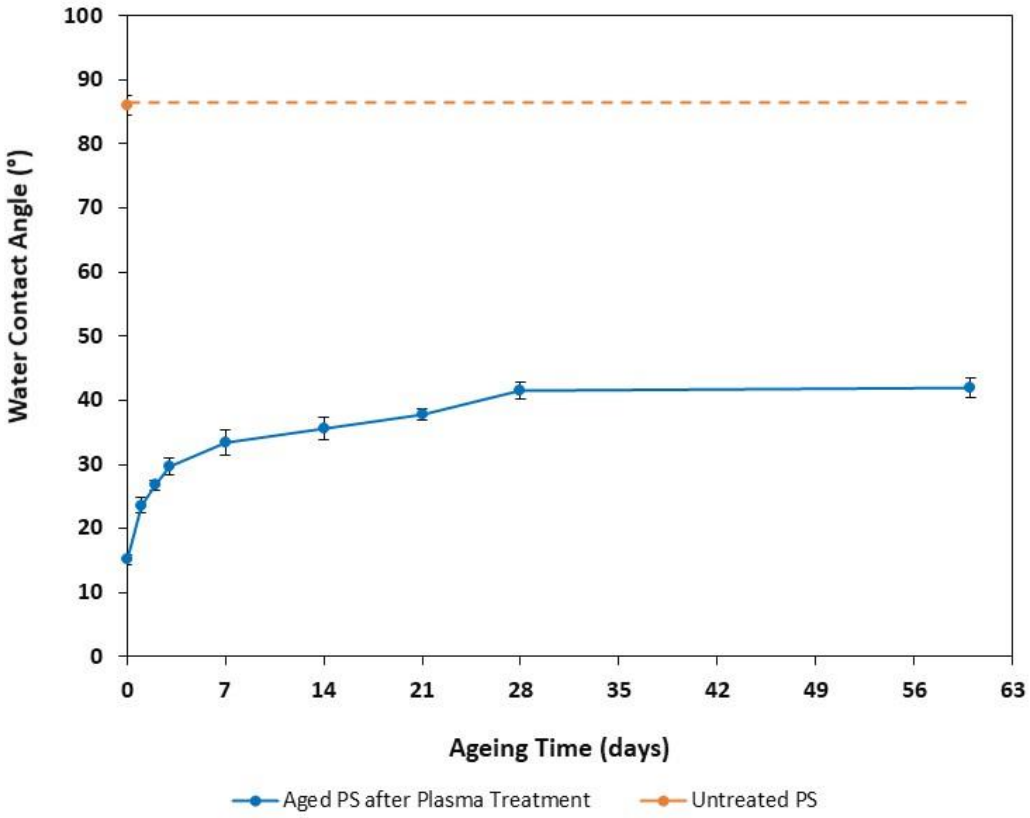

Figure 7.6: Development of apparent water contact angle on PS foam skin after O_2 plasma treatment as function of ageing times.

Table 7.5: Surface composition analysis of O_2 plasma-treated PS over ageing times.

Ageing Time (days)	C%	O%	N%	O/C[a)]
0	81.17	18.38	0.32	22.64
1	83.66	15.63	0.56	18.68
2	84.36	14.78	0.72	17.52
3	84.65	14.48	0.69	17.11
7	85.17	14.22	0.47	16.70
14	85.88	13.75	0.22	16.01
21	85.92	13.23	0.68	15.40
28	85.75	13.30	0.78	15.51
60	86.15	13.12	0.61	15.23
Untreated	99.49	0.47	-	0.47

[a)]Traces of Si < 0.20%

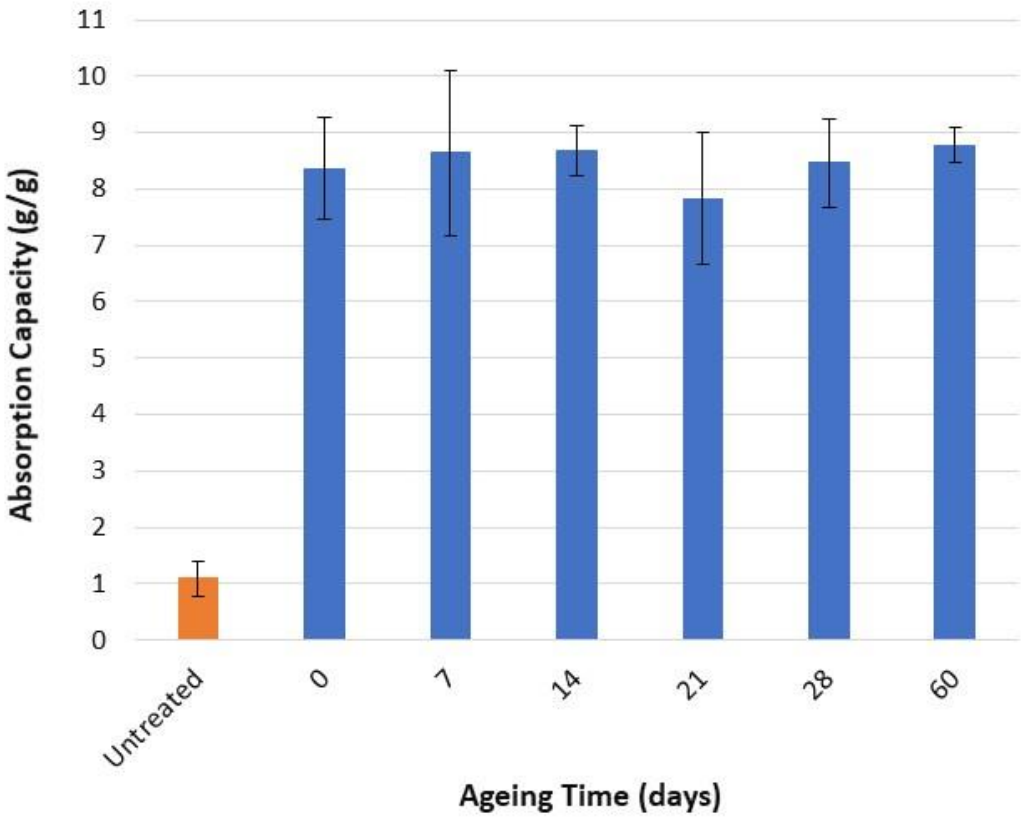

Figure 7.7: Absorption capacity of plasma-treated PS foam with BSA 8 wt% (γ: 52.03 mN/m) over different ageing times.

7.4 Discussion

Liquid absorption and retention properties of a porous media, such as PS foam fundamentally depends on both its structural and wetting characteristics.[133] The high porosity and open-cell content of the PS foam are among the crucial structural parameters, which determine the potential for the foam samples to uptake significant liquid quantities. This was reflected in the large gaseous space within the foam matrix as the porosity represents the volume of gaseous cells to the sample volume.[62] The formation of larger cells and thinner cellular membranes can be attributed to the low foam density.[154] A previous work reported an increase in water absorption capacity of polyurethane foam from 0.6 to 6.8 vol% due to a decrease in the foam density from 116 to 42 kg/m^3, respectively.[153] The high interconnectivity of the gaseous voids (open cells) also increased the gaseous space available to be filled by absorbed liquids, while the isolated and closed cells had no contribution to the liquid absorption capacity.[153] Others found a strong relationship between the improved liquid absorption capacity of polyurethane foam with an increase in the pore

connectivity.[133] Regardless of these attributes, pore surface wettability is a crucial enabler for liquid penetration into PS foam voids under a capillary pressure (ΔP_c) generated on the foam pores and is key for exploiting the open space in the foam. This pressure is determined by the liquid surface tension, size and wettability of pores as described by Young-Laplace equation (7.7):

$$\Delta P_c = \frac{2\gamma \cos\theta}{r} \qquad (7.7)$$

where γ is the liquid surface tension, θ is the liquid contact angle on pore surface, r is the radius of the foam pore. Accordingly, smaller pores with higher hydrophilic surface absorbed the wetting liquid before larger pores due to their higher negative capillary pressure.[133,134,236] The corresponding capillary forces are based on the discrepancy of surface energy on the wet and dry pore surfaces as the wicking liquid tends to wet the pore surfaces.[136,137]

The hydrophobicity and low surface energy of PS foam restrict the interactions between the pore surfaces and water-based fluids.[156] This prevents the liquid penetration into the foam pores as demonstrated in the low absorption capacity of untreated PS foam samples. Thus, the PS foam efficiency as a soak-away is currently limited for food packaging despite the large pore volume. However, the pore surfaces of PS foam had higher hydrophilicity and surface energy after the oxygen plasma treatment.[237] The plasma treatment decreased the WCA on PS foam skin and led to rapid wicking of water into the foam porous structure. The improved foam hydrophilicity allowed the liquid to wet the foam pores and increased their capillary pressure. This resulted in a substantial increase in the liquid wicking and absorption capacity,[133,134,156] and plasma-treated PS foam with BSA 8 wt% had an absorption capacity around 8 times that of the untreated foam. The pore surfaces were modified through diffusion of the excited gaseous species of plasma into the foam porous structure. This was manifested in activation of the interconnected pores and implanting polar functional groups on their surfaces.[238,239] On the other hand, the plasma treatment had no effect on the absorption capacity of PS foam with water of low surface tension (γ: 31.54 mN/m). This is due to the already high wetting affinity of the liquid to wet the pore surfaces facilitating the liquid penetration into the foam porous structure.[134] However, liquids with such low surface tensions are not typical of meat

exudate.[43] This effect could be analogous to the use of chemical surfactants in the foam as a means of reducing the exudate surface tension.

The O_2 plasma treatment improved the hydrophilicity of the PS foam pores by increasing the oxygen content on the treated surfaces.[240] This corresponded to an increase in O/C from 0.47% to 22.64% for untreated and plasma-treated PS foam samples respectively. These results are in line with published research, with different studies reporting comparable improvements in surface hydrophilicity and oxygen contents of plasma-treated PS.[240–242] The exposure to the excited plasma species induces hydrogen abstraction and chain scission of PS structure with the primary target being the aromatic rings.[243] This results in formation of reactive radical sites on the treated PS surface.[244] The reaction between these sites and excited oxygen molecules in the plasma glow led to the introduction of different polar oxygen groups including C-OH, C=O, COOH and O-C(=O)-O, which contributed to the decrease in WCA to 15.13°.[240,241] These functional groups have been reported in previous studies on plasma-treated PS material.[240,242,245] The presence of aromatic rings in the PS structure accounted for the satellite π-π* peak. The C 1s spectrum after the plasma treatment revealed a decrease in π-π* peak intensity, which can be ascribed to a targeting of the C=C bonds within the aromatic rings. This may have resulted in opening the rings and generating new polar oxygen groups, such as the carbonate group O-C(=O)-O and carboxyl group (O=C-OH) as described by other studies.[240,245] The plasma-treated PS can remain reactive due to unreacted radical sites, and the presence of a small nitrogen peak may originate from the post-treatment reaction between the atmospheric air and available radical sites. The presence of small amounts of other elements on the PS structure is assumed to originate from the PS oxidation in the case of oxygen and contamination in the case of silicon.[221,246]

Polymeric materials functionalized with oxygen plasma experience hydrophobic recovery as a result of ageing. This corresponds to a decay of polar oxygen groups and a tendency of the polymer surface to lose some of the gained hydrophilicity.[240] The plasma-treated PS foam showed reduction in the surface wettability with an increase in the WCA over time. Previous studies on aged PS after plasma treatments showed similar tendency of PS surface to become more hydrophobic with decreases in surface oxygen content during ageing time.[221,240,242] Although WCA increased to 41.90° after 60 days, it remained significantly lower than WCA of 86.01° for untreated PS

foam. This was consistent with the decrease in O% and O/C ratios over the same storage time. The ageing effect can occur due to reorientation of the PS polymer chains leading to burying of the oxygen groups into the polymer matrix. The formation of hydroperoxides on the treated PS surface can also facilitate the ageing process. These hydroperoxide products are unstable leading to decay in the surface polarity and hydrophilicity. However, the ageing process resulted only in a partial loss of the surface wettability and oxygen concentration. Therefore, the plasma treatment induced a permanent increase in the foam wettability.[240] The maintained improvement in the foam wettability allowed liquids, even with high surface tensions, to wet the foam pores. The corresponding negative capillary pressures acting on the pores provided the PS foam with liquid sucking functionality. This was evident with a maintained high absorption capacity of aged PS foam with BSA 8 wt% at more than 8 times that of untreated PS foam. Thus, it is viable to fully treat the PS foam with plasma whether in the form of a finished absorbent food tray or sheet. This can be achieved through perforation of the foam skin to allow the excited plasma species to penetrate the internal foam pores.

7.5 Closure

This work has demonstrated the viability of using plasma surface treatment, rather than chemical wetting agents, to improve the liquid uptake of open-cell polymeric foam. The exposure of the porous structure of PS foam to the plasma introduced polar oxygen groups onto the pore surfaces and improved their wettability. This increased the capillary pressure acting on the pores allowing larger liquid uptake and absorption. The plasma-treated foam samples had a substantial and durable increase in their liquid absorption capacity (g/g) of 8 times higher than the pristine foam samples. Therefore, one cubic meter of the PS foam sheet gained liquid absorption capacity of about 365 kg after plasma treatment in comparison with only about 45 kg for untreated PS foam. The wettability increases experienced partial loss due to the decrease in the oxygen groups under the effects of the ageing phenomenon. However, the aged foam pores maintained surface wettability distinctly higher than the untreated foam pores after 60 days post plasma treatment. This was sufficient for the liquids to wet the pore surfaces inducing instant liquid wicking and absorption, with no drop in performance over time. This showed the efficiency and practicality of using plasma technology for improving liquid scavenging within food packaging. This ensures higher absorption capacity and rapid

wicking of any excessive food liquid, and thus, helps take the exuded liquid away from the packaged food. The open-cell polymeric foams can be used as soak-away for meat exudate or other food juices in form of whole packaging trays (acting as both package and soak-away) or absorbent pad without the need for chemical wetting agents.

Chapter 8

Conclusions and Recommendations

8.1 Introduction

The development of innovative and sustainable solutions for the liquid management within plastic food packaging plays a part in meat wastage and recyclability of food packaging. Exudate isolation from the packaged fresh meat not only helps maintain the quality and safety of meat products, but it also reduces the meat waste. This contributes to the food security for the growing world population. The packaging solutions developed in this work are sustainable, enabling full recyclability of the resulting plastic packaging waste. Liquid isolation in the plastic film packaging was investigated to introduce new technologies that can trap the meat exudate within a single plastic material. This involved liquid retention in recesses with specially modified geometry, recesses with modified surface wettability of recess walls and open-cell polymeric foam with modified pore surface wettability.

8.2 Conclusions

Three different food packaging solutions were developed to retain the meat exudate in plastic film or foam packaging itself. The assessment of the liquid retention capacities was performed against simulant liquids of meat exudate, covering a range of surface tensions and rheological properties might be exhibited by meat exudates. This work included four investigations as outlined below:

- Surface tension and rheological characterisation of pork exudate and simulant liquids
- Liquid retention in capillary recesses with raised rims
- Liquid retention in capillary recesses with localised surface modification by oxygen plasma surface treatment
- Liquid absorption of open-cell polymeric foam with surface modification by oxygen plasma surface treatment.

8.2.1 Characterisation of Pork Exudate and Simulant Liquids

Pork exudates were collected from fresh packaged pork meat that were sourced from four major retailers. The surface tension, shear viscosity and viscoelastic properties

were measured for these pork exudates. The pork exudates showed Newtonian-like shear flow behaviour with low shear viscosity in the range of 4-10 mPa.s. Some very weak elasticity was observed in pork exudates. The surface tension of all pork exudates was lower than pure water with measured values in the range of 52-60 mN/m.

The simulant liquids were formulated to mimic the surface tensions and rheological properties measured for pork exudate. These liquids were formulated and characterised for their surface tensions, shear viscosity and viscoelastic properties. This included the formulation of aqueous CMC 1 wt% solutions with different added portions of surfactant. Aqueous BSA 8 wt% simulant and surfactant simulants were also formulated. All these simulant liquids showed low and constant shear viscosities < 10 mPa.s. The addition of surfactant allowed to formulate these liquids with high, medium and low surface tensions as described in Chapter 4. BSA 8 wt% solution was formulated to mimic the presence of proteins in real meat exudate. The exudate simulants were indicative of real exudate and performed similarly where side by side evaluation was performed.

8.2.2 Capillary Recesses with Raised Rims

The integration of raised thin rims on to PET recesses with extended sizes showed substantial increases in their liquid retention capacity. The thin raised rims acted as a means of enhancing the valving functionality of recess openings throughout increasing their expansion angles. The liquid menisci on the recess openings were more stable and resistant to liquid drainage. For PET recesses with opening diameter of 9 mm, the present of raised rims increased their retention capacity with pork exudate by 2.76 times in comparisons with recesses with no rims. This can allow to manufacture meat trays with retention capacity of around 2900 mL/m^2 which is comparable with current absorbent pads. These plastic trays can also be made from other mono-plastic materials, such as PE and PP. This results in plastic meat trays that are easy to clean and fully recyclable. The manufacturing of plastic meat trays with arrays of rim-integrated recesses can be easily scaled up and incorporated in to the existing tray forming process.

8.2.3 Capillary Recesses with Localised Plasma Surface Treatment

Surface modification of PET recess walls by localised oxygen plasma treatment was an effective means to increase the liquid retention capacity of the treated recesses. Plasma-treated PET recesses of extended sizes demonstrated a considerable and long-lasting

increase in their liquid retention capacity (2.24 times) when compared with untreated PET samples. The localised oxygen plasma treatment introduced polar oxygen groups onto the PET recess surface resulting in an increase in surface wettability and energy. The treated recesses were able to exploit the capillary valving functionality that is based on wetting variation between the treated walls and untreated edges of recesses. This allowed to form more stable menisci within the treated recesses and prevent liquid drainage, even after 60 days of ageing. Therefore, plastic meat trays can be manufactured from mono-plastic materials, such as PET, PE and PP for exudate isolation with potential capacity of around 2900 mL/m^2. This liquid capacity, and the relative improvement offered by the modification vs standard recesses were very similar to the benefits provided by the capillary recesses reported previously (Chapter 5) and comparable both with current absorbent pads. These trays are also easy to clean and enter closed loop recycling. This demonstrated the viability of using plasma treatment in food packaging to effectively isolate any excessive exudate. The plasma technology is already used in packaging and can be scaled up to be a continuous treatment process for food packaging by using atmospheric plasma technology.

8.2.4 Open-Cell Polymeric Foam with Plasma Surface Treatment

Oxygen plasma treatment of open-cell PS foam revealed improvement in wettability of the foam porous structure. The exposure of the porous structure of PS foam to the plasma introduced polar oxygen groups onto the pore surfaces and improved their wettability. This increased the capillary pressure acting on the pores allowing larger liquid uptake and absorption. The plasma-treated foam samples had a substantial and durable increase in their liquid absorption capacity (g/g) of 8 times higher than the pristine foam samples. This corresponded to liquid absorption capacity of 365 kg for one cubic meter of the PS foam sheet after plasma treatment in comparison with only about 45 kg for untreated PS foam. The wettability increases experienced partial loss due to the decrease in the oxygen groups under the effects of the ageing phenomenon. However, the aged foam pores maintained surface wettability distinctly higher than the untreated foam pores after 60 days post plasma treatment. This was sufficient for the liquids to wet the pore surfaces inducing instant liquid wicking and absorption, with no drop in performance over time. This demonstrated the viability of using plasma surface treatment, rather than chemical wetting agents, to improve the liquid/exudate uptake of open-cell polymeric foam. The open-cell polymeric foams can be used as soak-away

for meat exudate or other food juices in form of whole packaging trays (acting as both package and soak-away) or absorbent pad without the need for chemical wetting agents.

8.2.5 Commercialisation

The developed packaging solutions resulted in two patents with successful scaling-up and commercialisation of a plastic padless meat tray that is based on the geometrical modification of liquid-holding recesses. This commercialised plastic padless tray has already been placed on the shelves of major retailers in Europe under the trademarked name “kp Zapora®”. This innovative tray is the winner of two global awards in packaging sustainability; “WorldStar 2022 Award” from the World Packaging Organisation (https://worldstar.org/winners_detail/2937/2022/%20/Food/), and “Best in Class Sustainable Design 2022 Award” form PAC Global Awards. (https://www.pac-awards.com/2022-winners) kp Zapora® tray is manufactured by a simple and low-cost thermoforming process of single plastic film integrated with innovative design as shown in Figure 8.1. Currently available in Europe, the manufacturing process is readily transferable to any area of our world to address the global challenges of food waste and packaging recycling. By isolating the exudate released from packaged meat, this innovative padless tray can restrict meat spoilage and provide hygienic presentation of the packaged meat, reducing meat waste. This fully recyclable tray is also made from a single polymeric material (PET), minimising the plastic packaging footprint and preserving both marine and agriculture dependent food systems through capturing and recycling post-consumer plastic packaging. In broader context, the padless tray technology helps save the resources and energy used in food packaging. It also promotes use of recyclable packaging within society due to easy cleaning and recycling.

Figure 8.1: Padless plastic meat tray (kp Zapora®) with liquid-holding recesses, based on the geometry modification of recesses vs conventional plastic meat tray with absorbent meat pad (trays source: Klockner Pentaplast Group).

8.3 Recommendations for Future Work

This research has developed means for improving the recyclability of fossil-fuel based mono-material packaging, with focus on packaging of protein products (meat, poultry, fish, seafoods). The current packaging solutions disclosed in this work can also equally transfer to scavenge the excreted liquids of other liquid-exuding food products, such as soft and prepared fruits. On the other hand, the plastic packaging materials investigated are still derived from non-renewable sources aligned with existence of the fossil fuel industry. The vision of a net-zero carbon for food packaging is not complete, a key step would be the transition of food packaging towards renewable bioderived materials. Therefore, future work is recommended for exploring the potential of using the technologies developed in this research with bio-derived plastics in place of PET. This involves adoption of approaches that are based on the capillarity and wettability for liquid isolation within bio-derived plastic packaging, leading to further sustainability improvements of food packaging. The lid is still multicomponent due to the complexity of gas barrier requirements in film. This is being addressed with a follow-on project. Further, an evaluation of scale-up and large capital investment of plasma treatment is required to identify any potential issues in its usage for the developed packaging solutions.

Appendix

A.1 Measurement of Open-Cell Content of Foam Samples

Open-cell content of PS foam was measured by a gas pycnometer (ULTRAPYC 1200e-Quantachrome Instruments, USA) using nitrogen gas as stated in the experimental procedures of the standard measurement method ASTM D6226-10. The pycnometer is based on gas displacement method to measure the volume of solid material occupying the sample chamber (pycnometer sample volume). PS foam samples were prepared by cutting the foam sheet into cylinders (diameter: 3.80 cm) with a sharp cutting disk. The geometrical volume of PS foam cylinders was measured via a digital calliper. The measurement method included placing PS foam samples in the sample chamber and introducing nitrogen gas into the chamber until reaching an initial pressure (P_1) of 34.5 kPa (5 psig). The chamber valve was then opened to allow the nitrogen gas to expand into reference chamber reaching a lower stable pressure (P_2). The volume measured by nitrogen pycnometer was the volume of the PS foam sample displacing pycnometer chamber. This volume was calculated from volume of pycnometer chambers and working pressures (P_1 and P_2). The measurements were carried out at temperature of 23 ± 1 °C. The open-cell content was then determined from the ratio of open-cell volume of PS sample (difference between the pycnometer volume and geometrical volume) to geometrical sample volume.[211,212]

A.2 Surface Energy Determination of Samples

Surface energy determination of polymer surfaces is important to understand and characterise the wetting behaviours of different liquids on sample surfaces. This was based on Fowkes' theory of surface free energy. According to Fowkes, any interface exhibits a certain surface energy that is consisting of polar component (γ_s^p) and dispersive component (γ_s^d). These surface energy components are attributed to different molecular interactions present on a surface. For example, dipole forces account for polar component and London forces for dispersive component. This theory was developed by Owens-Wendt to consider the contribution of hydrogen bonding in polar component of surface energy. The total surface energy (γ_s^{tot}) of a solid surface is the sum of both polar and dispersive components as: $\gamma_s^{tot} = \gamma_s^p + \gamma_s^d$

The surface tension (γ_l) of liquids has also polar and dispersive components. Based on Owens-Wendt method, liquids with known components of their surface energy can be used to determine the surface energy components of a solid surface. Therefore, polar (DI water) and non-polar (diiodomethane) liquids were used to produce sessile drops on sample surfaces. The polar (γ_l^p) and dispersive (γ_l^d) surface tension components for water were 51.0 and 21.8 mN/m, and for diiodomethane were 0 and 50.8 mN/m respectively.[76,204] Contact angle measurements of sessile drops of these liquids were repeated six times at temperature of 20 ± 1 °C. The average contact angle values were compensated in Owens-Wendt model as shown in equation (A.2.1) to calculate the surface energy and its components of sample surfaces.

$$\gamma_l (1 + \cos \theta_e) = 2\sqrt{\gamma_s^d \gamma_l^d} + 2\sqrt{\gamma_s^p \gamma_l^p} \qquad \text{(A.2.1)}$$

A.3 Geometrical Dimensions of PET Recesses with Varied Rim Heights and Widths

Table A.3.1: Geometrical dimensions of PET recesses with different rim heights.

	Measured dimensions (mm) of PET recesses with opening diameter of 9 mm				
Nominal rim height	Rim height (*b*)	Rim width (*w*)	Diameter (*d*)	Depth (*h*)	Draft Angle (α, º)
0.1	0.115 ± 0.016	0.495 ± 0.018	8.879 ± 0.103	5.088 ± 0.004	6.650 ± 0.212
0.2	0.182 ± 0.013	0.460 ± 0.016	8.906 ± 0.086	5.060 ± 0.031	7.024 ± 0.34
0.5	0.485 ± 0.003	0.577 ± 0.022	8.894 ± 0.110	5.008 ± 0.020	6.489 ± 0.190
1	1.011 ± 0.034	0.502 ± 0.005	9.012 ± 0.025	4.962 ± 0.105	6.771 ± 0.266
2	1.791 ± 0.042	0.578 ± 0.065	8.987 ± 0.058	4.933 ± 0.022	6.767 ± 0.231

Table A.3.2: Geometrical dimensions of PET recesses with different rim widths.

	Measured dimensions (mm) of PET recesses with opening diameter of 9 mm				
Nominal rim width	Rim width (*w*)	Rim height (*b*)	Diameter (*d*)	Depth (*h*)	Draft Angle (α, º)
0.2	0.229 ± 0.038	1.902 ± 0.018	9.027 ± 0.090	5.078 ± 0.004	6.767 ± 0.404
0.3	0.293 ± 0.017	1.919 ± 0.038	8.960 ± 0.026	5.120 ± 0.052	6.737 ± 0.739
0.5	0.578 ± 0.065	1.791 ± 0.042	8.987 ± 0.058	4.933 ± 0.022	6.767 ± 0.231
1	0.962 ± 0.021	1.962 ± 0.012	8.916 ± 0.055	5.082 ± 0.050	7.933 ± 0.666
2	1.982 ± 0.015	1.990 ± 0.012	8.700 ± 0.042	5.072 ± 0.023	6.500 ± 0.283
5	4.985 ± 0.039	1.963 ± 0.021	8.760 ± 0.064	5.062 ± 0.022	7.233 ± 0.643

References

1. Biji KB, Ravishankar CN, Mohan CO, Srinivasa Gopal TK. Smart packaging systems for food applications: a review. J Food Sci Technol. 2015 Oct 24;52(10):6125–35.

2. Brody AL, Bugusu B, Han JH, Sand CK, McHugh TH. Innovative food packaging solutions. J Food Sci. 2008 Oct;73(8).

3. Gaikwad KK, Singh S, Ajji A. Moisture absorbers for food packaging applications. Environ Chem Lett. 2019 Jun 15;17(2):609–28.

4. Lee KT. Quality and safety aspects of meat products as affected by various physical manipulations of packaging materials. Meat Sci. 2010 Sep;86(1):138–50.

5. Schumann B, Schmid M. Packaging concepts for fresh and processed meat – Recent progresses. Innov Food Sci Emerg Technol. 2018 Jun 1;47:88–100.

6. Kakadellis S, Woods J, Harris ZM. Friend or foe: Stakeholder attitudes towards biodegradable plastic packaging in food waste anaerobic digestion. Resour Conserv Recycl. 2021 Jun 1;169.

7. Zhao X, Cornish K, Vodovotz Y. Narrowing the Gap for Bioplastic Use in Food Packaging: An Update. Environ Sci Technol. 2020 Apr 21;54(8):4712–32.

8. Geueke B, Groh K, Muncke J. Food packaging in the circular economy: Overview of chemical safety aspects for commonly used materials. J Clean Prod. 2018 Aug 20;193:491–505.

9. Licciardello F. Packaging, blessing in disguise. Review on its diverse contribution to food sustainability. Trends Food Sci Technol. 2017 Jul 1;65:32–9.

10. PlascticsEurope. Plastics-the Facts 2021 An analysis of European plastics production, demand and waste data [Internet]. [cited 2022 Jan 24]. Available from: https://plasticseurope.org/knowledge-hub/plastics-the-facts-2021/

11. Rydz J, Musiol M, Zawidlak-Wegrzyńska B, Sikorska W. Present and Future of Biodegradable Polymers for Food Packaging Applications. In: Biopolymers for Food Design. Elsevier Inc.; 2018. p. 431–67.

12. Alexandratos N, Bruinsma J. World Agriculture towards 2030/2050: the 2012 revision [Internet]. WORLD AGRICULTURE. 2012 Jun [cited 2022 Jan 24]. Available from: https://www.fao.org/3/ap106e/ap106e.pdf

13. Cole MB, Augustin MA, Robertson MJ, Manners JM. The science of food security. npj Sci Food. 2018 Dec;2(1).

14. Global food losses and food waste – Extent, causes and prevention [Internet]. Rome; 2011 [cited 2022 Jan 24]. Available from: https://www.fao.org/3/i2697e/i2697e.pdf

15. Global Initiative on Food loss and Waste Reduction [Internet]. Rome; 2015 [cited 2022 Jan 24]. Available from: http://www.fao.org/3/i4068e/i4068e.pdf

16. Dilkes-Hoffman LS, Lane JL, Grant T, Pratt S, Lant PA, Laycock B. Environmental impact of biodegradable food packaging when considering food waste. J Clean Prod. 2018 Apr 10;180:325–34.

17. Ahmed I, Lin H, Zou L, Brody AL, Li Z, Qazi IM, et al. A comprehensive review on the application of active packaging technologies to muscle foods. Food Control. 2017 Dec 1;82:163–78.

18. Gouvêa DM, Mendonça RCS, Lopez MES, Batalha LS. Absorbent food pads containing bacteriophages for potential antimicrobial use in refrigerated food products. LWT - Food Sci Technol. 2016 Apr 1;67:159–66.

19. Van Rooyen LA, Allen P, O'Connor DI. The application of carbon monoxide in meat packaging needs to be re-evaluated within the EU: An overview. Meat Sci. 2017 Oct 1;132:179–88.

20. Lanzani F, Mauri R. Sheet of expanded plastics material with absorbent properties towards aqueous liquids [Internet]. United States: United States; US5833894, 1998 [cited 2020 Oct 26]. Available from: https://patents.google.com/patent/US5833894A/en

21. Bekele S, Douglas RE, Vaughn GF, Kinard D, Kannankeril C. Absorbent pad with controlled rate of wicking [Internet]. United States: United States; US7025198, 2006 [cited 2020 Oct 26]. Available from: https://patents.google.com/patent/US7025198B2/en

22. Geyer R, Jambeck JR, Law KL. Production, use, and fate of all plastics ever made. Sci Adv. 2017 Jul 5;3(7).

23. The New Plastics Economy: Rethinking the future of plastics & catalysing action [Internet]. 2017 [cited 2022 Jan 24]. Available from: https://ellenmacarthurfoundation.org/the-new-plastics-economy-rethinking-the-future-of-plastics

24. Wood C, Border P. Plastic Food Packaging Waste [Internet]. 2019 Jul [cited 2022 Jan 24]. Available from: https://post.parliament.uk/research-briefings/post-pn-0605/

25. Walker TR, McGuinty E, Charlebois S, Music J. Single-use plastic packaging in the Canadian food industry: consumer behavior and perceptions. Humanit Soc Sci Commun. 2021 Dec 1;8(1).

26. Kumar R, Verma A, Shome A, Sinha R, Sinha S, Jha PK, et al. Impacts of

plastic pollution on ecosystem services, sustainable development goals, and need to focus on circular economy and policy interventions. Sustain [Internet]. 2021 Sep 1 [cited 2022 Apr 15];13(17):9963. Available from: https://doi.org/10.3390/su13179963

27. Beltran M, Tjahjono B, Bogush A, Julião J, Teixeira ELS. Food Plastic Packaging Transition towards Circular Bioeconomy: A Systematic Review of Literature. Sustainability [Internet]. 2021 Apr 1 [cited 2022 Apr 15];13(7):3896. Available from: https://www.mdpi.com/2071-1050/13/7/3896

28. Pettersen MK, Nilsen-Nygaard J, Hansen AÅ, Carlehög M, Liland KH. Effect of liquid absorbent pads and packaging parameters on drip loss and quality of chicken breast fillets. Foods [Internet]. 2021 Jun 1 [cited 2022 Apr 15];10(6). Available from: https://pubmed.ncbi.nlm.nih.gov/34200694/

29. Chisenga SM, Tolesa GN, Workneh TS. Biodegradable food packaging materials and prospects of the fourth industrial revolution for tomato fruit and product handling. Int J Food Sci. 2020;2020.

30. Tornberg E. Effects of heat on meat proteins - Implications on structure and quality of meat products. Meat Sci. 2005;70(3 SPEC. ISS.):493–508.

31. Huff-Lonergan E, Lonergan SM. Mechanisms of water-holding capacity of meat: The role of postmortem biochemical and structural changes. Meat Sci. 2005 Sep;71(1):194–204.

32. Pearce KL, Rosenvold K, Andersen HJ, Hopkins DL. Water distribution and mobility in meat during the conversion of muscle to meat and ageing and the impacts on fresh meat quality attributes - A review. Meat Sci. 2011 Oct;89(2):111–24.

33. Hertog-Meischke MJA den, Smulders FJM, van Logtestijn JG. The effect of storage temperature on drip loss from fresh beef. J Sci Food Agric [Internet]. 1998 Dec 1 [cited 2022 Apr 15];78(4):522–6. Available from: https://onlinelibrary.wiley.com/doi/10.1002/(SICI)1097-0010(199812)78:4%3C522::AID-JSFA150%3E3.0.CO;2-F

34. Warner RD. The Eating Quality of Meat-IV Water-Holding Capacity and Juiciness. In: Lawrie's Meat Science: Eighth Edition. Elsevier; 2017. p. 419–59.

35. Kim GD, Jung EY, Lim HJ, Yang HS, Joo ST, Jeong JY. Influence of meat exudates on the quality characteristics of fresh and freeze-thawed pork. Meat Sci. 2013 Oct 1;95(2):323–9.

36. Bowker BC, Zhuang H. Relationship between muscle exudate protein composition and broiler breast meat quality. Poult Sci. 2013;92(5):1385–92.

37. Bowker BC, Eastridge JS, Solomon MB. Measurement of Muscle Exudate

Protein Composition as an Indicator of Beef Tenderness. J Food Sci. 2014;79(7).

38. Savage AWJ, Warriss PD, Jolley PD. The amount and composition of the proteins in drip from stored pig meat. Meat Sci [Internet]. 1990 Jan 1 [cited 2018 Apr 6];27(4):289–303. Available from: https://www.sciencedirect.com/science/article/abs/pii/030917409090067G

39. Bowker BC, Eastridge JS, Solomon MB. Measurement of Muscle Exudate Protein Composition as an Indicator of Beef Tenderness. J Food Sci [Internet]. 2014 Jul 1 [cited 2018 Feb 14];79(7):C1292–7. Available from: http://doi.wiley.com/10.1111/1750-3841.12496

40. Savage AWJ, Warriss PD, Jolley PD. The amount and composition of the proteins in drip from stored pig meat. Meat Sci. 1990 Jan 1;27(4):289–303.

41. Xiong YL. Muscle proteins. In: Proteins in Food Processing: Second Edition. Elsevier Inc.; 2018. p. 127–48.

42. Bowker B, Gamble G, Zhuang H. Exudate Protein Composition and Meat Tenderness of Broiler Breast Fillets. Poult Sci. 2016 Jan 17;95(1):133–7.

43. Ursu AV, Marcati A, Michaud P, Djelveh G. Valorisation of industrial cooked ham by-products as functional ingredients. J Food Eng. 2016 Dec 1;190:54–60.

44. Di Luca A, Mullen AM, Elia G, Davey G, Hamill RM. Centrifugal drip is an accessible source for protein indicators of pork ageing and water-holding capacity. Meat Sci. 2011 Jun;88(2):261–70.

45. Laville E, Sayd T, Morzel M, Blinet S, Chambon C, Lepetit J, et al. Proteome changes during meat aging in tough and tender beef suggest the importance of apoptosis and protein solubility for beef aging and tenderization. J Agric Food Chem. 2009 Nov 25;57(22):10755–64.

46. Shibata-Ishiwatari N, Fukuoka M, Sakai N. Changes in the viscosity of expressible water in meat during heating: Description based on the denaturation kinetics of water-soluble proteins. Food Sci Technol Res. 2015;21(4):525–30.

47. Farouk MM, Mustafa NM, Wu G, Krsinic G. The “sponge effect” hypothesis: An alternative explanation of the improvement in the waterholding capacity of meat with ageing. Meat Sci. 2012 Mar;90(3):670–7.

48. Fernández A, Picouet P, Lloret E. Reduction of the spoilage-related microflora in absorbent pads by silver nanotechnology during modified atmosphere packaging of beef meat. J Food Prot. 2010;73(12):2263–9.

49. Zhang X, Wang H, Li N, Li M, Xu X. High CO2-modified atmosphere packaging for extension of shelf-life of chilled yellow-feather broiler meat: A special breed in Asia. LWT - Food Sci Technol. 2015;64(2):1123–9.

50. Lawrie RA, Ledward D. Lawrie's Meat Science: Seventh Edition. Lawrie's Meat Science: Seventh Edition. 2006. 1–442 p.

51. Kim GD, Jung EY, Lim HJ, Yang HS, Joo ST, Jeong JY. Influence of meat exudates on the quality characteristics of fresh and freeze-thawed pork. Meat Sci. 2013 Oct;95(2):323–9.

52. Realini CE, Marcos B. Active and intelligent packaging systems for a modern society. Meat Sci. 2014;98(3):404–19.

53. López-Rubio A, Almenar E, Hernandez-Muñoz P, Lagarón JM, Catalá R, Gavara R. Overview of Active Polymer-Based Packaging Technologies for Food Applications. Food Rev Int. 2004;20(4):357–87.

54. Laiewski S, Hessen TA, Hardy TR, Gilvin AF. Purge trap tray [Internet]. United States: United States; US4576278, 1986 [cited 2020 Oct 26]. Available from: https://patents.google.com/patent/US4576278

55. Otoni CG, Espitia PJP, Avena-Bustillos RJ, McHugh TH. Trends in antimicrobial food packaging systems: Emitting sachets and absorbent pads. Food Res Int. 2016 May 1;83:60–73.

56. Ren T, Qiao M, Huang TS, Weese J, Ren X. Efficacy of N-halamine compound on reduction of microorganisms in absorbent food pads of raw beef. Food Control. 2018 Feb 1;84:255–62.

57. Davidson RP, Becke GS, Minnett JC. Food tray with integrated liquid-retention system [Internet]. United States: United States; US8596490, 2013 [cited 2020 Oct 26]. Available from: https://patents.google.com/patent/US8596490B2/en

58. Christodoulou C. Food packaging tray made of expanded polystyrene with ability to absorb moisture internally, of a single layer structure, without surface cover with membranes (non - laminated); products and method [Internet]. United States: United States; US 2006/0060478, 2006 [cited 2022 Apr 16]. Available from: https://patents.google.com/patent/US20060060478A1/en

59. Wiegers W. Tray for packaging portions of meat or similar foods [Internet]. United States: United States; US6598740, 2003 [cited 2020 Oct 26]. Available from: https://patents.google.com/patent/US6598740B1/en

60. Bland DG, Stobby WG, Rose GD, Mork SW, Staples TL, McCann GD. Absorbent, extruded thermoplastic foams [Internet]. United States: United States; US006071580, 2000 [cited 2021 Feb 15]. p. 580. Available from: https://patents.google.com/patent/US6071580A/en

61. Colombo EA, Braddon JJ. Food package with integral juice absorbing bottom [Internet]. United States: United States; US6695138, 2004 [cited 2020 Oct 26]. Available from: https://patents.google.com/patent/US6695138B1/en

62. Pinto J, Athanassiou A, Fragouli D. Surface modification of polymeric foams

for oil spills remediation. J Environ Manage. 2018 Jan 15;206:872–89.

63. Gunashekar S, Pillai KM, Church BC, Abu-Zahra NH. Liquid flow in polyurethane foams for filtration applications: a study on their characterization and permeability estimation. J Porous Mater. 2015 Jun 1;22(3):749–59.

64. LaRue JM, Cappel CE, Petlak FA. Container having internal reservoir [Internet]. United States: United States; US7921992, 2011 [cited 2020 Oct 26]. Available from: https://patents.google.com/patent/US7921992B2/en?oq=+7921992

65. Jensen R, Versteylen S. Consumer food storage package with absorbent food pad [Internet]. United States: United States; US 2008/0199577, 2008 [cited 2021 Aug 6]. p. 1–10. Available from: https://patents.google.com/patent/US20080199577A1/en

66. Durdag K, Pendleton B, Hamlyn R, Gunn V, Etchells M. Biodegradable polymer non-woven absorbent pad with absorbency and antimicrobial chemistry [Internet]. United States: United States; US 8828516, 2014 [cited 2021 Aug 6]. p. 1–34. Available from: https://patents.google.com/patent/US8828516B2/en

67. Colombo EA. Highly absorbent open cell polymer foam and food package comprised thereof [Internet]. United States: United States; US7175021, 2007 [cited 2022 Apr 17]. Available from: https://patents.google.com/patent/US7175021B2/en

68. Karbowiak T, Debeaufort F, Voilley A. Importance of surface tension characterization for food, pharmaceutical and packaging products: A review. Crit Rev Food Sci Nutr. 2006 Jun 1;46(5):391–407.

69. Grundke K, Pöschel K, Synytska A, Frenzel R, Drechsler A, Nitschke M, et al. Experimental studies of contact angle hysteresis phenomena on polymer surfaces - Toward the understanding and control of wettability for different applications. Adv Colloid Interface Sci. 2015 Aug 12;222:350–76.

70. Wang Z, Elimelech M, Lin S. Environmental Applications of Interfacial Materials with Special Wettability. Environ Sci Technol. 2016 Mar 1;50(5):2132–50.

71. Si Y, Yu C, Dong Z, Jiang L. Wetting and spreading: Fundamental theories to cutting-edge applications. Curr Opin Colloid Interface Sci. 2018 Jul 1;36:10–9.

72. Rapp BE. Surface Tension. In: Microfluidics: Modelling, Mechanics and Mathematics [Internet]. Elsevier; 2017 [cited 2022 Apr 17]. p. 421–44. Available from: https://linkinghub.elsevier.com/retrieve/pii/B9781455731411500204

73. Ebnesajjad S. Surface tension and its measurement. In: Handbook of Adhesives

and Surface Preparation. Elsevier Inc.; 2011. p. 21–30.

74. Rudawska A, Jacniacka E. Analysis for determining surface free energy uncertainty by the Owen-Wendt method. Int J Adhes Adhes. 2009 Jun;29(4):451–7.

75. Altay BN, Ma R, Fleming PD, Joyce MJ, Anand A, Chen T, et al. Surface Free Energy Estimation: A New Methodology for Solid Surfaces. Adv Mater Interfaces. 2020 Mar 1;7(6).

76. Awaja F, Gilbert M, Kelly G, Fox B, Pigram PJ. Adhesion of polymers. Prog Polym Sci. 2009 Sep;34(9):948–68.

77. Ozean C, Hasirci N. Evaluation of surface free energy for PMMA films. J Appl Polym Sci. 2008 Apr 5;108(1):438–46.

78. Bonn D, Eggers J, Indekeu J, Meunier J. Wetting and spreading. Rev Mod Phys. 2009 May 27;81(2):739–805.

79. Awaja F. Autohesion of polymers. Polymer (Guildf). 2016 Aug 5;97:387–407.

80. Ralston J, Popescu M, Sedev R. Dynamics of wetting from an experimental point of view. Annu Rev Mater Res. 2008;38:23–43.

81. Stammitti-Scarpone A, Acosta EJ. Solid-liquid-liquid wettability and its prediction with surface free energy models. Adv Colloid Interface Sci. 2019 Feb 1;264:28–46.

82. Patnaik A, Rengasamy RS, Kothari VK, Ghosh A. Wetting and wicking in fibrous materials. Text Prog [Internet]. 2006 [cited 2022 Apr 18];38(1):1–105. Available from: https://www.tandfonline.com/doi/abs/10.1533/jotp.2006.38.1.1

83. Otitoju TA, Ahmad AL, Ooi BS. Superhydrophilic (superwetting) surfaces: A review on fabrication and application. J Ind Eng Chem. 2017 Mar 25;47:19–40.

84. Al-Zaidi E, Fan X. Effect of aqueous electrolyte concentration and valency on contact angle on flat glass surfaces and inside capillary glass tubes. Colloids Surfaces A Physicochem Eng Asp. 2018 Apr 20;543:1–8.

85. Schuster JM, Schvezov CE, Rosenberger MR. Construction and calibration of a goniometer to measure contact angles and calculate the surface free energy in solids with uncertainty analysis. Int J Adhes Adhes. 2018 Dec 1;87:205–15.

86. Meiron TS, Marmur A, Saguy IS. Contact angle measurement on rough surfaces. J Colloid Interface Sci. 2004 Jun 15;274(2):637–44.

87. Wenzel RN. Resistance of solid surfaces to wetting by water. Ind Eng Chem [Internet]. 1936 Aug 1 [cited 2022 Apr 18];28(8):988–94. Available from: https://pubs.acs.org/doi/abs/10.1021/ie50320a024

88. Yuan Y, Lee TR. Contact angle and wetting properties. Springer Ser Surf Sci

[Internet]. 2013 [cited 2022 Apr 18];51(1):3–34. Available from: https://link.springer.com/chapter/10.1007/978-3-642-34243-1_1

89. Johnson RE, Dettre RH. Contact angle hysteresis. III. Study of an idealized heterogeneous surface. J Phys Chem [Internet]. 1964 [cited 2022 Apr 18];68(7):1744–50. Available from: https://pubs.acs.org/sharingguidelines

90. Valipour M. N, Birjandi FC, Sargolzaei J. Super-non-wettable surfaces: A review. Colloids Surfaces A Physicochem Eng Asp. 2014 Apr 20;448(1):93–106.

91. Yao X, Song Y, Jiang L. Applications of bio-inspired special wettable surfaces. Adv Mater. 2011 Feb 8;23(6):719–34.

92. Rizvi A, Chu RKM, Lee JH, Park CB. Superhydrophobic and oleophilic open-cell foams from fibrillar blends of polypropylene and polytetrafluoroethylene. ACS Appl Mater Interfaces. 2014 Dec 10;6(23):21131–40.

93. Ionov L, Houbenov N, Sidorenko A, Stamm M, Minko S. Smart microfluidic channels. Adv Funct Mater. 2006 Jun 6;16(9):1153–60.

94. Ou J, Perot B, Rothstein JP. Laminar drag reduction in microchannels using ultrahydrophobic surfaces. Phys Fluids. 2004;16(12):4635–43.

95. Di Mundo R, D'Agostino R, Palumbo F. Long-lasting antifog plasma modification of transparent plastics. ACS Appl Mater Interfaces. 2014 Oct 8;6(19):17059–66.

96. Introzzi L, Fuentes-Alventosa JM, Cozzolino CA, Trabattoni S, Tavazzi S, Bianchi CL, et al. "Wetting enhancer" pullulan coating for antifog packaging applications. ACS Appl Mater Interfaces. 2012 Jul 25;4(7):3692–700.

97. Juncker D, Schmid H, Drechsler U, Wolf H, Wolf M, Michel B, et al. Autonomous microfluidic capillary system. Anal Chem. 2002 Dec 15;74(24):6139–44.

98. Figliuzzi B, Buie CR. Rise in optimized capillary channels. J Fluid Mech. 2013;731:142–61.

99. Hamraoui A, Nylander T. Analytical approach for the Lucas-Washburn equation. J Colloid Interface Sci. 2002;250(2):415–21.

100. Liu H, Cao G. Effectiveness of the Young-Laplace equation at nanoscale. Sci Rep. 2016 Apr 1;6.

101. Extrand CW. Forces, pressures and energies associated with liquid rising in nonuniform capillary tubes. J Colloid Interface Sci. 2015 Jul 5;450:135–40.

102. Lu G, Wang XD, Duan YY. Study on initial stage of capillary rise dynamics. Colloids Surfaces A Physicochem Eng Asp. 2013;433:95–103.

103. Siebold A, Nardin M, Schultz J, Walliser A, Oppliger M. Effect of dynamic contact angle on capillary rise phenomena. Colloids Surfaces A Physicochem Eng Asp. 2000 Jan 15;161(1):81–7.

104. Stange M, Dreyer ME, Rath HJ. Capillary driven flow in circular cylindrical tubes. Phys Fluids. 2003;15(9):2587–601.

105. Wang Q, Graber ER, Wallach R. Synergistic effects of geometry, inertia, and dynamic contact angle on wetting and dewetting of capillaries of varying cross sections. J Colloid Interface Sci. 2013;396:270–7.

106. Dreyer M, Delgado A, Path HJ. Capillary rise of liquid between parallel plates under microgravity. J Colloid Interface Sci. 1994 Mar 1;163(1):158–68.

107. Barozzi GS, Angeli D. A note on capillary rise in tubes. Energy Procedia. 2014;45:548–57.

108. Radulovic J, Sefiane K, Shanahan MER. Capillary rise of superspreaders. J Colloid Interface Sci. 2011;361(2):643–8.

109. Bao J, Wang L. Capillary imbibition of water in discrete planar cracks. Constr Build Mater. 2017 Aug 15;146:381–92.

110. Chen JM, Huang PC, Lin MG. Analysis and experiment of capillary valves for microfluidics on a rotating disk. Microfluid Nanofluidics. 2008 May;4(5):427–37.

111. Thio THG, Soroori S, Ibrahim F, Al-Faqheri W, Soin N, Kulinsky L, et al. Theoretical development and critical analysis of burst frequency equations for passive valves on centrifugal microfluidic platforms. Med Biol Eng Comput. 2013 May;51(5):525–35.

112. Wang S, Zhang X, Ma C, Yan S, Inglis D, Feng S. A review of capillary pressure control valves in microfluidics. Biosensors. 2021 Oct 1;11(10).

113. Cho H, Kim HY, Kang JY, Kim TS. How the capillary burst microvalve works. J Colloid Interface Sci. 2007 Feb 15;306(2):379–85.

114. Feng Y, Zhou Z, Ye X, Xiong J. Passive valves based on hydrophobic microfluidics. Sensors Actuators, A Phys. 2003 Nov 15;108(1–3):138–43.

115. Glière A, Delattre C. Modeling and fabrication of capillary stop valves for planar microfluidic systems. Sensors Actuators, A Phys. 2006 Aug 14;130–131(SPEC. ISS.):601–8.

116. Yildirim E. Modeling and Analysis of a Microfluidic Capillary Valve. J Polytech. 2017;20(2):487–94.

117. Leu TS, Chang PY. Pressure barrier of capillary stop valves in micro sample separators. Sensors Actuators, A Phys. 2004 Sep 21;115(2-3 SPEC. ISS.):508–15.

118. Du X, Zhang P, Liu Y, Wu Y. A passive through hole microvalve for capillary flow control in microfluidic systems. Sensors Actuators, A Phys. 2011 Feb;165(2):288–93.

119. Kazemzadeh A, Ganesan P, Ibrahim F, He S, Madou MJ. The Effect of Contact Angles and Capillary Dimensions on the Burst Frequency of Super Hydrophilic and Hydrophilic Centrifugal Microfluidic Platforms, a CFD Study. PLoS One. 2013 Sep 12;8(9).

120. Wang Z, Yen HY, Chang CC, Sheng YJ, Tsao HK. Trapped liquid drop at the end of capillary. Langmuir. 2013 Oct 1;29(39):12154–61.

121. Agonafer DD, Lopez K, Palko JW, Won Y, Santiago JG, Goodson KE. Burst behavior at a capillary tip: Effect of low and high surface tension. J Colloid Interface Sci. 2015 Oct 1;455:1–5.

122. Tsougeni K, Papageorgiou D, Tserepi A, Gogolides E. "Smart" polymeric microfluidics fabricated by plasma processing: Controlled wetting, capillary filling and hydrophobic valving. Lab Chip. 2010;10(4):462–9.

123. Ishida T, McLaughlin D, McLaughlin D, Tanaka Y. First-come-first-store microfluidic device of droplets using hydrophobic passive microvalves. Sensors Actuators, B Chem. 2018;254:1005–10.

124. Davies RM, Taylor G. The mechanics of large bubbles rising through extended liquids and through liquids in tubes. Proc R Soc London Ser A Math Phys Sci [Internet]. 1950 Feb 7 [cited 2022 May 24];200(1062):375–90. Available from: https://ui.adsabs.harvard.edu/abs/1950RSPSA.200..375D/abstract

125. Extrand CW. Spontaneous Draining of Liquids from Vertically Oriented Tubes. Langmuir. 2017 Nov 14;33(45):12903–7.

126. Kumar A, Ray S, Das G. Draining phenomenon in closed narrow tubes pierced at the top: an experimental and theoretical analysis. Sci Rep. 2018 Dec 1;8(1).

127. Extrand CW. Drainage from a Fluid-Handling Component because of Inclination. Langmuir. 2018 Jan 9;34(1):126–30.

128. Kohlhoff D, Ohshima M. Open cell microcellular foams of polylactic acid (PLA)-based blends with semi-interpenetrating polymer networks. Macromol Mater Eng. 2011 Aug 15;296(8):770–7.

129. Sun M, Chen C, Chen L, Su B. Hierarchically porous materials: Synthesis strategies and emerging applications. Front Chem Sci Eng. 2016 Sep 1;10(3):301–47.

130. Gong L, Kyriakides S, Jang WY. Compressive response of open-cell foams. Part I: Morphology and elastic properties. Int J Solids Struct. 2005 Mar;42(5–6):1355–79.

131. Liu PS, Chen GF. Porous Materials: Processing and Applications. Porous Materials: Processing and Applications. Elsevier Inc.; 2014. 1–560 p.

132. Ceglia G, Merlin A, Viot P, Schmitt V, Mondain-Monval O. Porous materials with tunable mechanical properties. J Porous Mater. 2014 Nov 15;21(6):903–12.

133. Pinto J, Athanassiou A, Fragouli D. Effect of the porous structure of polymer foams on the remediation of oil spills. J Phys D Appl Phys. 2016 Mar 1;49(14).

134. Unsal E, Dane JH, Schwartz P. Effect of liquid characteristics on the wetting, capillary migration, and retention properties of fibrous polymer networks. J Appl Polym Sci. 2005 Jul 5;97(1):282–92.

135. Staples TL, Shaffer DG. Wicking flow in irregular capillaries. Colloids Surfaces A Physicochem Eng Asp. 2002 May 23;204(1–3):239–50.

136. Masoodi R, Tan H, Pillai KM. Darcy's law-based numerical simulation for modeling 3D liquid absorption into porous wicks. AIChE J. 2011 May;57(5):1132–43.

137. Masoodi R, Pillai KM. A general formula for capillary suction-pressure in porous media. J Porous Media. 2012;15(8):775–83.

138. Xiong Q, Baychev TG, Jivkov AP. Review of pore network modelling of porous media: Experimental characterisations, network constructions and applications to reactive transport. J Contam Hydrol. 2016 Sep 1;192:101–17.

139. Narayana Iyer KA, Pantina R, Deshpande AP. Modelling and simulation of drop spreading on fibrous porous media. J Text Inst. 2014 Mar;105(3):294–303.

140. Mao N, Russell SJ. Capillary pressure and liquid wicking in three-dimensional nonwoven materials. J Appl Phys. 2008;104(3).

141. Kim J, Kim HY. On the dynamics of capillary imbibition. J Mech Sci Technol. 2012 Dec 1;26(12):3795–801.

142. Martic G, Blake TD, De Coninck J. Dynamics of imbibition into a pore with a heterogeneous surface. Langmuir. 2005 Nov 22;21(24):11201–7.

143. Jiang S, Agarwal S, Greiner A. Low-Density Open Cellular Sponges as Functional Materials. Angew Chemie - Int Ed. 2017 Dec 4;56(49):15520–38.

144. Markert B. A biphasic continuum approach for viscoelastic high-porosity foams: Comprehensive theory, numerics, and application. Arch Comput Methods Eng. 2008 Dec;15(4):371–446.

145. Chu RKM, Mark LH, Park CB. Scalable Fabrication of Microcellular Open-Cell Polymer Foams. Adv Eng Mater. 2022 Mar 1;24(3).

146. Hou J, Zhao G, Zhang L, Wang G, Li B. High-expansion polypropylene foam prepared in non-crystalline state and oil adsorption performance of open-cell foam. J Colloid Interface Sci. 2019 Apr 15;542:233–42.

147. Lee ST, Kareko L, Jun J. Study of thermoplastic PLA foam extrusion. J Cell Plast. 2008 Jul;44(4):293–305.

148. Sauceau M, Fages J, Common A, Nikitine C, Rodier E. New challenges in polymer foaming: A review of extrusion processes assisted by supercritical carbon dioxide. Prog Polym Sci. 2011 Jun;36(6):749–66.

149. Fan C, Wan C, Gao F, Huang C, Xi Z, Xu Z, et al. Extrusion foaming of poly(ethylene terephthalate) with carbon dioxide based on rheology analysis. J Cell Plast. 2016;52(3):277–98.

150. Tomin M, Kmetty Á. Polymer foams as advanced energy absorbing materials for sports applications—A review. J Appl Polym Sci. 2022 Mar 5;139(9).

151. Obi BE. FLEXIBLE FOAMS. In: Polymeric Foams Structure-Property-Performance [Internet]. William Andrew Publishing; 2018 [cited 2022 May 29]. p. 299–331. Available from: https://doi.org/10.1016/B978-1-4557-7755-6.00010-0

152. Zanderighi L. Influence of active packaging on the shelf-life of minimally processed fish products in a modified atmosphere. Packag Technol Sci. 2001 Nov;14(6):267–74.

153. Thirumal M, Khastgir D, Singha NK, Manjunath BS, Naik YP. Effect of foam density on the properties of water blown rigid polyurethane foam. J Appl Polym Sci. 2008 Mar 5;108(3):1810–7.

154. Duong HTT, Burford RP. Effect of foam density, oil viscosity, and temperature on oil sorption behavior of polyurethane. J Appl Polym Sci. 2006 Jan 5;99(1):360–7.

155. Wang G, Zeng Z, Wu X, Ren T, Han J, Xue Q. Three-dimensional structured sponge with high oil wettability for the clean-up of oil contaminations and separation of oil-water mixtures. Polym Chem. 2014 Oct 21;5(20):5942–8.

156. Safinia L, Wilson K, Mantalaris A, Bismarck A. Atmospheric plasma treatment of porous polymer constructs for tissue engineering applications. Macromol Biosci. 2007 Mar 8;7(3):315–27.

157. Cowan-Ellsberry C, Belanger S, Dorn P, Dyer S, Mcavoy D, Sanderson H, et al. Environmental safety of the use of major surfactant classes in North America. Crit Rev Environ Sci Technol. 2014 Sep 2;44(17):1893–993.

158. Rebello S, Asok AK, Mundayoor S, Jisha MS. Surfactants: Toxicity, remediation and green surfactants. Environ Chem Lett. 2014;12(2):275–87.

159. Lee KT, Goddard JM, Hotchkiss JH. Plasma modification of polyolefin surfaces. Packag Technol Sci. 2009 Apr;22(3):139–50.

160. Fabbri P, Messori M. Surface Modification of Polymers: Chemical, Physical, and Biological Routes. In: Modification of Polymer Properties. Elsevier Inc.; 2017. p. 109–30.

161. Deng J, Wang L, Liu L, Yang W. Developments and new applications of UV-induced surface graft polymerizations. Prog Polym Sci. 2009 Feb;34(2):156–93.

162. Nemani SK, Annavarapu RK, Mohammadian B, Raiyan A, Heil J, Haque MA, et al. Surface Modification of Polymers: Methods and Applications. Adv Mater Interfaces. 2018 Dec 21;5(24).

163. Wang J, Chen H, Wang X, Yuan Z. Facile method to prepare a transparent superhydrophobic PET film. Appl Phys A Mater Sci Process. 2016 Nov 1;122(11).

164. Valipour Motlagh N, Khani R, Rahnama S. Super dewetting surfaces: Focusing on their design and fabrication methods. Colloids Surfaces A Physicochem Eng Asp. 2015 Nov 5;484:528–46.

165. Ma M, Hill RM. Superhydrophobic surfaces. Curr Opin Colloid Interface Sci. 2006 Oct;11(4):193–202.

166. Ozdemir M, Yurteri CU, Sadikoglu H. Physical polymer surface modification methods and applications in food packaging polymers. Crit Rev Food Sci Nutr. 1999;39(5):457–77.

167. Johansson KS. Surface Modification of Plastics. In: Applied Plastics Engineering Handbook: Processing, Materials, and Applications: Second Edition. Elsevier Inc.; 2017. p. 443–87.

168. Ebnesajjad S. Plasma Treatment of Polymeric Materials. In: Surface Treatment of Materials for Adhesive Bonding. Elsevier; 2014. p. 227–69.

169. Vesel A, Mozetic M. New developments in surface functionalization of polymers using controlled plasma treatments. J Phys D Appl Phys. 2017 Jun 29;50(29).

170. Ozdemir M, Yurteri CU, Sadikoglu H. Physical polymer surface modification methods and applications in food packaging polymers. Crit Rev Food Sci Nutr [Internet]. 1999 [cited 2022 May 29];39(5):457–77. Available from: https://www.tandfonline.com/doi/abs/10.1080/10408699991279240

171. Van Deynse A, Cools P, Leys C, De Geyter N, Morent R. Surface activation of polyethylene with an argon atmospheric pressure plasma jet: Influence of applied power and flow rate. Appl Surf Sci. 2015 Feb 15;328:269–78.

172. Vandencasteele N, Reniers F. Plasma-modified polymer surfaces: Characterization using XPS. J Electron Spectros Relat Phenomena. 2010 May;178–179(C):394–408.

173. Mandolfino C, Lertora E, Gambaro C. Effect of cold plasma treatment on surface roughness and bonding strength of polymeric substrates. Key Eng Mater. 2014;611–612:1484–93.

174. Puliyalil H, Filipič G, Cvelbar U. Selective Plasma Etching of Polymers and Polymer Matrix Composites. In: Non-Thermal Plasma Technology for Polymeric Materials: Applications in Composites, Nanostructured Materials, and Biomedical Fields. Elsevier; 2018. p. 241–59.

175. Morent R, De Geyter N, Leys C. Effects of operating parameters on plasma-induced PET surface treatment. Nucl Instruments Methods Phys Res Sect B Beam Interact with Mater Atoms. 2008 Jun;266(12–13):3081–5.

176. Shenton MJ, Stevens GC. Surface modification of polymer surfaces: Atmospheric plasma versus vacuum plasma treatments. J Phys D Appl Phys. 2001 Sep 21;34(18):2761–8.

177. Tajima S, Komvopoulos K. Effect of reactive species on surface crosslinking of plasma-treated polymers investigated by surface force microscopy. Appl Phys Lett. 2006;89(12).

178. Wang J, Chen X, Reis R, Chen Z, Milne N, Winther-Jensen B, et al. Plasma modification and synthesis of membrane materials—a mechanistic review. Membranes (Basel). 2018 Sep 1;8(3).

179. Vesel A, Junkar I, Cvelbar U, Kovac J, Mozetic M. Surface modification of polyester by oxygen- And nitrogen-plasma treatment. Surf Interface Anal. 2008 Nov;40(11):1444–53.

180. Kostov KG, dos Santos ALR, Honda RY, Nascente PAP, Kayama ME, Algatti MA, et al. Treatment of PET and PU polymers by atmospheric pressure plasma generated in dielectric barrier discharge in air. Surf Coatings Technol. 2010 Jun;204(18–19):3064–8.

181. Cui NY, Upadhyay DJ, Anderson CA, Meenan BJ, Brown NMD. Surface oxidation of a Melinex 800 PET polymer material modified by an atmospheric dielectric barrier discharge studied using X-ray photoelectron spectroscopy and contact angle measurement. Appl Surf Sci. 2007 Feb 15;253(8):3865–71.

182. Homola T, Matoušek J, Hergelová B, Kormunda M, Wu LYL, Černák M. Activation of poly(ethylene terephthalate) surfaces by atmospheric pressure plasma. Polym Degrad Stab. 2012;97(11):2249–54.

183. Hegemann D, Brunner H, Oehr C. Plasma treatment of polymers for surface and adhesion improvement. Nucl Instruments Methods Phys Res Sect B Beam

Interact with Mater Atoms. 2003 Aug;208(1–4):281–6.

184. Markets and Markets. Pork Meat Market by Type, Packaging, and Application: Global Opportunity Analysis and Industry Forecast, 2021-2027 [Internet]. 2020 [cited 2022 Jun 1]. Available from: https://www.researchandmarkets.com/reports/5214893/pork-meat-market-by-type-packaging-and

185. Ritchie H, Roser M. Meat and Dairy Production - Our World in Data [Internet]. OurWorldInData. 2017 [cited 2022 Jun 1]. Available from: https://ourworldindata.org/meat-production

186. What is the liquid in my meat package? [Internet]. Meat Science. 2016 [cited 2022 Jun 2]. Available from: https://meatscience.org/TheMeatWeEat/topics/fresh-meat/article/2016/04/14/what-is-the-liquid-in-my-meat-package

187. Benchabane A, Bekkour K. Rheological properties of carboxymethyl cellulose (CMC) solutions. Colloid Polym Sci. 2008 Sep;286(10):1173–80.

188. Lopez CG, Rogers SE, Colby RH, Graham P, Cabral JT. Structure of sodium carboxymethyl cellulose aqueous solutions: A SANS and rheology study. J Polym Sci Part B Polym Phys. 2015 Apr 1;53(7):492–501.

189. Siritientong T, Aramwit P. Characteristics of carboxymethyl cellulose/sericin hydrogels and the influence of molecular weight of carboxymethyl cellulose. Macromol Res. 2015 Sep 1;23(9):861–6.

190. Arinaitwe E, Pawlik M. Dilute solution properties of carboxymethyl celluloses of various molecular weights and degrees of substitution. Carbohydr Polym. 2014;99:423–31.

191. Topală T, Bodoki A, Oprean L, Oprean R. Bovine serum albumin interactions with metal complexes. Clujul Med [Internet]. 2014 [cited 2022 Jun 2];87(4):5. Available from: /pmc/articles/PMC4620676/

192. Phan HTM, Bartelt-Hunt S, Rodenhausen KB, Schubert M, Bartz JC. Investigation of bovine serum albumin (BSA) attachment onto self-assembled monolayers (SAMs) using combinatorial quartz crystal microbalance with dissipation (QCM-D) and spectroscopic ellipsometry (SE). PLoS One. 2015 Oct 27;10(10).

193. Bujacz A. Structures of bovine, equine and leporine serum albumin. Acta Crystallogr Sect D Biol Crystallogr. 2012 Oct;68(10):1278–89.

194. Jian W, Wang L, Wu L, Sun YM. Physicochemical properties of bovine serum albumin-glucose and bovine serum albumin-mannose conjugates prepared by pulsed electric fields treatment. Molecules. 2018;23(3).

195. Onaș AM, Bîru IE, Gârea SA, Iovu H. Novel bovine serum albumin protein

backbone reassembly study: Strongly twisted β-sheet structure promotion upon interaction with go-pamam. Polymers (Basel). 2020 Nov 1;12(11):1–14.

196. Assadpour E, Jafari SM. An overview of biopolymer nanostructures for encapsulation of food ingredients. In: Biopolymer Nanostructures for Food Encapsulation Purposes. Elsevier; 2019. p. 1–35.

197. Jaishankar A, Sharma V, McKinley GH. Interfacial viscoelasticity, yielding and creep ringing of globular protein-surfactant mixtures. Soft Matter. 2011 Sep 7;7(17):7623–34.

198. Thi-Yen Le T, Hussain S, Tsay RY, Noskov BA, Akentiev A, Lin SY. On the equilibrium surface tension of aqueous protein solutions – Bovine serum albumin. J Mol Liq. 2022 Feb 1;347.

199. Guo Z, Zhang J, Zhang T, Li C, Zhang Y, Bai J. Liquid viscosities, excess properties, and viscous flow thermodynamics of triethylene glycol + water mixtures at T = (298.15, 303.15, 308.15, 313.15, and 318.15) K. J Mol Liq. 2012 Jan;165:27–31.

200. Huang J, Zeng S, Xiong S, Huang Q. Steady, dynamic, and creep-recovery rheological properties of myofibrillar protein from grass carp muscle. Food Hydrocoll. 2016 Dec 1;61:48–56.

201. Ewoldt RH, Johnston MT, Caretta LM. Experimental Challenges of Shear Rheology: How to Avoid Bad Data. In: Complex Fluids in Biological Systems [Internet]. Springer, New York, NY; 2015 [cited 2022 Jun 2]. p. 207–41. Available from: https://link.springer.com/chapter/10.1007/978-1-4939-2065-5_6

202. Chen H, Muros-Cobos JL, Holgado-Terriza JA, Amirfazli A. Surface tension measurement with a smartphone using a pendant drop. Colloids Surfaces A Physicochem Eng Asp. 2017 Nov 20;533:213–7.

203. Bidwell RM, Duran JLJ, Hubbard GL. Tables for the determination of the surface tensions of liquid metals by the pendant drop method [Internet]. Los Alamos, NM (United States); 1963 Jan [cited 2022 Jun 2]. Available from: http://www.osti.gov/servlets/purl/4607254/

204. Yang L, Chen J, Guo Y, Zhang Z. Surface modification of a biomedical polyethylene terephthalate (PET) by air plasma. Appl Surf Sci. 2009 Feb 1;255(8):4446–51.

205. Nisticò R. Polyethylene terephthalate (PET) in the packaging industry. Polym Test. 2020 Oct 1;90.

206. Maga D, Hiebel M, Aryan V. A comparative life cycle assessment of meat trays made of various packaging materials. Sustain. 2019 Oct 1;11(19).

207. Leite WO, Campos Rubio JC, Mata F, Hanafi I, Carrasco A. Dimensional and

Geometrical Errors in Vacuum Thermoforming Products: An Approach to Modeling and Optimization by Multiple Response Optimization. Meas Sci Rev. 2018 Jun 1;18(3):113–22.

208. Bergs T, Tombul U, Herrig T, Klink A, Klocke F. Experimental analysis of influence of discharge current, pulse interval time and flushing conditions on WEDM performance. Procedia Manuf. 2018 Jan 1;18:130–7.

209. Automated Digital Microscope ZEISS Smartzoom 5 [Internet]. Zeiss. [cited 2022 Jun 2]. Available from: https://www.zeiss.com/microscopy/int/products/imaging-systems/smartzoom-5.html

210. Francis L. Materials Processing - 1st Edition [Internet]. 1st Edition. 2015 [cited 2022 Jun 2]. Available from: https://www.elsevier.com/books/materials-processing/francis/978-0-12-385132-1

211. Laguna-Gutierrez E, Van Hooghten R, Moldenaers P, Rodriguez-Perez MA. Understanding the foamability and mechanical properties of foamed polypropylene blends by using extensional rheology. J Appl Polym Sci. 2015 Sep 1;132(33).

212. ASTM International. Standard Test Method for Apparent Density of Rigid Cellular Plastics [Internet]. 2020 [cited 2022 Jun 2]. Available from: https://www.astm.org/d1622_d1622m-14.html

213. Fischer ER, Hansen BT, Nair V, Hoyt FH, Dorward DW. Scanning Electron Microscopy. Curr Protoc Microbiol [Internet]. 2012 May 1 [cited 2022 Jun 2];25(1):2B.2.1-2B.2.47. Available from: https://onlinelibrary.wiley.com/doi/10.1002/9780471729259.mc02b02s25

214. Maire É, Adrien J, Petit C. Structural characterization of solid foams. Comptes Rendus Phys. 2014;15(8–9):674–82.

215. ASTM International. Standard Test Method for Open Cell Content of Rigid Cellular Plastics [Internet]. 2015 [cited 2022 Jun 2]. Available from: https://www.astm.org/d6226-10.html

216. Pandiyaraj KN, Selvarajan V, Deshmukh RR, Yoganand P, Balasubramanian S, Maruthamuthu S. Low pressure DC glow discharge air plasma surface treatment of polyethylene (PE) film for improvement of adhesive properties. Plasma Sci Technol [Internet]. 2013 Jan 1 [cited 2022 Jun 2];15(1):56–63. Available from: https://iopscience.iop.org/article/10.1088/1009-0630/15/1/10

217. Xie L, Dai Q, Du G, Deng Q, Liu G. Study on surface modification of polyethylene terephthalate(PET) film by RF-AR/O2 plasma treatment. Appl Mech Mater [Internet]. 2012 [cited 2022 Jun 2];200:94–8. Available from: https://www.scientific.net/AMM.200.194

218. Jucius D, Kopustinskas V, Grigaliunas V, Guobiene A, Lazauskas A, Andrulevičius M. Highly hydrophilic poly(ethylene terephthalate) films prepared by combined hot embossing and plasma treatment techniques. Appl Surf Sci. 2015 Sep 15;349:200–10.

219. Korin E, Froumin N, Cohen S. Surface Analysis of Nanocomplexes by X-ray Photoelectron Spectroscopy (XPS). ACS Biomater Sci Eng. 2017 Jun 12;3(6):882–9.

220. Dowling DP, Tynan J, Ward P, Hynes AM, Cullen J, Byrne G. Atmospheric pressure plasma treatment of amorphous polyethylene terephthalate for enhanced heatsealing properties. Int J Adhes Adhes. 2012 Jun;35:1–8.

221. Ba OM, Marmey P, Anselme K, Duncan AC, Ponche A. Surface composition XPS analysis of a plasma treated polystyrene: Evolution over long storage periods. Colloids Surfaces B Biointerfaces. 2016 Sep 1;145:1–7.

222. Junkar I, Vesel A, Cvelbar U, Mozetič M, Strnad S. Influence of oxygen and nitrogen plasma treatment on polyethylene terephthalate (PET) polymers. Vacuum. 2009 Aug 25;84(1):83–5.

223. Wardhani R, Putu S, Sanjoto BL, Nur H, Hari S. Numerical simulation of multipoint forming with circular die pins in hexagonal packing. Appl Mech Mater. 2014;493:589–93.

224. Sharma V, Jaishankar A, Wang YC, McKinley GH. Rheology of globular proteins: Apparent yield stress, high shear rate viscosity and interfacial viscoelasticity of bovine serum albumin solutions. Soft Matter [Internet]. 2011 Jun 7 [cited 2022 Jun 24];7(11):5150–60. Available from: https://pubs.rsc.org/en/content/articlehtml/2011/sm/c0sm01312a

225. Lanzaro A. A microfluidic approach to studying the injection flow of concentrated albumin solutions. SN Appl Sci [Internet]. 2021 Sep 1 [cited 2022 Jun 24];3(9). Available from: https://pubmed.ncbi.nlm.nih.gov/34723096/

226. McCool R, Martin PJ. Thermoforming process simulation for the manufacture of deep-draw plastic food packaging. Proc Inst Mech Eng Part E J Process Mech Eng [Internet]. 2011 Nov 13 [cited 2022 Jun 25];225(4):269–79. Available from: http://journals.sagepub.com/doi/10.1177/0954408911416292

227. Buntinx M, Willems G, Knockaert G, Adons D, Yperman J, Carleer R, et al. Evaluation of the Thickness and Oxygen Transmission Rate before and after Thermoforming Mono- and Multi-layer Sheets into Trays with Variable Depth. Polymers (Basel) [Internet]. 2014 Dec 22 [cited 2022 Jun 25];6(12):3019–43. Available from: http://www.mdpi.com/2073-4360/6/12/3019

228. Ashter SA. The Thermoforming Process. In: Thermoforming of Single and Multilayer Laminates. Elsevier; 2014. p. 13–38.

229. Morye SS. A comparison of the thermoformability of a PPE/PP blend with thermoformable ABS. Part I: Small deformation methods. Polym Eng Sci [Internet]. 2005 Oct 1 [cited 2022 Jun 25];45(10):1369–76. Available from: https://onlinelibrary.wiley.com/doi/10.1002/pen.20416

230. Throne J. Thermoforming. In: Applied Plastics Engineering Handbook: Processing, Materials, and Applications: Second Edition. Elsevier Inc.; 2017. p. 345–75.

231. Lv J, Zhou Q, Zhi T, Gao D, Wang C. Environmentally friendly surface modification of polyethylene terephthalate (PET) fabric by low-temperature oxygen plasma and carboxymethyl chitosan. J Clean Prod. 2016 Apr 1;118:187–96.

232. Nosonovsky M, Bhushan B. Roughness optimization for biomimetic superhydrophobic surfaces. Microsyst Technol [Internet]. 2005 Aug 15 [cited 2022 Jun 25];11(7):535–49. Available from: https://link.springer.com/article/10.1007/s00542-005-0602-9

233. Extrand CW. Drainage from a Fluid-Handling Component with Multiple Orifices due to Inclination or Rotation. Langmuir [Internet]. 2018 Apr 10 [cited 2022 Jun 25];34(14):4159–65. Available from: https://pubs.acs.org/sharingguidelines

234. Andersson H, Van der Wijngaart W, Griss P, Niklaus F, Stemme G. Hydrophobic valves of plasma deposited octafluorocyclobutane in DRIE channels. Sensors Actuators, B Chem. 2001 Apr 30;75(1–2):136–41.

235. Pankaj SK, Bueno-Ferrer C, Misra NN, Milosavljević V, O'Donnell CP, Bourke P, et al. Applications of cold plasma technology in food packaging. Trends Food Sci Technol. 2014 Jan 1;35(1):5–17.

236. Ravi S, Dharmarajan R, Moghaddam S. Measurement of Capillary Radius and Contact Angle within Porous Media. Langmuir [Internet]. 2015 Nov 5 [cited 2022 Jun 25];31(47):12954–9. Available from: https://pubs.acs.org/doi/abs/10.1021/acs.langmuir.5b03113

237. Canal C, Gaboriau F, Vílchez A, Erra P, Garcia-Celma M, Esquena J. Topographical and Wettability Effects of Post-Discharge Plasma Treatments on Macroporous Polystyrene-Divinylbenzene Solid Foams. Plasma Process Polym [Internet]. 2009 Oct 14 [cited 2022 Jun 25];6(10):686–92. Available from: https://onlinelibrary.wiley.com/doi/10.1002/ppap.200950011

238. Safinia L, Datan N, Höhse M, Mantalaris A, Bismarck A. Towards a methodology for the effective surface modification of porous polymer scaffolds. Biomaterials. 2005 Dec 1;26(36):7537–47.

239. Sahnia L, Wilson K, Mantalaris A, Bismarck A. Through-thickness plasma modification of biodegradable and nonbiodegradable porous polymer

constructs. J Biomed Mater Res - Part A [Internet]. 2008 Dec 1 [cited 2022 Jun 26];87(3):632–42. Available from: https://pubmed.ncbi.nlm.nih.gov/18189299/

240. Vesel A. Modification of polystyrene with a highly reactive cold oxygen plasma. Surf Coatings Technol. 2010 Oct 15;205(2):490–7.

241. Dupont-Gillain CC, Adriaensen Y, Derclaye S, Rouxhet PG. Plasma-oxidized polystyrene: Wetting properties and surface reconstruction. Langmuir [Internet]. 2000 Oct 17 [cited 2022 Jun 26];16(21):8194–200. Available from: https://pubs.acs.org/doi/abs/10.1021/la000326l

242. Haïdopoulos M, Horgnies M, Mirabella F, Pireaux J-J. Angle-Resolved XPS Study of Plasma-Deposited Polystyrene Films after Oxygen Plasma Treatment. Plasma Process Polym [Internet]. 2008 Jan 10 [cited 2022 Jun 26];5(1):67–75. Available from: https://onlinelibrary.wiley.com/doi/10.1002/ppap.200700067

243. Davies J, Nunnerley CS, Brisley AC, Sunderland RF, Edwards JC, Krüger P, et al. Argon plasma treatment of polystyrene microtiter wells. Chemical and physical characterisation by contact angle, ToF-SIMS, XPS and STM. Colloids Surfaces A Physicochem Eng Asp. 2000 Dec 1;174(3):287–95.

244. Dhayal M, Alexander MR, Bradley JW. The surface chemistry resulting from low-pressure plasma treatment of polystyrene: The effect of residual vessel bound oxygen. Appl Surf Sci. 2006 Sep 15;252(22):7957–63.

245. Vesel A, Zaplotnik R, Kovac J, Mozetic M. Initial stages in functionalization of polystyrene upon treatment with oxygen plasma late flowing afterglow. Plasma Sources Sci Technol [Internet]. 2018 Sep 19 [cited 2022 Jun 26];27(9):094005. Available from: https://iopscience.iop.org/article/10.1088/1361-6595/aad486

246. Fricke K, Tresp H, Bussiahn R, Schröder K, Von Woedtke T, Weltmann KD. On the use of atmospheric pressure plasma for the bio-decontamination of polymers and its impact on their chemical and morphological surface properties. Plasma Chem Plasma Process [Internet]. 2012 Aug 11 [cited 2022 Jun 26];32(4):801–16. Available from: https://link.springer.com/article/10.1007/s11090-012-9378-8